

PEOPLE'S DEMOCRATIC REPUBLIC OF ALGERIA
MINISTRY OF HIGHER EDUCATION AND SCIENTIFIC RESEARCH
FERHAT ABBAS UNIVERSITY-SETIF-1
INSTITUTE OF OPTICS AND PRECISION MECHANICS

THESIS

Submitted to obtain

3rd Cycle LMD DOCTORATE

Domain: Science and Technology

Faculty: Optics and Precision Mechanics

Specialty: Optics and Applied Photonics

By

Asma ABCHI

Title

**Contribution to the study of storage and surface conditions on the
adhesive behavior of optical surfaces.**

Discussed publicly at: 05/11 /2022

Members of the assessment committee:

Chairman	Abdellah CHORFA	Prof	F.A.U.Setif1
Supervisor	Nabil BELKHIR	Prof	F.A.U.Setif1
Examiner	Zahra MALOU	Prof	F.A.U.Setif 1
Examiner	Abdelali HAYOUNE	MCA	ENP.Constantine
Examiner	Mohamed Rida BOUDICHICHA	MCA	ENP.Constantine

Acknowledgments

At the outset, I bow my head before the almighty **ALLAH**, the Lord of worlds who endowed me with the enough vehemence to complete the task. Words are not enough to praise and thank for all the things given.

My foremost thanks go to my supervisor Professor **Mr. Belkhir Nabil** for his knowledge, great experience and a lot of helpful and interesting discussions, and for his great support during all my studies, and his advice and opinions, which he did not hesitate to give with confidence in this work.

Special thanks to Professor **Mr. Juan Rubio Alonso** for his excellent knowledge and great discussions with invaluable influence on my work, and without his continuous support this study would not have been completed.

With immense pleasure, I would thank Professor **Mr. Fausto Rubio Alonso** for having welcomed me in his institute of ceramics and glass (ICV), Autonomous University, for his help, advice, and to have made available to me all possible means to carry out my experiments, and to have accepted to be an examining member of my thesis jury.

I would thank Professor **Mr Hilmi Ünlü**, for all the optical measurements made on my thin films in his laboratory at Istanbul Technical University (ITU).

Many thanks and regards to Professor **Mr. Abdellah Chorfa** for chairing the jury for this thesis.

I express my sincere gratitude to Professor **Mrs. Zahra Malou** for having accepted to be an examiner of this thesis and to participate in the jury.

My utmost gratitude to Professor **Mr. Abdelali Hayoune** for has agreed to be a member of the Board of this thesis.

A lot of thanks to Professor **Mr. Mohamed Rida Boudichicha** for having accepted to be an examining member of my thesis jury.

I would like to thank all the staff, lab engineer and PhD students at the Institute of Optics and precision Mechanics, for the friendly atmosphere, professionalism and a lot of help during my 5 years here.

Finally, out of the nonscientific community, I dedicated this work:

First of all to my mother **Nadia**, my father **Lehcene**, brothers (**Anes, Ali**), and my sister **Fatima El Zahra** for their support and encouragement throughout my education and life. They have instilled in me a work ethic and ambition that has led me this far.

I would also like to show my love and thanks to my husband **Mehdi** for giving me encouragement and support during my academic study, and while my family for everything they have done for me.

CONTENTS

ABSTRACT

GENERAL INTRODUCTION

CHAPTER.1 OPTICAL MATERIALS

1.1.INTRODUCTION.....	1
1.2.OPTICAL MATERIALS.....	1
<i>1.2.1. Optical glass.....</i>	<i>1</i>
<i>1.2.1.1. Properties of optical glass.....</i>	<i>2</i>
1.2.1.1.1. Refractive index and Abbe number.....	2
1.2.1.1.2. Transmittance coefficient of optical glass.....	4
<i>1.2.2. Optical Polymers.....</i>	<i>4</i>
<i>1.2.2.1. Properties of optical polymer.....</i>	<i>5</i>
1.2.2.1.1. Refractive index and Abbe number.....	5
1. PMMA(Poly methyl methacrylate).....	5
2. Polystyrene.....	5
3. Polycarbonate	5
1.2.2.1.2. Transmittance coefficient of PMMA.....	6
1.3. CHARACTERISTIC OF OPTICAL MATERIALS.....	6
<i>1.3.1. Optical surface states.....</i>	<i>6</i>
<i>1.3.1.1. Surface Roughness parameters.....</i>	<i>7</i>
1.3.1.1.1. Mean Height of the Surface.....	7
1. Root Mean Square Height value (Sq).....	7
2. Arithmetic mean height value(Sa).....	7
1.3.1.1.2. Skewness and Kurtosis.....	7
1. Skewness value(Ssk).....	7
2. Kurtosis value (Sku).....	8
1.3.1.1.3. Maximum Height of the Surface.....	8
1. Maximum peak height (Sp).....	8
2. Maximum pit height (Sv).....	8
3. Maximum height (Sz).....	8
1.4. CHARACTERIZATION TECHNIQUES.....	9
<i>1.4.1. Total integrated scattering (TIS)</i>	<i>9</i>
<i>1.4.2. Ultraviolet-visible- near infrared spectroscopy.....</i>	<i>10</i>
<i>1.4.3. Raman spectroscopy and correlative μ-SHG mapping.....</i>	<i>11</i>
<i>1.4.4. Infrared spectroscopy</i>	<i>12</i>
<i>1.4.5. Optical profilometry.....</i>	<i>13</i>
<i>1.4.6. Atomic Force Microscopy.....</i>	<i>14</i>
1.5. STORAGE EFFECT ON THE OPTICAL MATERIALS.....	15
<i>1.5.1. Medium nature effect on substrates.....</i>	<i>15</i>
<i>1.5.2. Duration effect on substrate.....</i>	<i>16</i>
<i>1.5.3. Temperature effect.....</i>	<i>16</i>

CHAPTER.2 THIN FILMS AND ADHESION

2.1. INTRODUCTION.....	17
2.2. THIN FILMS.....	17
<i>2.2.1. Deposition techniques of thin films.....</i>	<i>18</i>
<i>2.2.1.1. Physical methods.....</i>	<i>20</i>
<i>2.2.1.1.1. Evaporation</i>	<i>20</i>
<i>1. Vacuum evaporation.....</i>	<i>20</i>
<i>2. Electron beam evaporation.....</i>	<i>21</i>
<i>3. Laser beam evaporation (pulsed-laser deposition).....</i>	<i>22</i>
<i>4. Ion beam deposition.....</i>	<i>23</i>
<i>2.2.1.1.2. Sputtering</i>	<i>24</i>
<i>1. Magnetron sputtering deposition.....</i>	<i>24</i>
<i>2. Reactive sputtering deposition</i>	<i>25</i>
<i>2.2.1.2. Chemical methods.....</i>	<i>26</i>
<i>2.2.1.2.1. Sol- gel deposition</i>	<i>26</i>
<i>1. Hydrolysis</i>	<i>27</i>
<i>. Condensation</i>	<i>27</i>
<i>1. Spin coating technique</i>	<i>28</i>
<i>2. Dip-coating technique</i>	<i>29</i>
<i>2.2.1.2.2. Chemical bat deposition</i>	<i>30</i>
<i>2.2.1.2.3. Chemical vapour deposition (CVD).....</i>	<i>31</i>
<i>1. Thermal (CVD).....</i>	<i>33</i>
<i>2. Plasma-enhanced CVD (PECVD).....</i>	<i>33</i>
2.3.CHARACTERIZATION OF THIN FILMS.....	34
<i>2.3.1.Stress measurement</i>	<i>35</i>
<i>2.3.2. Hardness and Young's modulus</i>	<i>35</i>
<i>2.3.3. Density.....</i>	<i>36</i>
<i>2.3.4. Resistance to cracking</i>	<i>37</i>
<i>2.3.5. Band gap energy</i>	<i>37</i>
<i>2.3.6. Contact angle</i>	<i>38</i>
<i>2.3.7. X-ray diffraction</i>	<i>39</i>
<i>2.3.8. Scanning electron microscopy.....</i>	<i>40</i>
2.4. ADHESION BEHAVIOR	41
<i>2.4.1. Material Adhesion Mechanism</i>	<i>41</i>
<i>2.4.1.1. Chemical Bonding</i>	<i>41</i>
<i>2.4.1.2. Mechanical Bonding</i>	<i>42</i>
<i>2.4.1.3. Stress, Deformation, and Failure.....</i>	<i>42</i>
<i>2.4.1.4. Fracture</i>	<i>42</i>
<i>2.4.2. Surface energy.....</i>	<i>43</i>
<i>2.4.3. Methods of contact angle measurements.....</i>	<i>44</i>
<i>2.4.3.1. Sessile Drop Method.....</i>	<i>44</i>
<i>2.4.3.2. Wilhelmy method.....</i>	<i>45</i>
<i>2.4.3.3. Du Nouy ring method.....</i>	<i>46</i>
<i>2.4.3.4.Captive Bubble Method.....</i>	<i>47</i>
<i>2.4.3.5. Digi- Drop method.....</i>	<i>47</i>
2.5.SURFACE ROUGHNESS EFFECT ON ADHESION BEHAVIOR..	48

CHAPTER.3 PRACTICAL STUDY

3. PRACTICAL STUDY.....	50
3.1. SUBJECT.....	50
3.2. MATERIALS AND DEVICES	50
3.3. STORAGE EFFECT ON THE OPTICAL MATERIALS	51
3.3.1. <i>Experimental procedure</i>	51
3.3.1.1. <i>Samples preparation</i>	51
3.3.1.2. <i>Characterization procedure</i>	51
3.3.1.2.1. SF2 and FK	51
3.3.1.2.1.1. Optical profilometry.....	51
3.3.1.2.1.2.AFM instrument.....	51
3.3.1.2.1.3.Abbe Refractometer.....	52
3.3.1.2.2. BK7 and PMMA	52
3.3.1.2.2.1. Storage effect on the roughness (Rq).....	52
A.TIS technique	52
B. Optical interferometry.....	53
3.3.1.2.2.1. UV–visible spectrophotometer.....	53
3.3.1.3. <i>Preparation of the solution</i>	53
3.3.1.3.1. Silica sols Preparation	53
3.3.1.3.2. Zinc Sulfide preparation sols.....	54
3.3.1.4. <i>Digi Drop measurement.....</i>	55
3.3.1.5. <i>Thin film used.....</i>	55
3.3.1.5.1. Silica thin film	55
3.3.1.5.2. Chemical structural properties	55
3.3.1.5.3. Coating adherence behavior	56
3.3.1.5.4. Zinc Sulfide thin film	56
3.3.1.6. <i>Adhesion and cohesion measurement</i>	56
3.4. RESULTS AND DISCUSSION	57
3.4.1. <i>Storage effect on the sample’s optical proprieties.....</i>	57
3.4.2. <i>Silica sol-gel solution characterization</i>	58
3.4.3. <i>Surface roughness.....</i>	62
3.4.4. <i>Surface roughness Effect on the contact angle</i>	64
3.4.5. <i>Coating Silica characterization.....</i>	71
3.4.6. <i>Silica adhesion</i>	74
3.4.7. <i>Scratch test of Silica thin films</i>	79
3.4.8. <i>Adhesion behavior</i>	81
3.4.9. <i>Influence of polishing on the transmission of stored materials.....</i>	84
3.4.10. <i>Behavior of stored samples on the thin film deposition.....</i>	89
3.4.10.1. <i>Thin films solution characterization</i>	89
3.4.11. <i>Adherence behavior</i>	94
3.4.12. <i>Adhesion and cohesion behavior</i>	95

GENERAL CONCLUSION

REFERENCE

ABSTRACT

Surface properties can affect the efficiency and behavior of the optical material, so their improvement is more than desirable. One of the recommended solutions is thin films depositions. Thin films are important for applications in different fields, such as optical devices, environmental applications, telecommunications devices, energy storage devices, and so on. The deposition of thin layers should be successful in order to achieve the desired objectives. Indeed, adhesion and deposit quality are the essential factor for the judgment of a thin films.

In this context, this thesis aims to study the effect of storage conditions and the surface quality of certain optical materials on the adhesion of thin films. For this purpose, tests have been carried out in the synthesis and deposition of thin films by sol -gel and chemical bath deposition (CBD), as well as the study of the adhesion behavior of Zinc Sulfide and Silica thin films deposited with different concentration: 20, 30 and 40% on optical substrates. The tests were carried out on substrates made of optical materials (mineral glass and polymer) for long-term storage in various solutions (CK and PEG). Surfaces were treated with several techniques (Optical interferometry, TIS, AFM....) Their surface roughness was measured and compared ,the prepared solutions were analyzed by FTIR, Raman and photoluminescence Spectroscopy. The results obtained are therefore large variances and therefore clear conclusions are not easily drawn. The storage effect of the optical materials and their surface roughness on the adhesion phenomenon and the spreading factor of the deposited thin layers are established.

Keywords: Optical glass, PMMA, spreading coefficient, thin films, adhesion, contact angle, sol-gel, CBD, Silica, Zinc sulfide.

GENERAL INTRODUCTION

In recent years, surfaces and interfaces most often play a major role in the production or the use of optical materials in different areas of microelectronics, chemistry, physics, metrology and optics.

In reality, the optical materials differ among each other foremost, by their optical properties: refraction index, dispersion, and transmission, so on. As well as, with technical characteristics such as presence of bubbles and striae, roughness, and others. Reference parameters include thermo-optical, heat-engineering, electrical, mechanical, and different characteristics, including chemical stability ready optical parts are protected by optical coatings.

The roughness, morphology and precise shape of the structures actually result from the properties, physical-chemical surfaces and/or interfaces and how they are manufactured [1]. It is therefore permanently interesting to analyze them in order to know their characteristics. Historically, surface conditions have been evaluated visually and/or tactilely, and then measured on a profile using sensors with a more or less efficient signal processing [2].

In many fields, several surface analysis techniques (AFM, SEM, confocal microscopy, interferometric microscopy, and optical profilometry...) are used to monitor and improve the performance of materials in both research and industry. Morphological analysis is one means of controlling materials at the microscopic and sometimes [3]. In a fact, one of the most reliable techniques used more in this case optical methods.

Optical methods, based on the principle of light-matter interaction, such as the phenomena of interference, polarization and diffusion, given their non-destructive nature and without contact, are able to control and quantify in real time in very accurate and faster information on surface roughness, deformations of objects, and morphology of thin film [4].

The dependence of the thin film deposition by the adhesion phenomena is not the only problems in the process. Indeed, the surface quality plays a big role in the thin film quality that is way surfaces must be finished to obtain very fine surfaces before the deposition.

The optical surfaces are the most fished surface before the deposition process because of the functional aspect of these surfaces. In optical field, surface are finished by several process, the most used are the free abrasive grains polishing and the chemical mechanical polishing (CMP). In this last, the optical surface is polished under determined parameters with the use of special slurry containing a very fine abrasive grain and a special solution. The abrasive grains for the mechanical action and the slurry for the chemical one, the reason of the name of this process.

Thin film deposition was the subject of several studies regarding their adhesion and their corrosion resistance [5]. In optical applications, deposition technique must be chosen to perform high quality, functional surfaces, especially. When it is necessary to produce a layer stacking, sol- gel and chemical bath evaporation techniques are recommended in this case.

Chemical bath deposition and sol-gel are one of the most used thin films elaboration techniques. It is a simple, practical, and useful technique in different coatings. The extent of utilizing substrates impacts different physical qualities of the last material, as dispersion, refractive index, and roughness. Chemical bath deposition and sol-gel layer depositions were the subject of several studies regarding their adhesion and their corrosion resistance [6].

The study of the adhesion behavior of optical surfaces is an area of research is very important because of the spreading factor role in these processes and their necessity. However, the phenomena describing surface tensions are extremely complex, like all systems whose consequence is the random result of countless events. The results obtained are therefore large variances are not easily drawn, the adhesion and cohesion behavior need to be clarified, while knowing the difficulty of identifying the causes of this phenomenon.

Adhesion is usually a non equilibrium irreversible process in which phenomena such as surface roughness, molecular rearrangements, and plastic deformations give rise to adhesion hysteresis and a real adhesive energy order of magnitude greater than the thermodynamic work of adhesion. These non-equilibrium mechanisms are not easily investigated, but if understood they can be used to significantly improve and tailor the adhesive interactions between various substrates [7].

Generally, thin film adhesion is of technological importance in determining the wettability of liquids used, and is also of considerable theoretical interest. The adhesion of films has been investigated in several fields. Also, adhesion is significant in many branches of surface physics; it is a fundamental parameter because it depends directly on inters atomic and intermolecular forces. Thin films are of special interest in this connection because it is in such systems that conditions of true interfacial contact can most nearly be attained.

In polycrystalline thin film devices, the performance and reliability will critically depend upon the microstructure, grain size and distribution, and defect density, that are in turn affected by deposition and post-deposition conditions as well as the thickness of the films. In recent years, various methods have been evolved to prepare smart materials and structures in thin film form that have a wide range of applications [8].

Silica gel can occur in various forms; however, they show similar surface properties as porous glass, quartz as well as silicate and siloxane crystals. A common feature of these compounds is the occurrence on their surface of functional hydroxyl groups bonded with the skeleton by covalent bonds.

Silanol groups can exist on the surface as single, geminal and vicinal groups which can form so-called bounded pairs.

The thickness effect on the physical properties of ZnS films has been studied. In addition to this, various critical issues related to the optoelectronic properties of ZnS films as a function of thickness and the influence of residual strain on such properties need to be addressed in order to improve the performance of devices further making use of ZnS films.

When thin films are realized the adhesion behavior must be considered. Some techniques are used to define the adhesion between the sample and the layer. Indeed, the adhesion phenomenon can be easily studied via the contact angle or the surface energy. In this way, studies were performed to determine the correlation between the contact angle and the different parameters and it was found that the contact angle decreased with the expansion of Zinc sulfide, and silica concentration.

In this work thin films are optically characterized by measuring contact angle, transmittance, and adhesion behavior of the Zinc sulfide (ZnS) and Silica (SiO₂) and thin film deposited on optical materials (Dense Flint SF2, Fluorite Crown FK, and borosilicate -crown BK7,B270 supplier (SHOTT GMBH),Soda lime glass(SL), polycarbonate lens (PC), Poly Methyl Methacrylate (PMMA), and calculating theirs: refractive index (n_d), Abbe number and surface roughness. These films (ZnS ,SiO₂) are deposited respectively with different concentrations, by chemical bath deposition (CBD)and sol-gel (dip coating) for each sample polished with cerium oxide and silica abrasive grains. Here, it is shown how the surface roughness is influenced by the wettability of the liquids deposited.

This thesis consists of three main parts; theoretical and practical. The first consists of two chapters in the first part, Chapter 1, a detailed literature review is provided on the characterization techniques, properties, surface roughness measurements and parameters effect of the optical material substrates.

In the second part, chapter 2, summarizing the main types, techniques, and characterization of the thin film depositions as well as the parameters influencing the adhesion and finally the techniques for measuring the surface energy, contact angle and adhesion.

As for the practical process, chapter3, is divided into three parts: the first presents the sample preparation of optical materials, and an interpretation of the concentration impact of different optical substrate (20, 30, and 40%), and surface roughness measurement.

The second part presents the study of the adhesion and surface roughness (SF2,FK,BK7,andPMMA) effect on silica and Zinc sulfide thin film properties using the sol-gel and chemical bath deposition(CBD)methods.

Moreover, the last part presents the survey of the wettability and the adhesive effect on the glasses (SL,B270 and PC). It ends with the presentation of the essential results with their discussion. We conclude our thesis with a general conclusion and some final suggestions for further work.

CHAPTER .1



OPTICAL MATERIALS

CHAPTER.1 OPTICAL MATERIALS

1. OPTICAL MATERIALS

1.1 INTRODUCTION

Generally, the optical glass and optical polymers are key materials not only for the optical industry but because of the high leverage effect of optical systems also for most research and development activities as well as for virtually all technology [9].

In Physical and chemical applications ,storage effect of the optical glasses and polymers are one of the important parameters influence on the surface quality , optical and mechanical properties of the optical substrates, also this may be due to compliance with the storage conditions(duration, medium ,and environment)[9-10].

In this chapter is presented the determination of the optical material types, techniques and surface roughness parameters for the optical materials as starting from its optical characteristics and storage effect of optical materials.

1.2. OPTICAL MATERIALS

1.2.1. Optical glass

In the year 2009 there is the anniversary closely related to optical instrumentation. It was 125 years ago that Otto Schott, Ernst Abbe, and Carl Zeiss founded the company “Jenaer Glas werke Schott und Genossen”. Schott introduced new optical glasses as well as new development and production processes, which allowed optics to become a technology. Now the design and reliable production of highly powerful optical systems became possible with far reaching consequences, which can hardly be overestimated [10]. Besides, the optical glasses are in widespread use. The reason is that they can be produced in large quantities with very good homogeneity and with a rich variety of special properties, which cannot be found in natural materials [11].

Presently, on Schott categories of optical glasses are found significant grades of optical glass [11], fabricated of specialized manufactures. In general, these grades of optical glass are classified, in two significant groups, Flint and Crown glasses .In fact, several chemical subsistence is used in the elaboration of these glasses as fluorine, phosphate, boron, barium, and lanthanum [12-13].

Additionally, another of the glasses are of wide variety that makes them available for any application, a number of most glasses exists[14]:

-Vitreous silica: Vitreous silica is the most refractory glass in commercial usage, it can also be made by chemical reaction and fusion utilizing silica acid or SiCl_4 or organic-silicon compounds with a softening temperature of nearly 1700 °C, fused silica is rarely considered for molding

CHAPTER.1 OPTICAL MATERIALS

applications except in extremely rare cases and with specialized equipment. It is frequently used for optical fibers, astronomical mirrors, and as thermal or electrical insulators[13-14].

-Borosilicate: it is used for precision glass molded lenses where low thermal expansion and high resistance to chemical attack are required. Borosilicate is also considered to be crown glasses that possess lower refractive index and low to moderate dispersion properties which are useful for many optical designs, especially for correction of secondary color aberrations.

-Lanthanum oxide: This glass typically possesses higher hardness, higher transformation temperature and useful refractive index and dispersion properties. Higher index enables shorter overall system length and lower spherical aberration. Higher dispersion properties are useful in many optical designs for both consumer and high end optical systems.

- Aluminosilicate: it is noted for higher values of Young's modulus and high resistance to chemical attack. Applications are common where higher operating temperatures are encountered, or where higher than normal stress is anticipated in the design.

1.2.1.1. Properties of optical glass:

The optical glass is a glass with a special composition, which is used in the manufacture of optical parts and components, for example: lenses, prisms, optical fibers, and so on this glass has a specific property [15]. In the first, high homogeneity, as optical glass is an isotropic material, exactly and constant values, in time and in glass volume, for a refractive index of 1.47 to 2, respectively for dispersion coefficient of 20 to 90. Then, the spectrum of optical radiations has a non-selective transmission in the visible range, and high mechanical strength in scratching and automation. Also, the chemical stability in relation with atmospheric agents and solutions of weak acids, and finally, the optical density is altering in accuracy limits the colorless optical glass, becomes toughness of predictable ionizing radiation [16].

1.2.1.1.1. Refractive index and Abbe number:

Among the optical glass sorts, two groups are very useful in optical field; the Crown and the Flint, they are different by their chemical composition and then their optical proprieties.

Launey et al [17] studied the specific properties of the Crown and Flint glasses, these Glasses can be broadly categorized according to their chromatic dispersion, refractive index(n_d), and Abbe number(v_d) [18]. In Table 1.1 are presented the most characteristics of optical glasses for Crown and Flint glasses.

CHAPTER.1 OPTICAL MATERIALS

Characteristics of optical glass	Crown glasses (K)	Flint glasses(F)
Dispersion (D_{FC})	Lower	Higher
Refractive index(n_d)	1.4 - 1.55	1.54 - 1.65
Abbe number(v_d)	More than 50	Less than 50

Table 1.1. Specific characteristics for Crown glasses and Flint glasses [18].

Figure 1.1 is illustrated a Abbe diagram ($n_d - v_d$). This diagram is explained the different optical glass types by using the refractive index and Abbe number as coordinates. The left part of the diagram corresponding to high Abbe number contains the crown glasses [19]. The right part of the diagram corresponding to low Abbe number contains the flint glasses in the end. Besides the rough differentiation between crowns and flints, the diagram shows further areas of similar chemical composition, e.g., the region of barium flints (BAF) or the area of lanthanum crowns (LAK) [20,21]. According to their position in the diagram, the glasses get their labels.

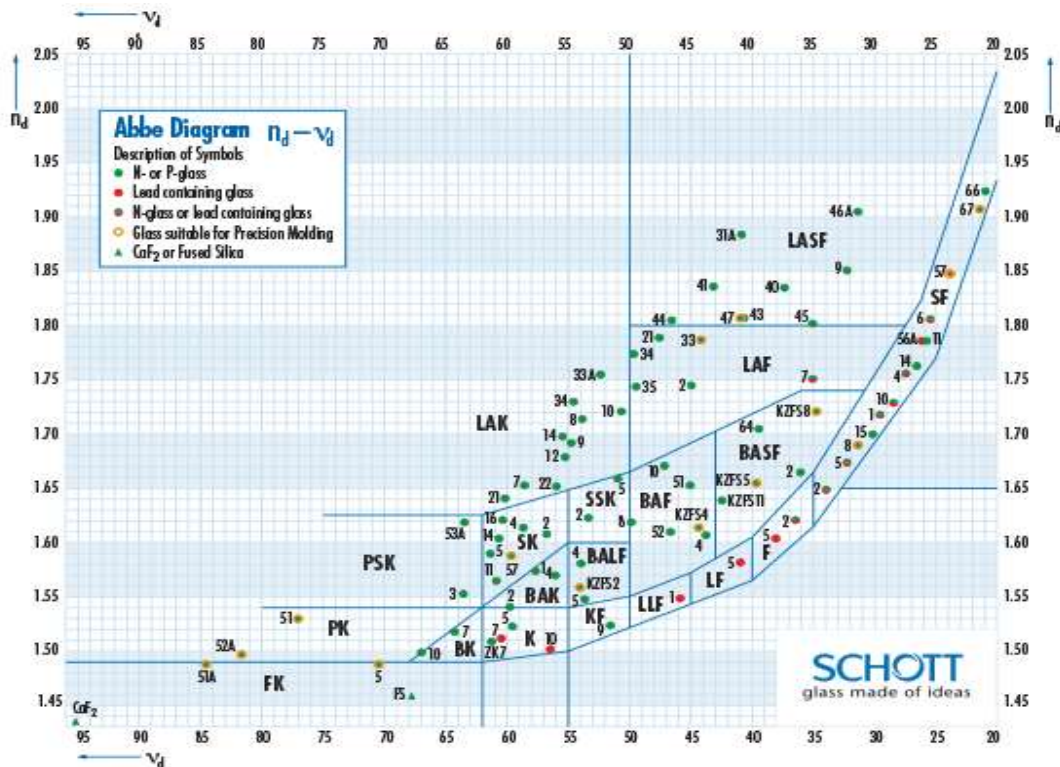


Figure 1.1. Abbe diagram of optical glasses (n_d, v_d)(Crowns and Flints)of society SCHOTT[21].

CHAPTER.1 OPTICAL MATERIALS

1.2.1.1.2. Transmittance coefficient of optical glass:

The UV transmittance edge does not only depend on the composition of the glass, but also on the thickness. With an increasing thickness the transmittance edge is shifted to longer wavelengths.

Figure 1.2 showed a comparison of the transmittance data of N-PK52A, N-SF57 and SF57 near the UV edge between different refractive indices, different composition and material thickness.

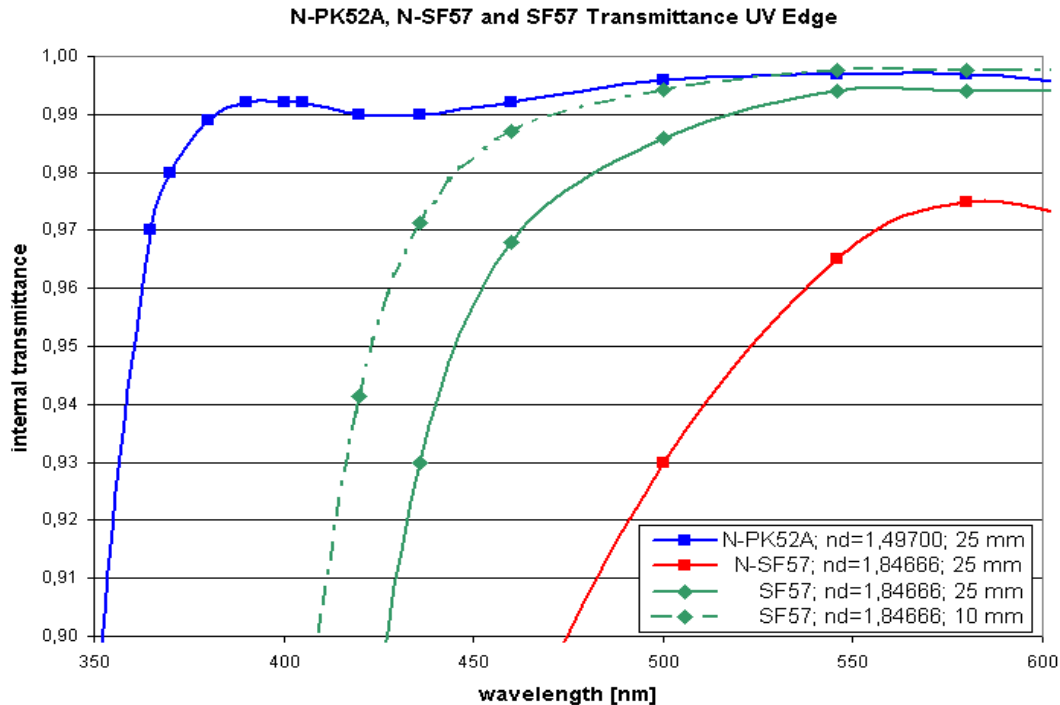


Figure1.2. Transmittance data of N-PK52A, N-SF57 and SF57 of society SCHOTT [21].

1.2.2. Optical Polymers

For centuries, glass proved to be the material of choice for all optical applications. During the 20th century, applications for glass elements and complex optical systems greatly expanded. Early uses of molded plastic elements included toy objectives, gauge windows and watch crystals. Throughout the 1970s and up to the present, high-grade optical polymers were developed specifically for optical applications [22]. These advancements in materials, coupled with improved mold design have enabled plastic optics to replace glass optics in a wide and growing number of applications. Abiona et al [23] demonstrated that a many molecular mass relative to small molecule compounds produces unique physical properties, including toughness, viscoelasticity, and a tendency to form glasses and semi crystalline structures rather than crystals.

Polymers are classified into different types on different basis as in the following enumeration, Classification based on the source of origin; the range of optical grade plastics continues to grow. An abbreviated list of some of the most important families of optical, for example: PMMA(Poly methyl methacrylate), Polystyrene, Polycarbonate.

CHAPTER.1 OPTICAL MATERIALS

1.2.2.1. Properties of optical polymer:

Optical polymer materials possess many unique properties, as well as refractive index, dispersive, and transmission. The optical properties of a polymer depend on many factors as its structure, composition, preparation methods, and processing conditions. Any negative influence on the optical properties of a polymer results in the polymer's aging, which affects the lifetime of the product. It has been found that scattering phenomena plays a major role in determining the optical properties of an optical polymer, include the following: PMMA (Poly methyl methacrylate), Polystyrene, and Polycarbonate [23-24].

1.2.2.1.1. Refractive index and Abbe number:

1. PMMA (Poly methyl methacrylate)

Henri et al [24] have reported that PMMA is an optically clear (transparent) thermoplastic .and it is one of the amorphous polymers that belongs to the acrylate family. Also, it is a clear, colorless polymer with a glass transition temperature range of 100 to 130°C, and a density of 1.20 g/cm³ at room temperature [25].

PMMA, also possesses very good optical properties, with a refractive index of 1.490 [26], and an Abbe number of 55.3, with a good clarity and excellent transmission properties throughout the visible portion of the spectrum [27].

2. Polystyrene

Polystyrene molecules are closely packed and have high density, tensile strength, and melting point; with a higher index of 1.59 and lower Abbe number 30.87 than PMMA. It is generally less expensive and tends to absorb somewhat in the deep blue spectrum. Polystyrene has a lower resistance to UV and is more easily scratched than acrylic.

A styrene lens, when paired with an appropriate acrylic lens offers an effective achromatic solution [28].

3. Polycarbonate

PC is commonly used for plastic lenses in eyewear, in medical devices, optical instrument, and exterior lighting fixtures. PC is known for its very high impact resistance and for the ability to perform over a wide range of temperatures (-137 to +124°C). Polycarbonate is similar to polystyrene in a refractive index 1.586 and Abbe number 29.9. Because of its high ductility, polycarbonate optic is not easily machined [29].

CHAPTER.1 OPTICAL MATERIALS

1.2.2.1.2. Transmittance coefficient of PMMA:

The experiments were performed on five types of substrates Polystyrene, Cyclic, Polycarbonate PMMA and, UV Acrylic. Transmission spectra of the used optical polymers were collected by UV-VIS-NIR Spectrometer (UV-3600 Shimadzu) in the spectral range from 300 to 1600 nm and are given in Figure.1. 3.

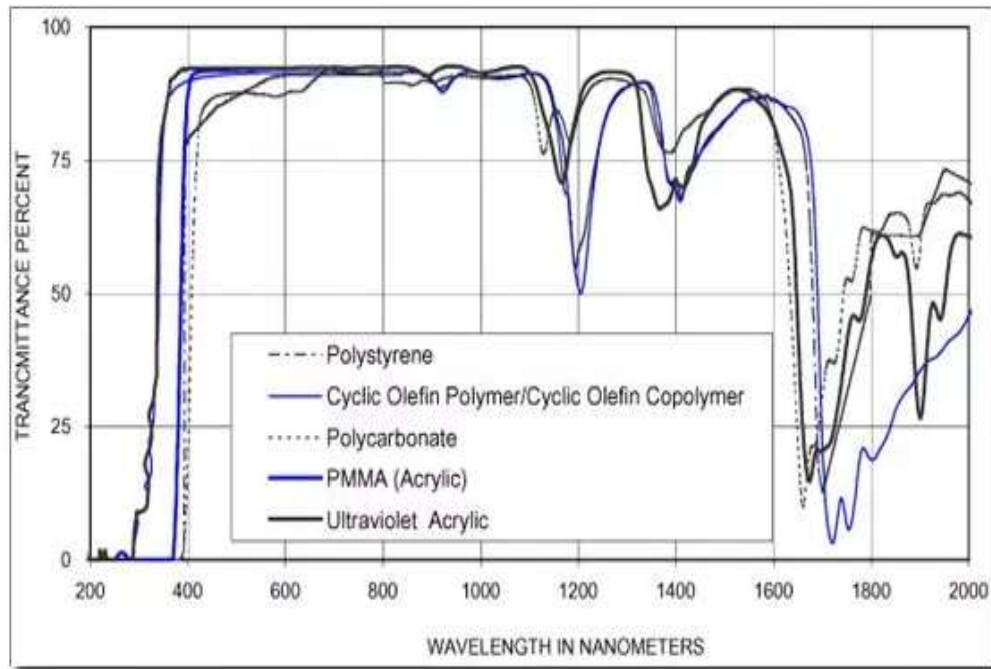


Figure. 1.3. Transmittance spectra of Polysterene, Cyclic, Polycarbonate PMMA and, UV Acrylic as a function of wavelength of society G-S [29].

1.3. CHARACTERISTIC OF OPTICAL MATERIALS

1.3.1. *Optical surface states*

Roughness is a characteristic of the surface state of a solid material; the geometric characterization of this parameter is delicate, since it is a statistical parameter that can't be characterized by a single measure, and because it is a variable dependent on three dimensions [30].

Usually Surface roughness measurement, Lee et al [31] have proposed a significant task in many engineering applications. Every surface has some type of texture that takes the form of peaks and valleys. These peaks and valleys vary in height and spacing and have properties inherent in the way the surface was produced. The development of non-contact-based roughness measurement techniques for engineering surfaces has received much consideration [32].

1.3.1.1.Surface Roughness parameters:

A single parameter of the surface roughness could not demonstrate a change in the manufacturing process [33]. Therefore, many parameters and methods were developed over the years to enable improved ways of surface roughness evaluation.

The definitions of the height parameters: Sa, Sq, Ssk, Sku, and Sz are given in the following sections.

1.3.1.1.1. Mean Height of the Surface

1. Root Mean Square Height value (Sq):

The root mean square height, or Sq parameter, is defined as the root mean square value of the surface departures $z(x, y)$ within the sampling area A.

$$Sq = \sqrt{\frac{1}{A} \iint_A z^2(x, y) dx dy} \quad (1.1)$$

2. Arithmetic mean height value (Sa):

The arithmetic mean height, or Sa parameter, is defined as the arithmetic mean of the absolute value of the height $z(x, y)$ within a sampling area A.

$$Sa = \frac{1}{A} \iint_A |z(x, y)| dx dy \quad (1.2)$$

The Sa and Sq parameters, (1.1) and (1.2) are strongly correlated to one another [34]. The Sq parameter has more statistical significance (standard deviation) and frequently has a more physical grounding than Sa. For example, Sq is directly related to surface energy and the way light is scattered from a surface [35].

1.3.1.1.2. Skewness and Kurtosis

1. Skewness value (Ssk):

Skewness is the ratio of the mean of the height values $z(x, y)$, cubed and the cube of Sq within a sampling area A.

$$Ssk = \frac{1}{Sq^3} \frac{1}{A} \iint_A z^3(x, y) dx dy \quad (1.3)$$

This parameter can be positive, negative or zero, and is unit-less since it is standardized by Sq. The Ssk parameter (1.3) describes the shape of the topography height distribution. For a surface with a random (or Gaussian) height distribution that has symmetrical topography, the skewness is zero. The skewness is gotten from the amplitude distribution curve; it is the measure of the profile symmetry about the mean line. This parameter cannot distinguish if the profile spikes are uniformly distributed above or below the mean plane and is strongly influenced by isolated peaks or isolated valleys. It represents the bias, either in the upward or downward direction of an amplitude distribution curve. Moreover, the Ssk parameter correlates well with load carrying ability and porosity [36].

CHAPTER.1 OPTICAL MATERIALS

2. Kurtosis value (Sku):

The Sku parameter,(1.4) is a measure of the sharpness of the surface height, $z(x, y)$ distribution and is the ratio of the mean of the fourth power of the height values and the fourth power of Sq within the sampling area A.

$$Sku = \frac{1}{Sq^4} \frac{1}{A} \iint_A z^4(x, y) dx dy \quad (1.4)$$

Kurtosis is completely positive and unit-less, and characterizes the spread of the height distribution. A surface with a Gaussian height distribution has a kurtosis value of three. In contrast to Ssk, utilization of this parameter not only detects whether the profile spikes are evenly distributed, but also provides a measure of the spikiness of the area a spiky surface will have a high kurtosis value and a bumpy surface will have a low kurtosis value[37].

The Ssk and Sku parameters can be less mathematically more stable than other parameters since they use high order powers in their equations, leading to faster error propagation [38].

1.3.1.1.3. Maximum Height of the Surface

1. Maximum peak height (Sp):

The Sp parameter,(1.5) represents the maximum peak height, that is to say, the height of the highest point on the surface.

$$Sp = \max_A z(x, y) \quad (1.5)$$

2. Maximum pit height (Sv):

The Sv parameter, (1.6) represents the maximum pit height, i.e. the height of the lowest point on the surface. As heights are counted from the mean plane and are signed, Sp is always positive and Sv is always negative.

$$Sv = |\min_A z(x, y)| \quad (1.6)$$

3. Maximum height (Sz):

The Sz parameter,(1.7) is the maximum height of the surface, i.e. is sum of the absolute values of Sp and Sv,

$$Sz = Sp + Sv \quad (1.7)$$

The maximum height parameters are to be used with caution as they are delicate to isolated peaks and pits, which may not be significant. However, Sz can be relevant on surfaces that have been filtered with a low-pass filter to characterize the amplitude of waviness on the work piece. Also, maximum height parameters will succeed in finding unusual conditions, such as a sharp spike or burr on the surface that may be indicative of poor material or poor processing [39-40].

The Figure 1.4 represented the surface roughness parameter.

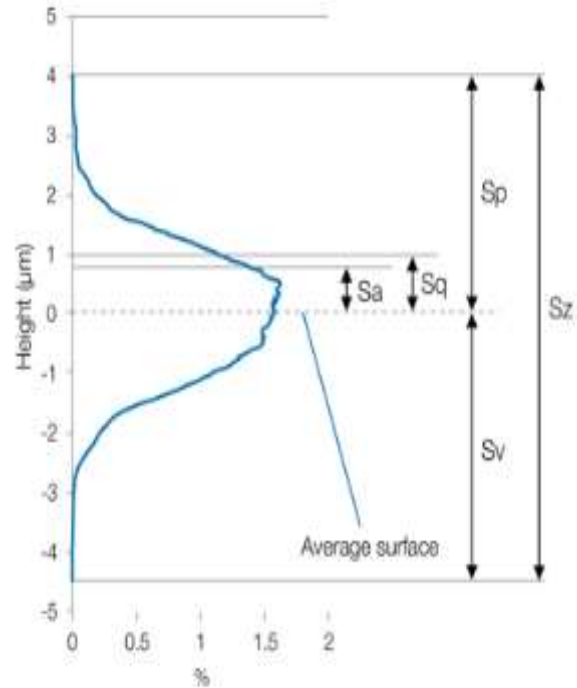
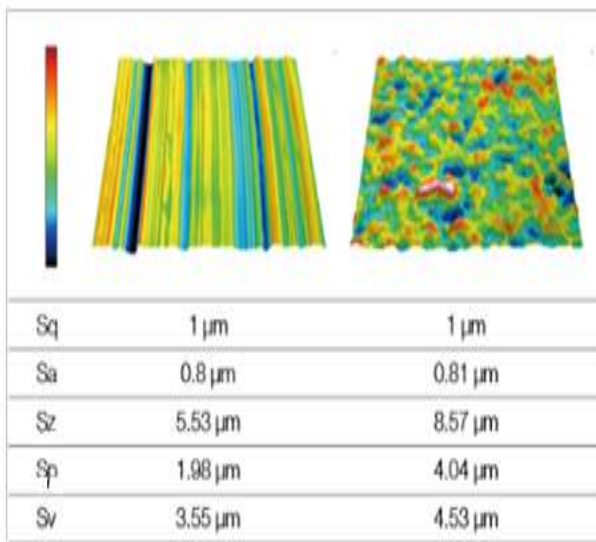


Figure 1.4. Graphical explanation of 3D surface roughness parameters (Sq,Sa,Sz,SpandSv)[38].

1.4. Characterization techniques

1.4.1. Total integrated scattering (TIS)

The TIS measurements are based on collection of scattered light with integrating Coblenzspheres. In reality, the Coblentz sphere is a hemisphere coated with a highly reflective metal layer [41]; the detector and the sample are mounted on the same side of the hemisphere and the backward scattering is measured.

The scattered radiation in the wide angular range (often from 2deg to 85deg) after one reflection is imaged onto the detector in the Coblentz sphere and this arrangement is less sensitive to scattering by air particles than integrating spheres [42]. TIS measurement setup is illustrated in Figure 1.5.

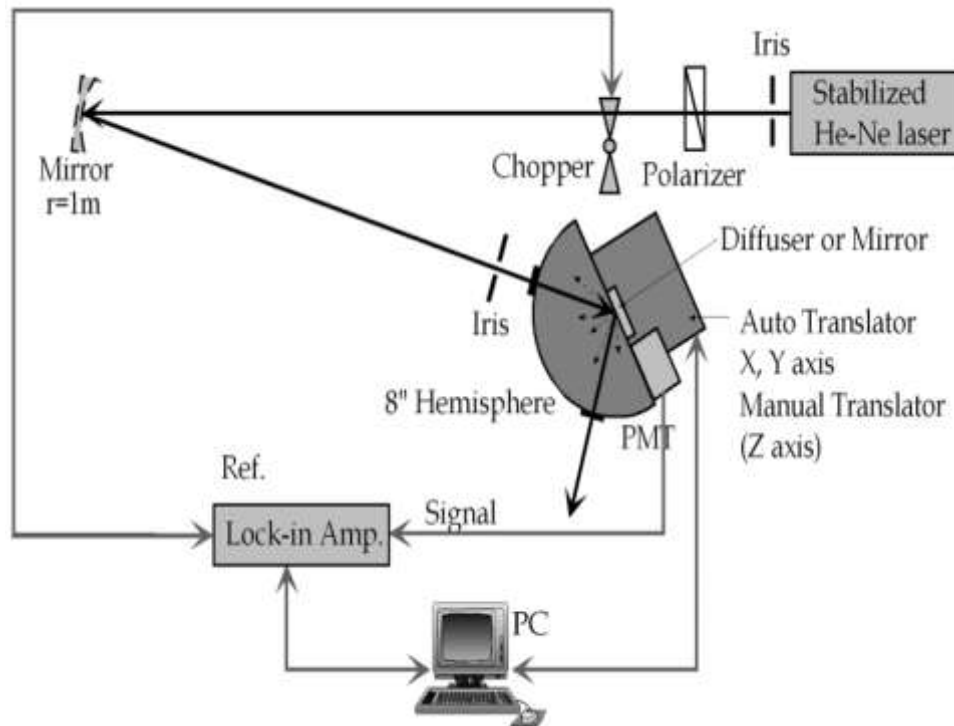


Figure 1.5. Schematic of TIS measurements technique setup [42].

To verify the internally built TIS setup, a stabilized He-Ne laser was used as a light source and the light source was modulated at about 1000 Hz for noise reduction. An 8-inch integrated hemi-sphere was used for 45° angle of incidence measurements and a PMT as a photodetector. For TIS mapping, a mirror was attached to the hemisphere using computer controlled auto translator [43].

1.4.2. Ultraviolet-visible- near infrared spectroscopy

UV/VIS/NIR spectroscopy is a powerful analytical procedure for determining the optical properties (transmittance, reflectance and absorbance) of liquids and solids represented in Figure 1.6. It can be used to characterize semiconductor materials, coatings, glass and many other research and manufacturing materials [44]. Furthermore, it worked in the optical range between 175 nm and 3300 nm. Optical spectroscopy refers to a set of technique which is based on the interaction between light and matter. Various techniques will be used to probe the structure of the glasses before and after poling but also to characterize the transmission region of the glasses [45].

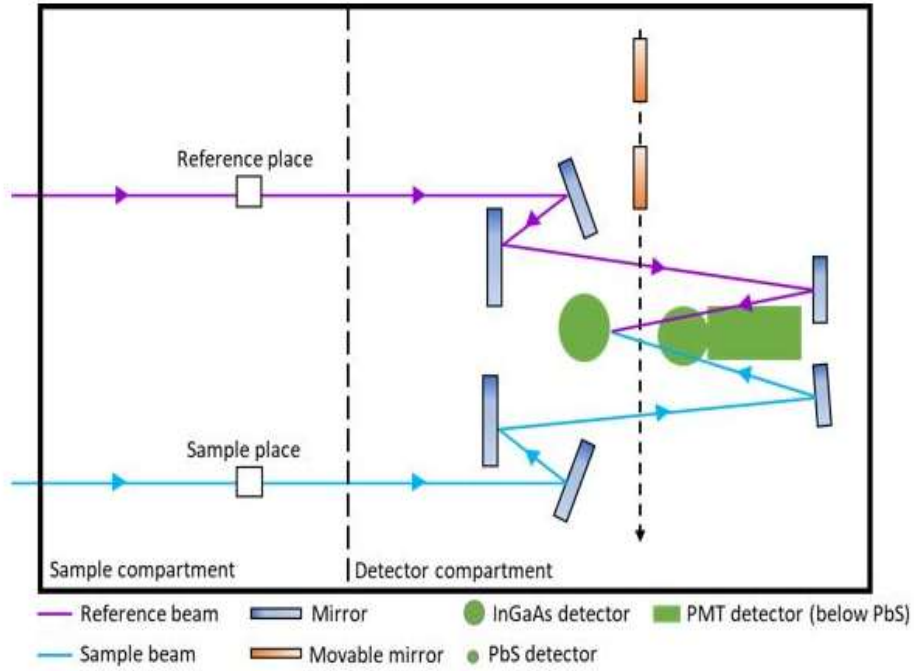


Figure 1.6. Principle of UV/VIS/NIR spectroscopy [44].

1.4.3. Raman spectroscopy and correlative μ -SHG mapping

Micro-Raman and micro-SHG measurements were recorded in backscattering mode on a modified micro-Raman spectrometer HR800. A representation of the assembly is presented on Figure 1.7. A continuous laser operating at 532 nm is utilized for Raman and a picoseconds laser at 1064 nm is used for micro-SHG measurements [46]. The utilization of a confocal microscope and a motorized stage (X, Y, Z) enables 3D mapping with good spatial resolution ($0.5\mu\text{m}$). Verily, typical resolution used for Raman is 2.5 cm^{-1} . Measurements of the SHG response were performed using a doughnut radial polarization to probe the electric field in the Z direction. Raman spectroscopy is complementary to infrared spectroscopy presented before. The main difference is that it uses light in the visible, which does not correspond to the energy level [47].

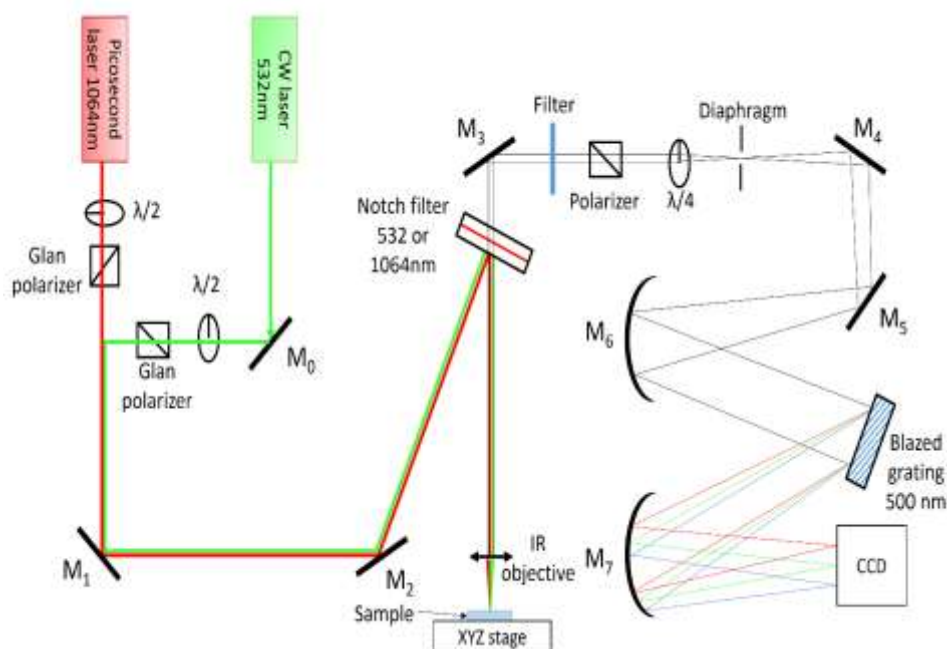


Figure 1.7. Principle of the combined Raman / SHG microscope setup [47].

1.4.4. Infrared spectroscopy

Infrared spectroscopy is based on the light and matter interaction in the infrared system. The infrared region can be separated into three regions, the near-infrared (NIR), the mid-infrared (MIR) and the far-infrared (FIR). Depending on the community of user, these three regions can vary in term of wavelength. In this technique, Wilson et al[48] have presented the norm ISO 20473 is used to define the three regions and specifies that the NIR spans from 0.78 to 3 μm , the MIR spans from 3 to 50 μm and the FIR from 50 to 1000 μm . Measurements were performed using three different techniques: IR in specular reflectance mode, IR in transmission mode and Attenuated Total Reflectance (ATR).

These various techniques are complementary, as they do not penetrate the sample in the same depth. The most frequent use of the absorption spectroscopy in Mid-IR lies in the identification of substances through their characteristic molecular vibrations. In general, molecules with a similar structure are not in gaseous phase at room temperature, and high temperatures are needed to perform gaseous spectroscopy. However, in order to work at room temperature, it is possible to carry out spectroscopy in liquid phase, dissolving the target molecules in a Mid-IR transparent solution [49]. In both gaseous and liquid spectroscopy, the detected absorption peaks are several of cm^{-1} wide.

Additionally, to detect these bands, techniques and components spanning a wide frequency range are required in this structure [50]; a combined technique is Fourier-Transform Infrared Spectroscopy (FT-IR) [51]. In this scheme, sketched in Figure 1.8, using a broadband source,

CHAPTER.1 OPTICAL MATERIALS

normally a lamp, an interferometric design is recorded from the light interacting with the sample. By using the Fourier Transform approach, it is possible to reconstruct the absorption spectrum of the substance under analysis.

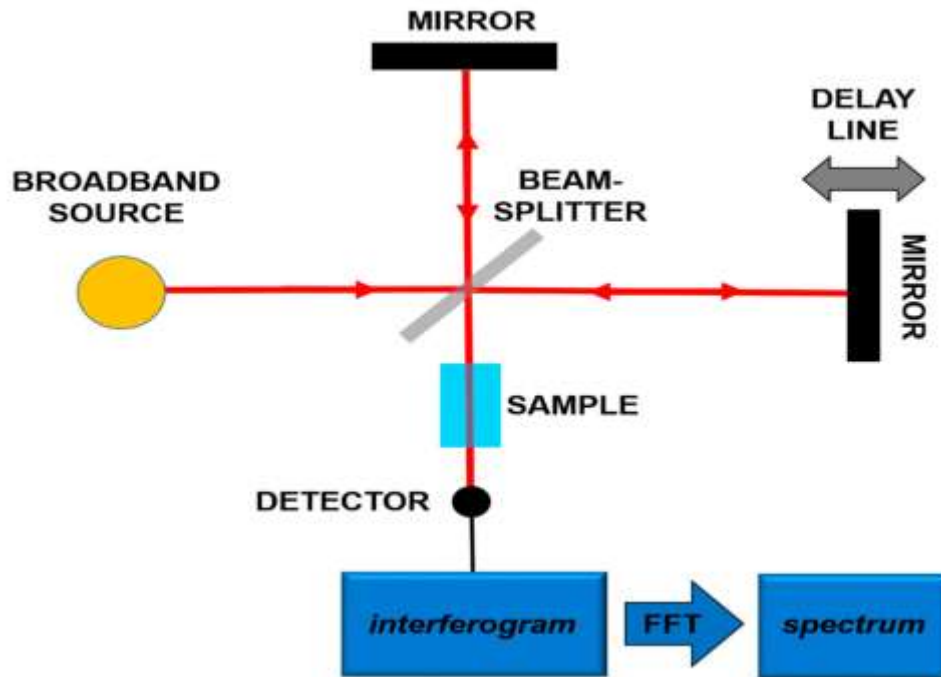


Figure 1.8. Principles of the Fourier-Transform Infrared Spectroscopy (FT-IR)[52].

1.4.5. Optical profilometry

Surface roughness has a significant influence on the performance of mechanical, electrical, and optical systems [53]. Generally; there are lots of optical measurement instruments dependent on various principles. Figure 1.9 is a schematic diagram of the optical profilometry.

Profilometry is rendered information about the surface features and topography of the surface. In conventional contact mode profiling, a mechanical stylus comes in contact with the surface to trace the surface features. On the opposite, non-contact optical profilometry is able to trace the surface topography and evaluated the roughness without damaging the actual surface features. It uses optical light interference principles to scan and measure topographic features of various materials as well as, glass, ceramics, metals and, polymers. Although these noncontact measurement instruments can offer very high accuracy, they are very sensitive to mechanical vibration, air turbulence, and temperature variation[54].

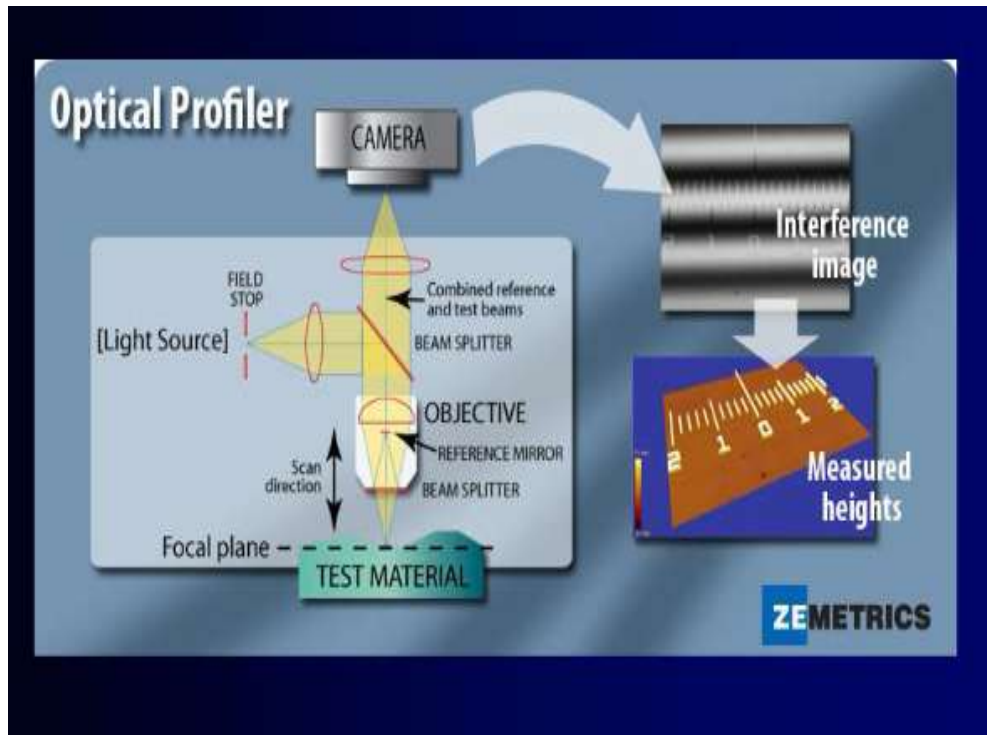


Figure 1.9. Schematic of non-contact optical profilometry [53].

1.4.6 Atomic Force Microscopy

Finotet al [54] have reported the atomic Force Microscopy (AFM) is a technique which consists of scanning the surface of a sample with a probe not only to visualize its topography yet, additionally to measure surface properties of a sample.

An AFM is included a nanometer size sharp tip, which is placed at the edge of a cantilever. As the tip is brought closer to the surface [55], attraction forces interact with it, causing the cantilever to flex towards the surface. When the tip contacts the surface, repulsion forces assume control over the attraction forces. During an AFM measure, the deflection of the cantilever is checked by means of a laser beam focused on top of the cantilever [56]. Any deflections of the cantilever will cause the reflected beam to deviate [57]. Four photodiodes permit recording these changes [58]. The deflection is hence constant over time and a precise map of the surface topography can be obtained [59-60]. The principle of the AFM measurement is summarized on Figure 1.10.

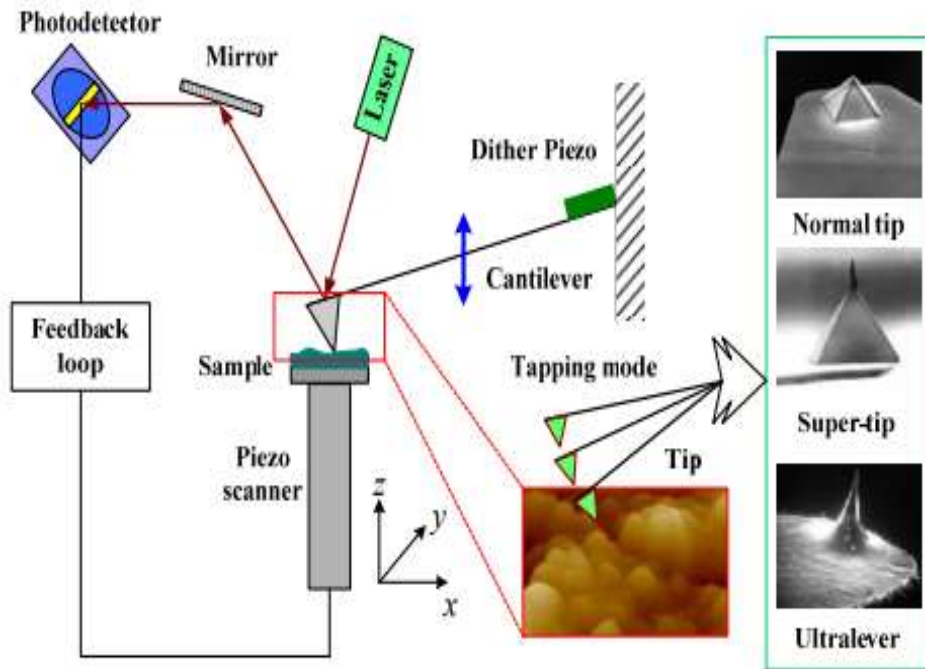


Figure 1.10 .Schematic of AFM technique setup [60].

1.5. Storage effect on the optical materials

1.5.1 Medium nature effect on substrates

Theoretically, the influence of the ambient environment in the state of the optical surface is determined. It was found that the admissible storage times of polished optical articles prior to coating deposition or gluing is less than the value set by industry standards. A change in the storage conditions at a given limit of production can result in a change in the state of the polished surfaces of optical parts.

In fact, the process of manufacturing optical parts (grinding, polishing, cleaning, washing, depositing optical vacuum and chemical coatings) the optical surfaces are exposed to water, acids, alkalis, organic liquids, the ambient atmosphere, and so on. In addition, the lower the chemical stability of optical glass [61], the more it should be taken into account in the technological process of surface roughness on optical materials[62]. This deterioration of the surface can change the optical and mechanical properties of the layer, such as spectral characteristics, adhesion, hardness, and abrasion resistance. The imperfections or failures of the technologies can lead to the degradation of important optical and technical characteristics [63].

CHAPTER.1 OPTICAL MATERIALS

1.5.2. Duration effect on substrate

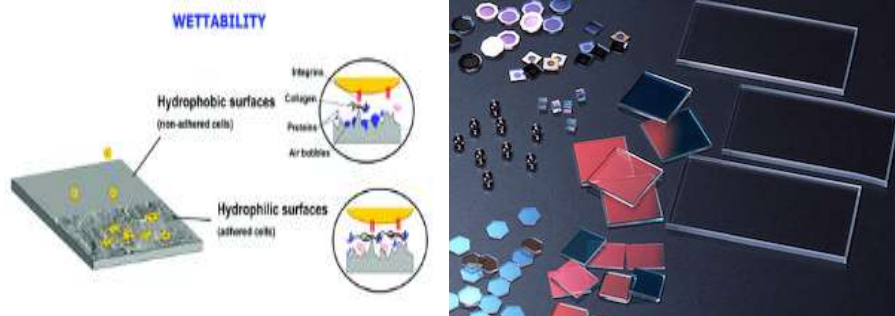
The optical storage of glasses was proposed, to realize a longer storage duration, and have been studied extensively in the last decade [64-65]. However, many difficult problems still remain and must be overcome for practical application.

An indicator of surface damage of a sample of silicate glass exposed to a moist atmosphere is a hygroscopic deposit comprised of droplets uniformly covering the entire surface. After tests, the surface of the glass is examined in reflected light [66]. This criterion could be suitable for comparing the properties of optical glasses with one another. Any changes in the surface layer of optical glass can be supposed to start long before the hygroscopic deposit becomes noticeable. In addition, changes can also occur without the formation of a deposit [67].

1.5.3. Temperature effect

Recently, Stricker et al [68] have performed a pioneering experiment using the heat treatment, In order to determine the temperature effect on the optical glasses stocked, chemical reactions in the solid phase by ion exchange can occur by changing the chemical composition of the glass surface and the deposited layer . This change results in a variation of the structure, and therefore of the refraction index, dispersion, density, also, the inter-diffusion changes the optical properties and influences the adhesion according to the reactions produced [69].

CHAPTER.2



THIN FILMS AND ADHESION

2. THIN FILMS AND ADHESION

2.1. INTRODUCTION

Thin film can be defined as a thin layer of material, where the thickness is varied from several nanometers to few micrometers. Like all materials, the structure of thin films is divided into amorphous and polycrystalline structure depending on the preparation conditions as well as the material nature [70]. The properties of thin films are extremely sensitive to the method of preparation, several techniques have been developed, and it is Depending on the desired film properties) for the deposition of the thin films of the metals, alloys, ceramic, polymer and superconductors on a variety of the substrate materials [71].

The vast varieties of thin film materials, their deposition, processing and fabrication techniques, spectroscopic characterization, optical characterization probes, physical properties, and structure-property relationships are the key features of such devices and basis of thin film technologies [72].

Most deposition techniques follow these three major sequences:

- Synthesis of the deposition species.
- Conveyance from source to substrate.
- Deposition and adhesion of the source onto the substrate and subsequent film growth.

Mellali et al [73] developed the apparent adhesion is usually measured by applying an external force to the thin film structure to a level that causes failure between the film and substrate, or in material near the interface. This applied force put energy into the system that causes strain and fracturing of chemical bonds. The loss of adhesion is called deadhesion and can occur over a large area to give film delamination from the substrate or over a small area to cause pinholes in the film.

This chapter concerns the techniques and methods of thin films deposition, with the corresponding characteristic of thin film material, morphology, mechanical, optical and adhesion behavior of these layers, indeed measurement techniques of contact angle.

2.2. THIN FILMS

Orava et al [74] have mentioned the techniques for producing thin film materials are exceptionally numerous, the nature of these materials is only multiplying: glass, insulators, semiconductors, polymers and superconductors, their applications covering several disciplines: optics, microelectronics, mechanics, chemistry, etc. In addition, the development of many surface analysis techniques, the increasingly precise control of parameters involved in the repository and a better understanding of the thin-film material growth.

CHAPTER.2 THIN FILMS AND ADHESION

2.2.1. Deposition techniques of thin films

Deposition techniques can be classified into physical and chemical methods[75,76], as shown in Figure 2.1 .Furthermore, the Table 2.2 revealed different methods of thin film deposition with a corresponding application of the deposited films.

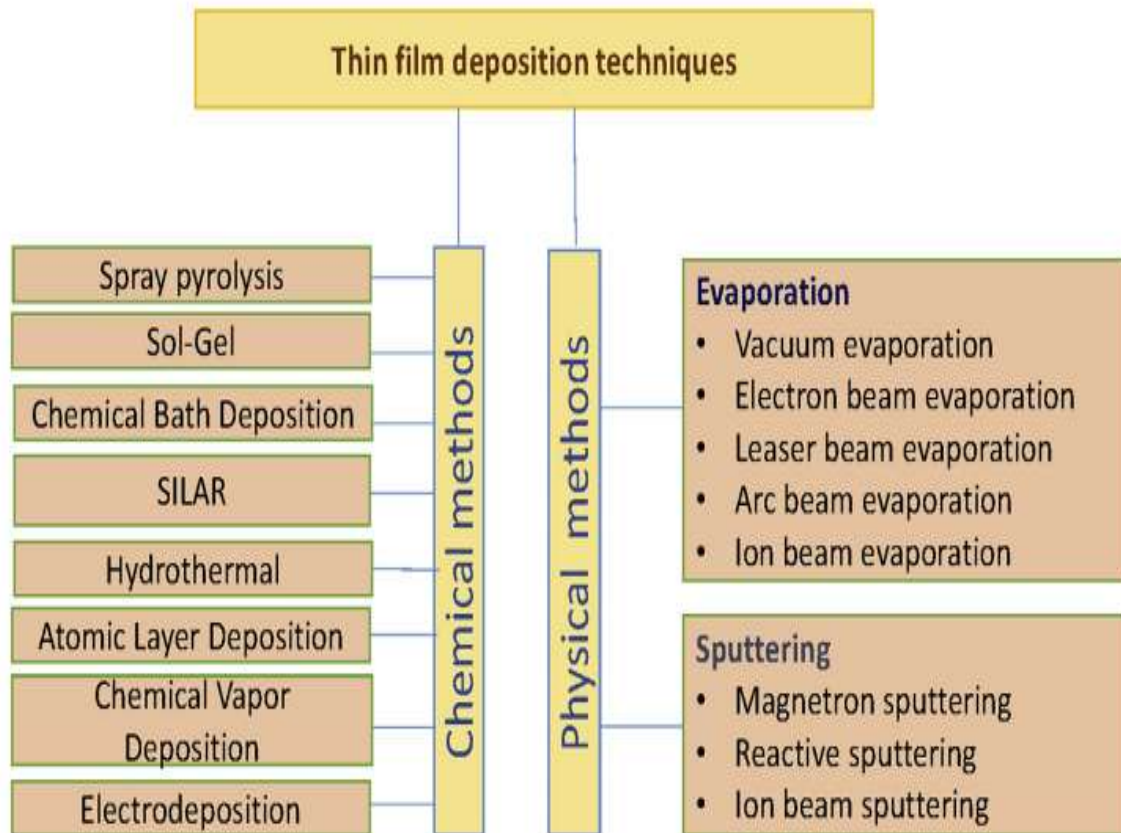


Figure 2.1. Schematic of brief classification of thin film deposition techniques [76].

CHAPTER.2 THIN FILMS AND ADHESION

Deposition method	Thin film	Material Application
Ultrasonic spray pyrolysis (USP)	ZnO. SnO ₂ –Fe ₂ O ₃ .TiO ₂ . Gd-CeO ₂ .	Solar cell.Sensors. Metal oxide coating.Solid oxide fuel cell.Photocatalysis [77].
Chemical bath deposition (CBD)	ZnS. PbS.ZnO.	Solar cell.Optoelectronics. Photocatalysis [78,79].
Successive ionic layer adsorption and reaction (SILAR)	CdO. ZnO.CuO.	Gas sensing. Photocatalysis. Supercapacitor [80,81].
Sol-gel method	TiO ₂ .TiO ₂ –SiO ₂ . CZTS.	Solar cell. Photocatalysis. Gas sensing.Self cleaning [82,83].
Electrodeposition	Cu ₂ O. Ga-CdS. Co(OH) ₂ . WO ₃ .	Optoelectronics. Solar cell. Supercapacitor. Photocatalysis [84,85].
Chemical vapour deposition (CVD)	B: ZnO. F:Mn ₃ O ₄ .	Solar cell. Optoelectronics. Photocatalysis. Gas sensing [86,87].
Plasma enhanced-chemicalvapourdeposition	TiO ₂ .SiO ₂ .	Antireflecting coating. Dielectric application. Biomedical applications. Photocatalysis [88,89].
Magnetron sputtering	TiO ₂ – SiO ₂ .CdTe	Photocatalysis. Solar cell [90,91].
Laser evaporation	NiMoS ₂ .TiO ₂ /Au/ TiO ₂ .	Dye-sensitized solar cells. Photocatalysis [92,93].

Table 2.1. Various thin film deposition method with corresponding applications.

CHAPTER.2 THIN FILMS AND ADHESION

2.2.2.1. *Physical methods:*

2.2.2.1.1. **Evaporation**

It is one of the oldest and extensively used techniques for semiconductor thin film deposition at industrial scale. Pessoa et al[94] have proposed the inter conversion between solid and vapor phase takes place under vacuum environment. There are several evaporation methods available for thin film deposition. During the evaporation process, vacuum effect causes ejection of atoms from the source, whereas [95], for ion plating process[96], the growing film is exposed to concurrent ion bombardment [97]. Indeed, this process has been reported to be performed using different configurations. These are molecular beam epitaxial, reactive evaporation and activate reactive evaporation. MBE is used for growing epitaxial through the active interaction of distinct or many atomic or molecular beams on the surface of a heated crystalline substrate material[98]. The evaporation occurs at an ultra-high vacuum for deposition of the controlled composition of uniform thickness of the thin film from specific deposition rate [99].

1. Vacuum evaporation:

It is a widely used technique for the deposition of functional thin film on the variety of substrates. The vacuum helps to settle vapors of coating particles on the substrate where it converts back into the solid phase [100]. Certainly, the evaporation is carried out by electron beam heating or electrical heating. Wei et al [101] have discussed that it is a simple technique for the synthesis of amorphous film and used to protect textiles from metal nano particle deposition. The basic sequential steps for thermal or vacuum evaporation are given below:

- The vapor is created from subjecting the target material to very high temperature by subliming or boiling.
- The ejected vapour from the target material is transported to the substrate through a vacuum.
- Condensation of the vapour takes place to form a solid thin film on the surface of the substrate, and further repeatability of the deposition cycles result in thin film growth and nucleation.

During the thermal evaporation process, the target material vaporized from the thermal process sources gets to the substrate material with minimal interference. The process is often carried out at a high vacuum pressure (HV), and the trajectory of the movement of the target material to the substrate is a straight path trajectory termed a line of sight [102] as shown in Figure 2.2. Vapour flux is created by heating the surface of source material to a sufficiently elevated temperature in a vacuum.

The flux can then condense on the surface material to form a thin film. In addition, the vacuum environment creates a safe zone to reduce gaseous contaminants in the deposition process to an

CHAPTER.2 THIN FILMS AND ADHESION

acceptable and minimal level and allows the evaporated atoms to undergo essentially collision less transport from the source onto the substrate. The thermal vaporization rate might be very high compared to other PVD processes [103]. Tungsten wire coils are commonly used as the source of the thermal heat or by using a high energy electron beam for heating the target material to an elevated temperature [104].

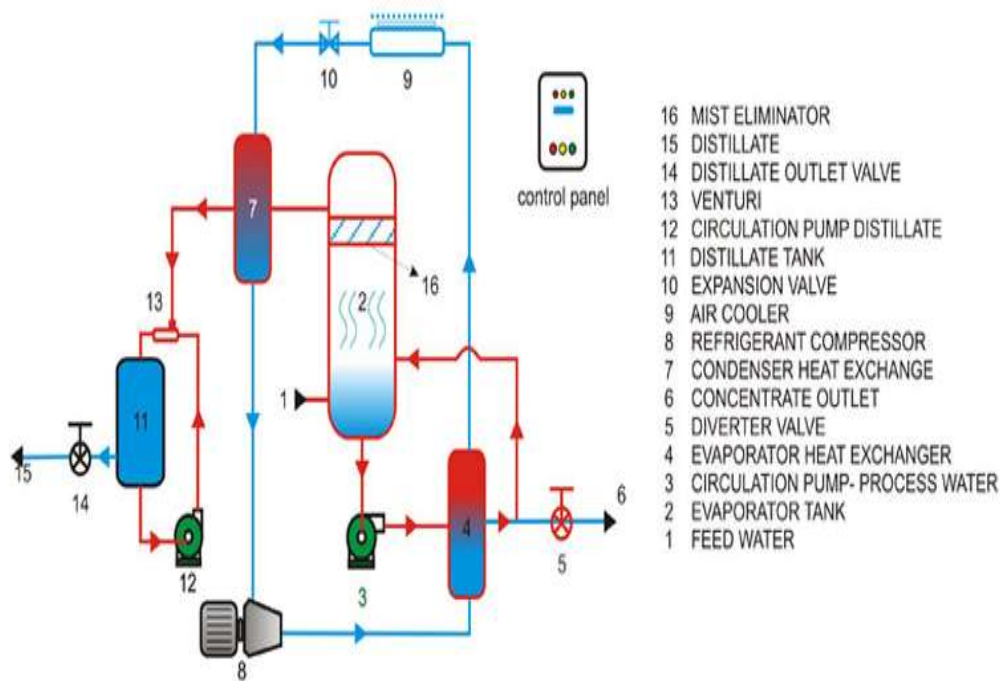


Figure 2.2.Schematic of Vacuum evaporation process.

2. Electron beam evaporation:

This is another vacuum based and convenient technique for thin film deposition. It involves the electron beam heating to evaporate the material to be deposited. This method produces vapour transports clouds inside the vacuum after irradiation of evaporate by electron beam from an electron. Yang et al [105] have demonstrated that the electron beam evaporation is a powerful technique to deposit oxide films with high crystalline, controlled stoichiometry and high deposition rate by optimizing the deposition parameters.

The various advantages of electron beam evaporation are:

- Electron beam vapour deposition uses a high energy beam of electrons bombards the sample material, causing vaporization.
- It is multiple source capability.
- It operates under lower ambient pressure.
- It provides superiority to control the deposition rate [106].

CHAPTER.2 THIN FILMS AND ADHESION

Figure 2.3 presents a schematic representation of an electron beam evaporation system [107]. Where the intensive beam of electrons is generated from a filament and steered through both electric and magnetic field to hit the target and vaporize it under vacuum environment. Thin films prepared by electron beam evaporation are of good quality and purity [108]. Large categories of materials can be prepared by electron beam evaporation technique [109] such as amorphous and crystalline semiconductors [110], metals [111], oxides[112],and molecular materials [113].

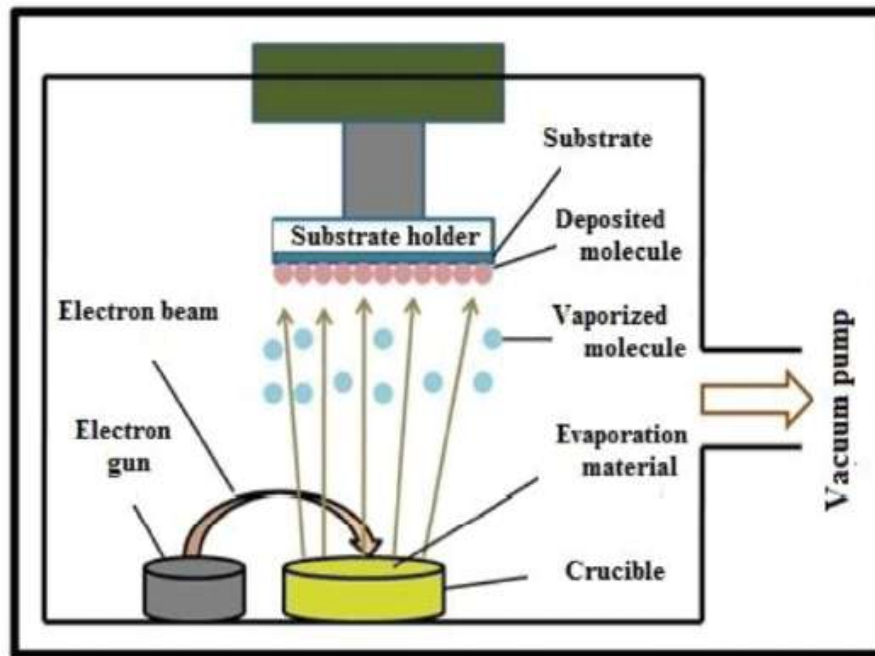


Figure 2.3. Schematic of electron beam evaporation.[109].

3. Laser beam evaporation (pulsed-laser deposition):

Pulsed-laser deposition (PLD) is another physical deposition technique to deposit the thin film coating system [114]. During the thin-film deposition process, the laser beam is utilized to ablate the material for depositing the thin films inside a vacuum chamber, as shown in Figure 2.4.

It is a laser based physical vapour deposition method and is most preferable for complex oxides[115]. PLD involves the ablation of the target material after irradiation from pulsed laser source under vacuum atmosphere. The ejected matter is in the form of plasma, which carries high kinetic energy. Finally, it gets gradually settled on the substrate. This method has several advantages, such as [116-117]:

- The film thickness can be controlled by tuning deposition parameters
- PLD is a faster and sophisticated technique.
- It allows the ablation of only selected area.

CHAPTER.2 THIN FILMS AND ADHESION

- It provides a precise transfer of stoichiometry from target to substrate.
- The prepared film possesses a high crystalline.

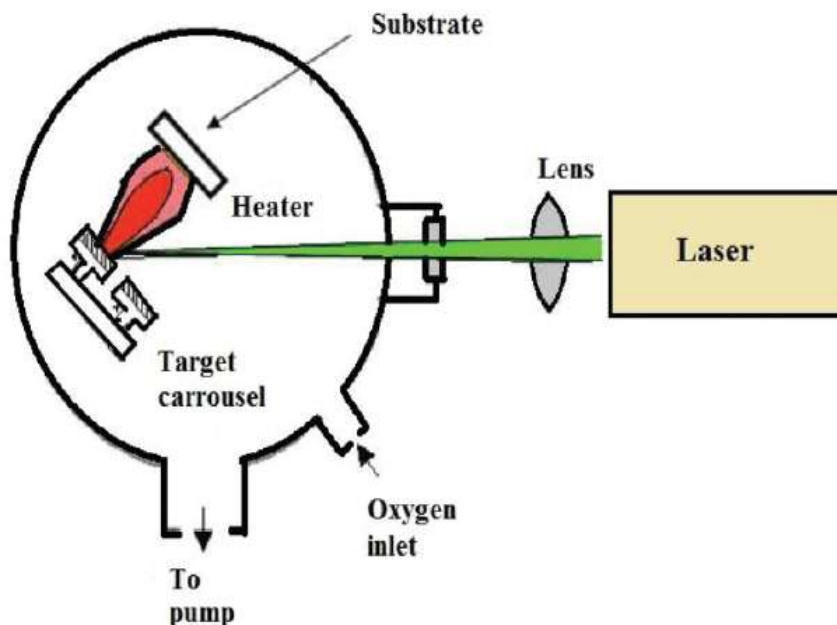


Figure 2.4. Schematic of pulsed-laser deposition [117].

4. Ion beam deposition:

Ion beam deposition (IBD) as illustrated in Figure 2.5, is a coating method in which beams of ions are employed to apply materials to the surface of a substrate. An IBD set up is typically made up of a deposition target, ion optics, and an ion source. Mass analyzers can also be incorporated if desired to monitor the species deposited in order to prevent impurities and avoid contamination [118]. The amount of energy applied determines the landing patterns of the ion beams. While low energy enables appropriate landing of ions on the surface of the substrate, high energy causes implantation of atomic ions into the substrate and fragmentation of molecular ions [119].

IBD is a direct beam deposition process that directly applies an ionized particle beam onto the substrate surface to fabricate thin film coatings on the substrate surface. At low energy, molecular ion beams would deposit intact, whereas at high deposition energy, molecular ions fragment and atomic ions penetrate further into the material [120]. Besides being able to independently control the process parameters (ion energy, temperature, and arrival rate of atomic species), films resulting from IBAD technique adhere more strongly to the substrate[121].

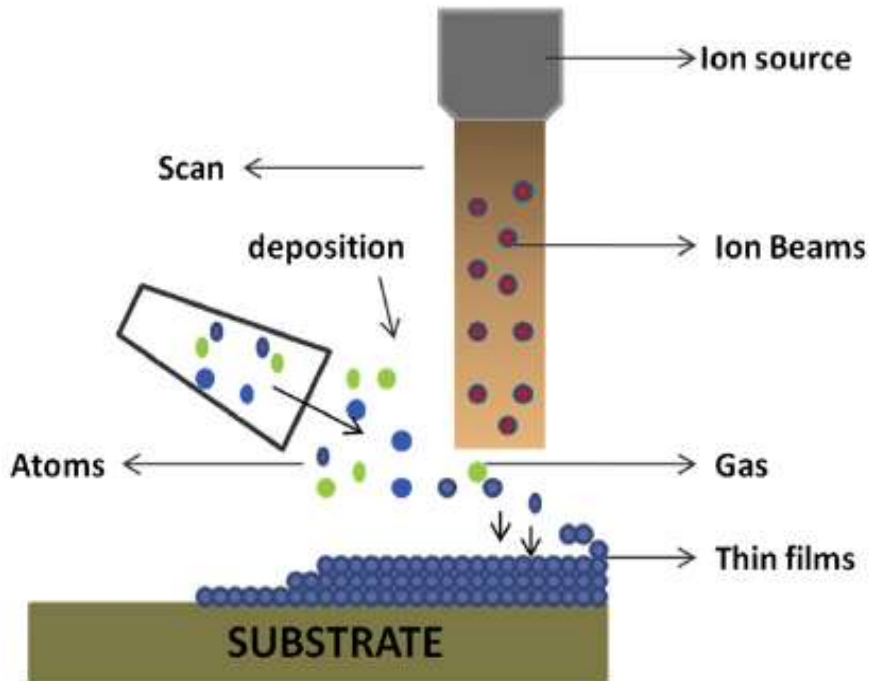


Figure 2.5. Schematic of the Ion beam deposition [122].

2.2.1.1.2. Sputtering

Sputtering is a vital and a prominent procedure among the PVD processes. It's a non-thermal vaporization process whereby an individual atom escapes from the target surface due to atomic collision cascades by suitable high energy ion bombardment. Unlike evaporation, the source is no longer created by thermal but by ion impact on the target. Also, Dumitru et al [123] have presented the target to substrate distance is shorter and, in many cases, it has outperformed other PVD processes with more functionality and performance as improved adhesion and thicker film. During the sputtering process, atoms are removed from the surface of the target material by the transfer of sustaining momentum from an atomic-sized energetic bombarding particle, usually gaseous ion accelerated from plasma [124]. Sputtering deposition can be achieved in a vacuum at low pressure plasma of <0.67 Pa where the sputtered particles are in line of sight and can also be done at a higher plasma pressure of 0.67 to 4 Pa, indeed, energetic particles sputtered or reflected from the sputtering target are formalized by gas phase collision before they reach the substrate surface. Sputtering is also being used as an etchant for cleaning the surface of solid materials and for pattern delineation because of its potential to eject atoms from an electrode surface [125].

1. Magnetron sputtering deposition:

The sputtering technique, as illustrated in Figure 2.6, it is a physical vapor deposition method that involves pushing materials from a source known as a target to the surface of a substrate. During sputtering, particles ejected from the target possess an energy of up to 100 000 eV; however, only a small proportion of them are ionized [126]. The energized ions shoot in straight lines to impinge on

CHAPTER.2 THIN FILMS AND ADHESION

the substrate, causing re-emission of the already deposited materials from the surface of the substrate [127], i.e. re-sputtering. Another way by which sputtering is achieved is by allowing ions from the target to collide with gaseous atom at high pressure, moderating the motion of the ions, causing them to diffuse towards the substrate and condense on the surface of the substrate[128].

The impact energy of the ions in the gaseous case depends on the gas pressure and can be modified by changing the latter, and the typical gases used are inert, with similar atomic weight to the target. The pulsing process leads to the creation of super-dense plasma exquisite properties, which result, creating more uniform thin films and the possibility of achieving a smooth surface coating with complex and irregular shaped substrate materials [129].

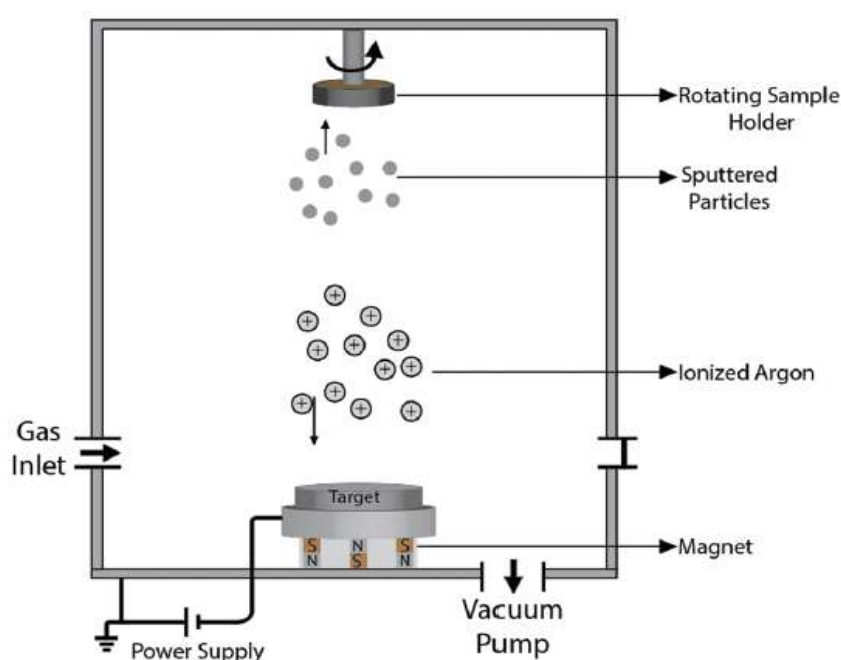


Figure 2.6. Schematic illustration of a magnetron sputtering method [127].

2. Reactive sputtering deposition:

Reactive sputter deposition is used for creating the compound thin film. During sputtering, a reactive gas such as nitrogen or oxygen is introduced to the deposition chamber and gas react with the target material to form a compound thin film on the surface of the substrate. This process is referred to as reactive sputtering [130]. An increase in reactive gas causes the topmost layer of the target material to transform from a single phase to compound phase, which often results in changes in the properties such as the conductivity, e.g., conductive surfaces become non-conductive, and vice versa[131]. The inert gas usually used for this process is Argon and it's possible to combine the inert gas with ionized non-inert gas (reactive gas) or introduced the ionized non-inert gas alone in the chamber [132]. The percentage of reactive gas added to the chamber is controllable to produce a specific stoichiometric ratio of the compound. The resulting deposited thin film is different from the target [133], the diagram of reactive sputtering is presented in Figure 2.7.

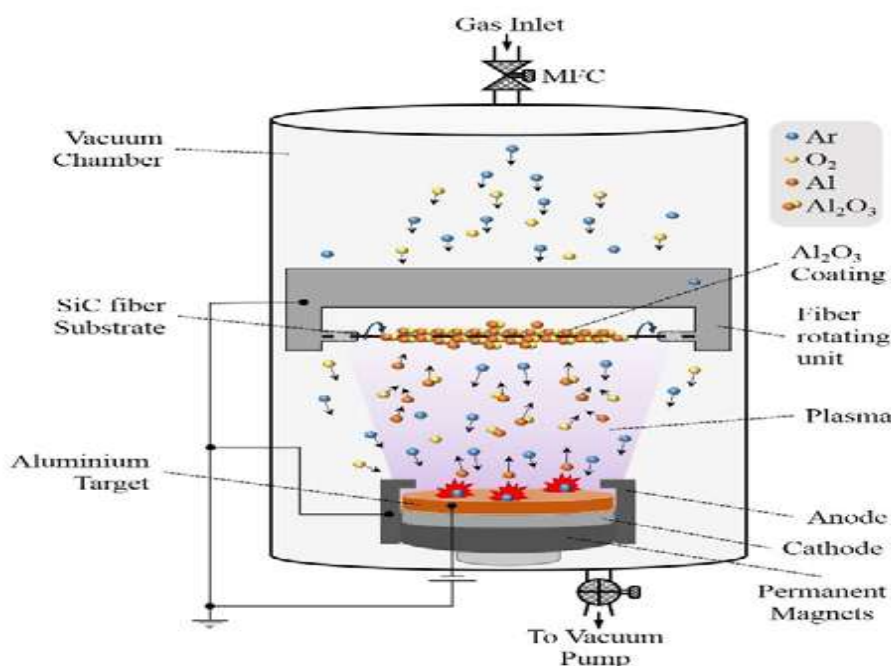


Figure 2.7. Schematic of reactive sputtering of Al_2O_3 [133].

2.2.1.2. Chemical methods

2.2.1.2.1. Sol-gel deposition:

The sol-gel technique is broadly used for the synthesis of oxide materials. Levage et al [134] have presented that; this technique is one ease and pure technique to manufacture thin films on metal or glass substrate. The formation of thin films of sol-gel involves three steps: (a) preparation of the precursor solution (b) deposition of sol on the substrate by using appropriate methods (c) thermal treatment for the deposited film [135].

This method works under low-temperature processing and gives better homogeneity for multicomponent materials. The word (sol) means the formation of a colloidal suspension and (gel) means the conversion of (sol) to viscous gels or solid materials. Two routes are used to prepare transition metal oxides (TMOs) as follows [136]:

- Preparing of inorganic precursors via inorganic salts in aqueous solution.
- Preparing of metal alkoxide precursors via metal alkoxides in non aqueous solvents.

The sol-gel process, depending on the precursors, may be divided into two classes, namely inorganic precursors (chlorides, nitrates, sulfides, etc.), and alkoxide precursors [137].

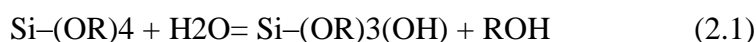
The extensively used precursors are tetramethoxy silane and tetraethoxy silane. In this process, the reaction of metal alkoxides and water, in the presence of acid or base, forms a one phase solution that goes through a solution-to-gel transition to form a rigid, two-phase system comprised of solid

CHAPTER.2 THIN FILMS AND ADHESION

metal oxides and solvent filled pores [138]. The physical and electrochemical properties of the resultant materials largely depend on the type of catalyst used in the reaction (see Figure 2.8). In the case of silica alkoxides, the acid catalyzed reaction results in weakly cross-linked linear polymers. These polymers entangle and form additional branches leading to gelation. Whereas, base-catalyzed reaction, due to rapid hydrolysis and condensation of alkoxide silanes, forms highly branched clusters [139].

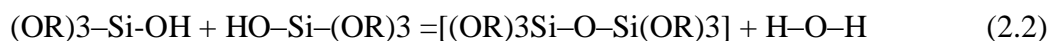
This difference in cluster formation is due to the solubility of resultant metal oxides in the reaction medium. The solubility of the silicon oxide is more in an alkaline medium which favors the inter-linking of silica clusters than an acidic medium [140]. A general procedure of sol-gel includes two stages, namely hydrolysis (2.1), condensation (2.2).

A. Hydrolysis:



The complete hydrolysis to form $\text{M}(\text{OH})_4$ is very difficult to achieve. Instead, condensation may occur between either two $-\text{OH}$ or $\text{M}-\text{OH}$ groups and an alkoxy group to form bridging oxygen and a water or alcohol molecule. A condensation reaction between two $-\text{OH}$ with the elimination of water is shown below [141]. The condensation reaction (2.2) between two hydroxylated metal species leads to $\text{M}-\text{O}-\text{M}$ bonds following release of water (oxolation). The reaction between a hydroxide and an alkoxide leads to form $\text{M}-\text{O}-\text{M}$ bonds following release of an alcohol (alkoxolation).

B. Condensation:



The hydrolysis and the polycondensation reactions are initiated at numerous sites and the kinetics of the reactions are therefore complex. When a sufficient number of interconnected $\text{M}-\text{O}-\text{M}$ bonds are formed in a particular region, they interact cooperatively to form colloidal particles or a sol. With time, the colloidal particles link together to form a three-dimensional network [142-143].

The possible mechanisms for both acid and base catalyzed reactions in case of silicon alkoxides are as shown in the Figure 2.8.

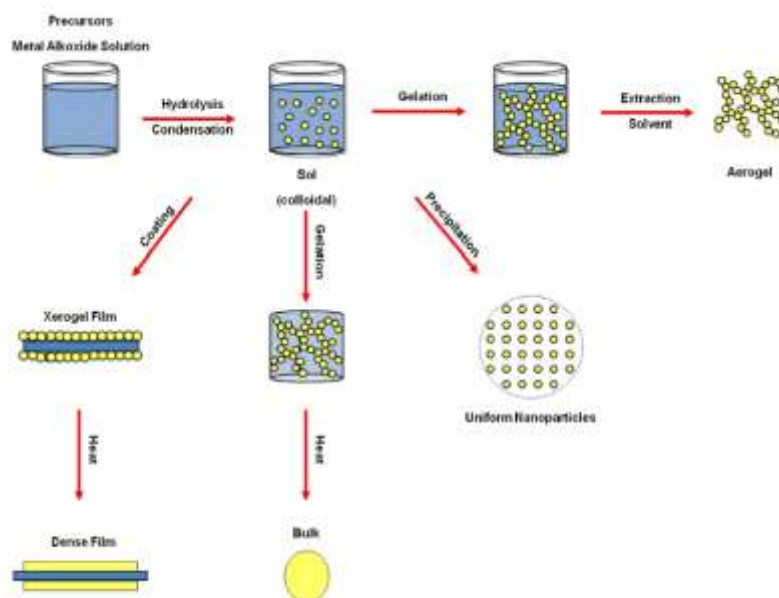


Figure 2.8. Sol–gel synthesis processes of optical glass materials in different forms, such as monosize nanoparticles, aerogels, and xerogels, in thin film [143].

The previous description provides the preparation of the precursor solution. In order to make thin film from the precursor solution, there are two processes for the production of the films, dip-coating, and spin-coating techniques.

1. Spin coating technique

Another technique is also available for usage after the precursor solution is prepared, known as spin coating or spinning. Sol is placed on the uniformly rotating horizontal disc to produce a uniform coating by means of adhesive and centrifugal force. The thickness of the film is controlled by angular velocity, concentration, and viscosity of the sol [144].

The slurry which is used in this method is similar to other fabrication methods. As shown in Figure 2.9, a certain amount of the slurry is placed on the center of the spin axis above the supporting layer, and will be spread over the plate by its rotation. Constant speed rotation of the axis and centrifugal force allows the slurry to form a uniform layer. The angular velocity of the spin is an important parameter in determining the thickness of the layer, and has an inverse relation to each other. In addition, the speed of the rotation can be adjusted in order to fabricate coating layers of desirable thickness [145]. Like the other methods containing slurry, the composition and the viscosity of the slurry determine the thickness of the resulting layer. Lower viscosity causes lower adherence of the slurry [146,147].

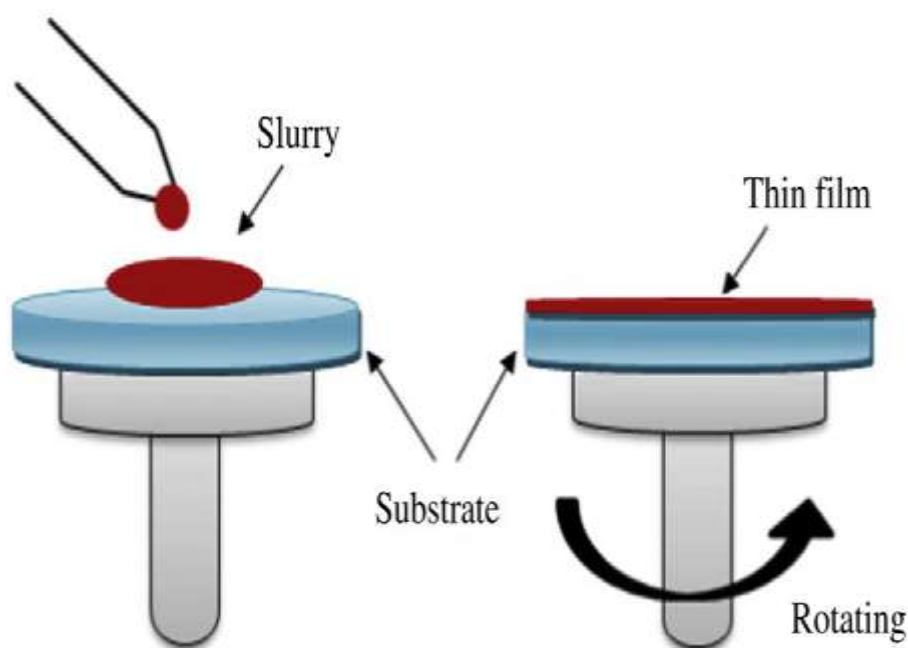


Figure 2.9. Schematic of spin-coating technique [147].

2. Dip-coating technique:

Dip-coating technique is almost used to fabricate transparent layers of oxides on a transparent substrate with a high degree of planarity and surface quality .

Kleinet al [148] have discussed this technique involves immersion of substrate to be coated with prepared sol with rapid drying. They are carried the uniform and quality films are obtained by optimizing dipping time, drying time, and number of cycles.

This sol gel method possesses several advantages over other traditional methods [149]:

- Sol-gel deposited film carries high optical quality and purity.
- It offers easier deposition of large area substrate optimum thickness.
- This technique is environmentally friendly and avoids washing after reaction.

The Dip-coating carries few drawbacks like:

- It is still struggling with adhesion and delamination.
- Stability of the synthesized film still needs to improve [150].

In the dip-coating method, the supporting layer is soaked in the slurry. Then the slurry jar comes down and a film of slurry is attached to the supporting layer [151,152]. After the coated slurry is dried at ambient temperature the supported layer with its new dip-coated layer is sintered [153]. The smoothness and thickness of the layer can be controlled by modifying the solid loads in the slurry and the draw-up speed of the supporting layer from the slurry jar [154]. Layers with the thickness of a few microns to hundreds of microns can be produced using this method [155]. The usual duration

CHAPTER.2 THIN FILMS AND ADHESION

for soaking the supporting layer in the jar initially is about 30 seconds [156]. The Figure 2.10 illustrates the dip-coating method.

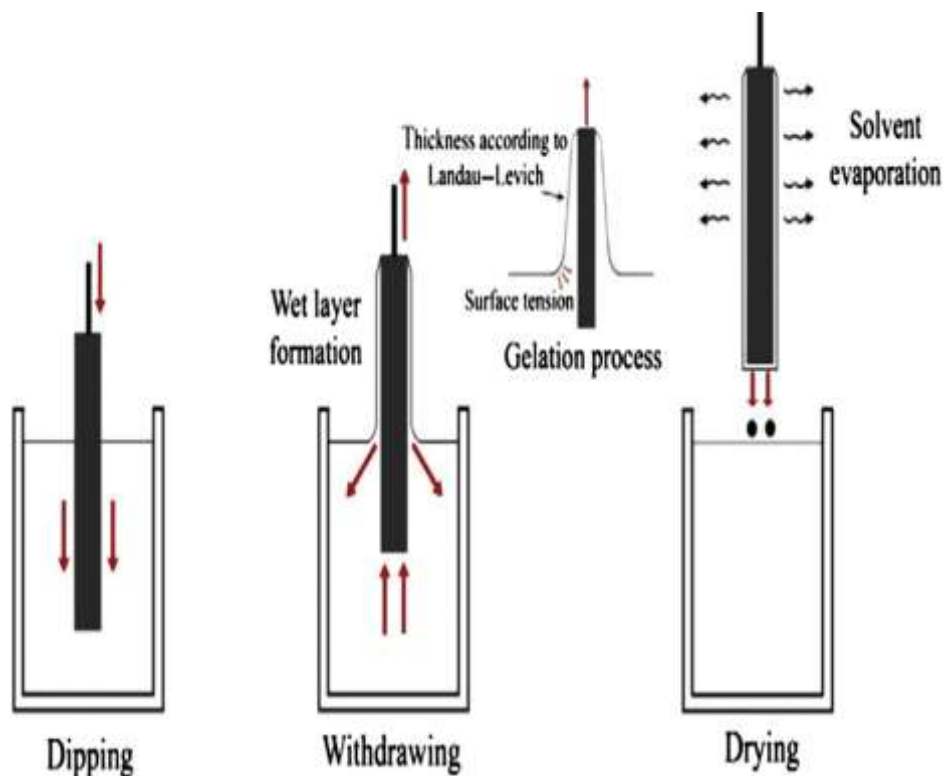


Figure 2.10 .Schematic of dip-coating technique [156].

2.2.1.2.2. Chemical bath deposition:

CBD is a method whose thin layers are arranged substrates immersed in dilute solutions containing metal ions and a source of chalcogenide [157], and to limit hydrolysis of metal ions, complexing agents are used . The CBD can be used to deposit any compound that satisfies the following four basic requirements as proposed by Ramasamy et al [158]. The compound can be made by simple precipitation. This, generally, although not exclusively, refers to the formation of a stoichiometric compound formed by ionic reaction.

- The compound should be relatively (and preferably highly) insoluble in the solution used.
- The compound should be chemically stable in the solution.
- If the reaction proceeds via the free anion, then this anion should be slowly generated, if the reaction is of the complex-decomposition type, then decomposition of the metal complex should similarly occur slowly [159].

The device we used in the CBD technique [160] to deposit ZnS is shown in the Figure 1.11.

The installation includes:

- Spade containing deposition solutions.
- Heating plate resistor used to heat the solution.

CHAPTER.2 THIN FILMS AND ADHESION

- Magnetic stirrer.
- PH meter to measure the pH value of the deposit solution.
- Programmable digital thermometer.

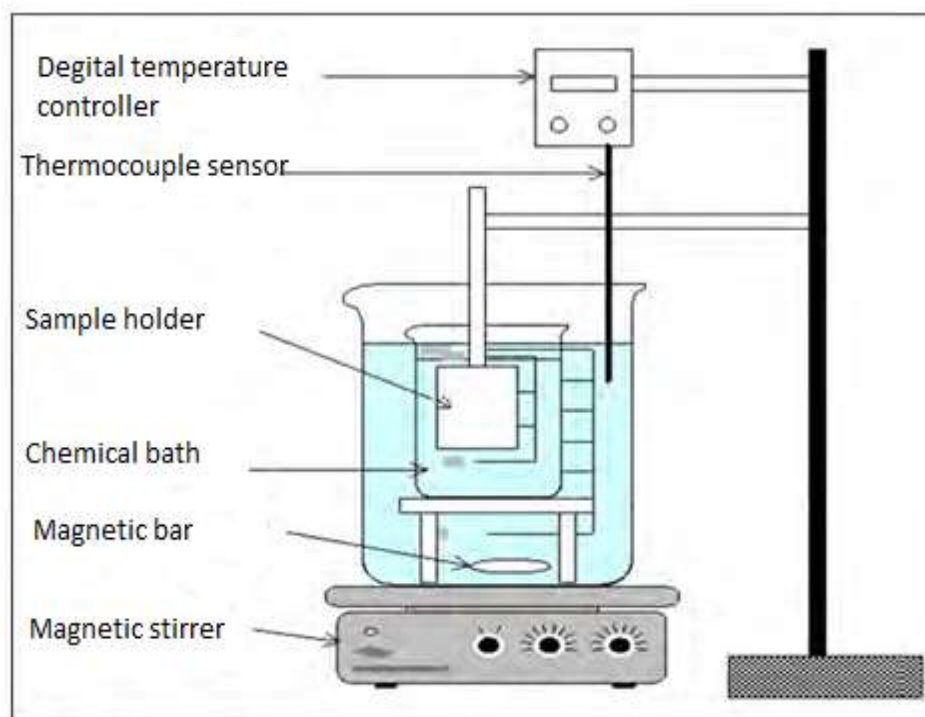


Figure 2.11. Experimental device used for chemical bath deposition (CBD).

2.2.1.2.3. *Chemical vapour deposition (CVD)*

Chemical bath deposition method is also known as solution growth technique or controlled precipitations [161]. It is the oldest method to deposit films on a substrate.

In CVD, film deposition on the surface is carried out at high temperature by cracking hydrocarbon gas under an inert atmosphere. The performance of thin film prepared by CVD depends on various factors such as reaction temperature, gas flow, substrate used, cooling rate and pressure. This method successfully synthesizes two dimensional hetero structures with excellent controllability, which has great importance in practical application. Under certain circumstances, CVD employed the use of plasma for temperature management. Basically, plasma is a glow discharge in field of low pressure[162]. The various advantages of CVD are:

- The synthesized films are well adherent and reproducible.
- It produces films of high density and purity.
- It is possible to control deposition rate, crystal structure and surface morphology.

However, CVD has some drawbacks, such as [163]:

- The use of flammable, toxic and corrosive precursor gases makes it unsafe.
- It is difficult to deposit multicomponent compound [164].

CHAPTER.2 THIN FILMS AND ADHESION

Several process factors and chemical reaction between the reactant and substrate are responsible for the quality of films produced during CVD, the quality of the film can be controlled and modified by using the combination of process parameter like flow rates[165], pressure, temperature, concentration of chemical species, reactor geometry, etc. [166]. The CVD reaction types possible are pyrolysis, reduction, oxidation, compound formation, disproportionate, and reversible transfer[167]. The chemical reaction taking place depends on the reactant (precursor) gas and the by-products[168]. In addition, the reaction has to be thermodynamically predicted, i.e., there is a need for availability of adequate energy for the reaction to take place and the Gibbs free energy (total energy) has to decrease in order to allow the temperature and pressure of the reaction to be altered [169].

The CVD process, usually characterized by volatile reaction, of by-products and unused precursor species. Many CVD reaction by-products are very hazardous volatile by-products such as H_2 , Cl_2 , HCl , HF or water vapour. Proper safety precaution is needed when using CVD[170]. Venting, scrubbing of by-products compounds are essential in CVD processes. CVD can be grouped based on energy used to drive the chemical reaction. Sources of energy can either be a photon, laser or temperature (thermal), the CVD process is presented in Figure 2.13.

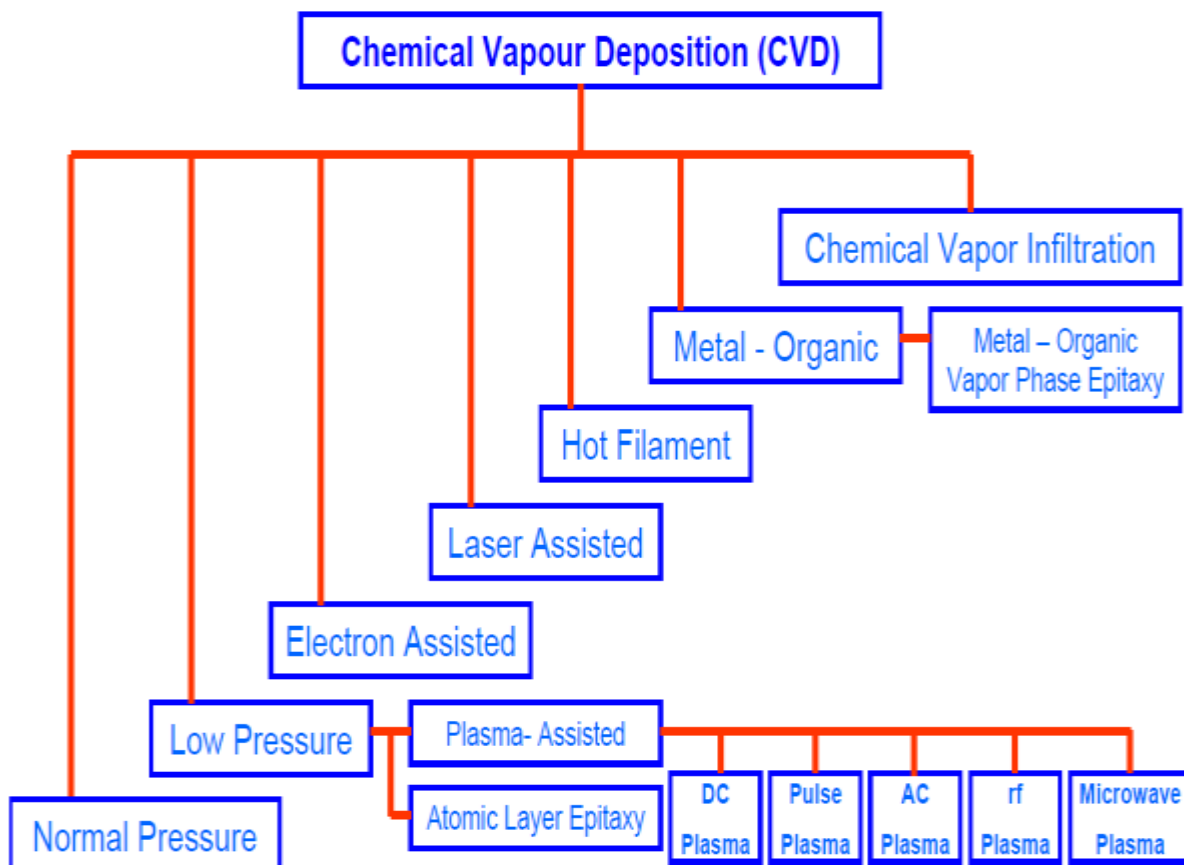


Figure2.13. Variants of Chemical Vapour Deposition.

CHAPTER.2 THIN FILMS AND ADHESION

1. Thermal CVD:

Thermal CVD is a CVD process for depositing a thin film on various materials. This process uses lamps or other methods to heat the substrate rapidly and activate the energy needed for the reaction to take place[171]. The growing film surface is exposed to thermal energy from either the condensing atoms or substrate heater to create the thin film. This thermal surface energy is responsible for mobilizing the atoms, which lead to the creation of thin film with uniform thickness and good surface coverage and finishing [172]. Since the thermal surface energy is dependent on the working temperature, an increase in temperature also resulted in a better thin film distribution on the surface of the substrate [173]. The surface chemistry and surface atom mobility are aided by the substrate temperature alone [174].

Figure 2.14 shows a schematic diagram of thermal CVD apparatus in the synthesis of carbon nanotubes.

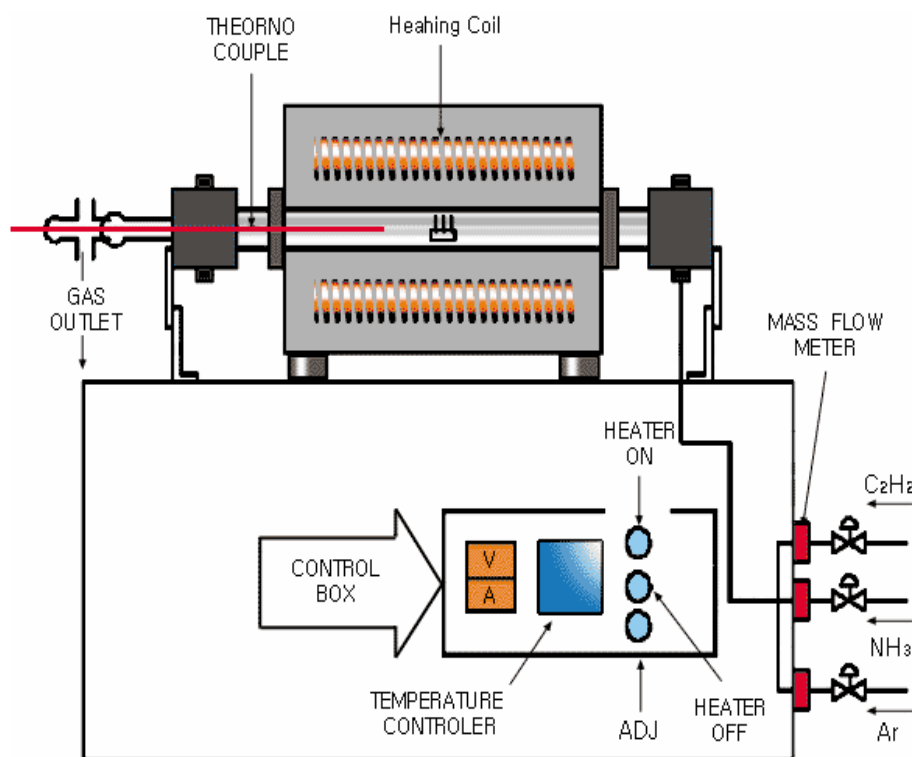


Figure 2.14. Schematic of thermal CVD methods[174].

2. Plasma-enhanced CVD (PECVD):

PECVD is a variant of CVD that is used to deposit a thin film from a gaseous state to a solid state on the substrate; the chemical reaction takes place after the creation of plasma in the reactor chamber and subsequently leads to deposition of a thin film on the surface of the substrate. PECVD uses an electrical source of energy to generate plasma and sustain the reaction process rather than

CHAPTER.2 THIN FILMS AND ADHESION

thermal energy for the majority of the CVD processes. In fact, the electrical energy is used to initiate homogeneous reactions for the creation of chemically active ions and radicals that can partake in heterogeneous reactions, which lead to layer formation on the substrate [175]; Figure 2.15 shows a schematic diagram of a typical plasma CVD apparatus with a parallel plate electrode structure. The main benefit of PECVD over thermal CVD processes is the possibility of deposition to take place at a very low temperature close to the ambient temperature and permit materials sensitive to temperature change to be worked on. Furthermore, the use of plasma to activate the gas phase chemistry opens up several new reaction paths for deposition at a significantly lower temperature [176].

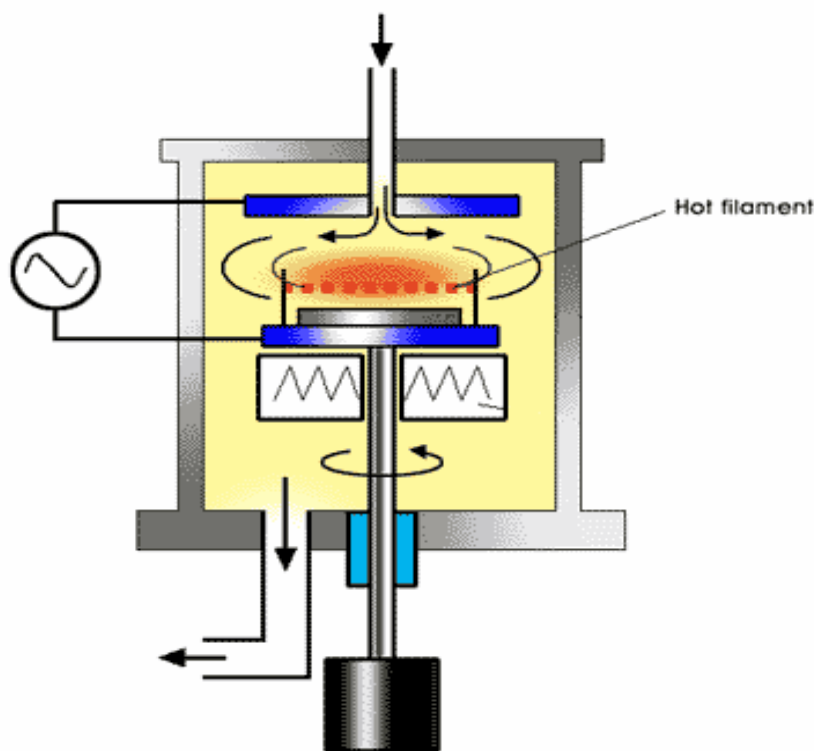


Figure 2.15. Schematic of plasma CVD methods [175].

2.3. CHARACTERIZATION OF THIN FILMS

In the past years the advancement in science has taken place mainly with the discovery of new materials. Characterization is an important step in the development of exotic materials. The complete characterization of any material consists of phase analysis, compositional characterization, structural and surface characterization, which have strong bearing on the properties of materials. In this section different analytical technique used to characterize our thin films are described with relevant principles of their operation and working.

CHAPTER.2 THIN FILMS AND ADHESION

2.3.1. Stress measurement

Stress is a physical quantity that expresses the internal forces that neighboring particles of a continuous material exert on each other. Besides, Ohring et al [177] have presented the control of the stress in a growing film is very important, since high values of either tensile or compressive stress, especially in combination with poor adhesion, can lead to cracking or delamination of the film from the substrate .

The total stress in the film can be divided onto, the thermal stress due to the mismatch of expansion coefficients of the substrate and the growing film and the intrinsic stress of the growing film because of the phase transformation, chemical reactions, recrystallization and concentration of defects during the film growth. The residual stresses (see Figure 2.16) cause also a lattice strain. It represents a stored energy in the lattice that plays an important role in the resistance of the film to plastic deformation [178].

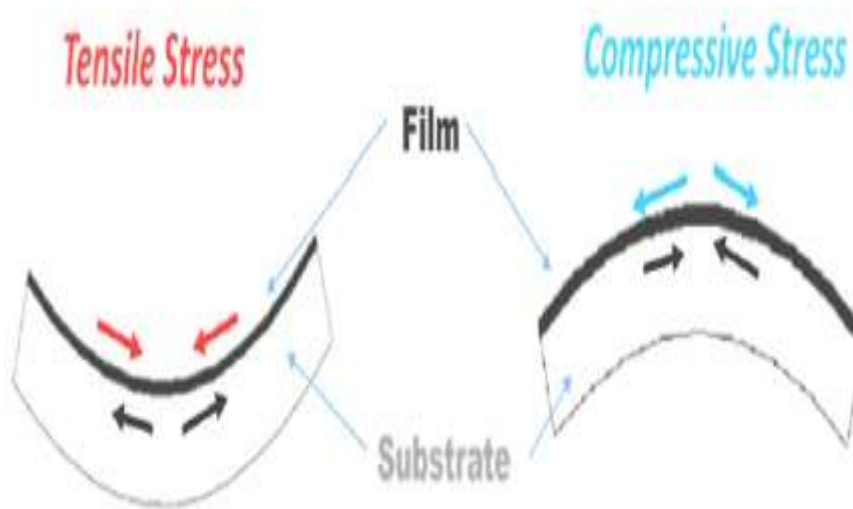


Figure 2.16. Tensile and Compressive Stress in a film [178].

If the coating was prepared at elevated temperatures and the thermal expansion coefficients of the substrate and the film are known, the thermal stress (2.3) can be calculated as:

$$\sigma_{th} = \frac{E_s}{1-\nu_s} \Delta\sigma\Delta T \quad (2.3)$$

Where σ_{th} , is the thermal stress of the film, $\Delta\sigma$ is the difference in thermal expansion coefficient of the film and the substrate, ΔT is the difference of the temperature before and after the deposition, E_s is the biaxial elastic modulus of the substrate, and ν_s is the Poisson's ratio of the substrate [179].

2.3.2. Hardness and Young's modulus

Hardness is a measure of how resistant a solid is to various shape changes when a compressive force is applied [180]. In other words, it is the resistance of a material to plastic deformation.

CHAPTER.2 THIN FILMS AND ADHESION

Various measurement techniques are used for the determination of hardness on the macro and micro scale [181]. Most of them are based on the measurement of the penetration resistance of the material to a permanent deformation by a special indenter [182]. The two most commonly used micro hardness tests in the case of thin-film measurements are [183]:

- Vickers hardness test (HV).
- Knoop hardness test (HK).

Special techniques to measure the micro hardness use micro indentation techniques [184]. Besides hardness, the elastic properties of the material can be determined from the maximum penetration depth compared to the residual depth of the indentation after the indenter has been removed [185].

In order to remove the elastic contribution to the displacement and determine the projected area of the load-displacement curve, the Oliver and Pharr model (2.4) can be used [186]:

$$S = \frac{dP}{dH} = \frac{2}{\sqrt{\pi}} E_r \sqrt{A} \quad (2.4)$$

Where $S = \frac{dP}{dH}$, is the experimentally measured stiffness of the upper portion of the unloading data, E_r is the reduced modulus, and A is the projected area of the elastic contact.

2.3.3. Density

The mass density of a thin film is measured in grams per cubic centimeter, or the areal density can be given in micrograms per square centimeter. Müller et al [187] have reported that the density depends on:

- Composition
- Arrangement of the atoms
- Closed porosity volume
- Definition of what constitutes a surface

Film density can be measured using geometry–property relationships or by displacement–floatation techniques. In the geometry–property techniques, the volume or area of the sample is determined as well as the mass of a specific volume or area. From this, the density can be calculated directly. For example, aluminum, which has a bulk density of 2.7 g/cm^3 , will form a film with an areal density of $27.0 \text{ micrograms/cm}^2$ for a 1000 Å film. Some bulk densities (g/cm^3) of common inorganic compound film materials are $\text{SiO}_2 = 2.20$ and $\text{TiO}_2 = 5.29$.

CHAPTER.2 THIN FILMS AND ADHESION

The film may be removed from the substrate and the density determined by displacement techniques. Pycnometry involves the displacement of a liquid or gas from a container of accurately known volume and the weight of the sample [188].

2.3.4. Resistance to cracking

One of the important mechanical parameters of the hardest thin films is their toughness and resistance to cracking [189]. Two most common methods for the determination of the film resistance to cracking are high indentation load test and bending test. In the high indentation load, test a diamond indenter penetrates into the surface of the film with a high indentation load $L > 250 \text{ mN}$ increasing up to its cracking. During the bending test, films deposited on the flexible substrate, typically molybdenum foil, are bent around the cylinder with a fixed diameter. After the test, cracks can be detected by the optical or electron microscopy [190]. Typical images are given in Figure 2.17.

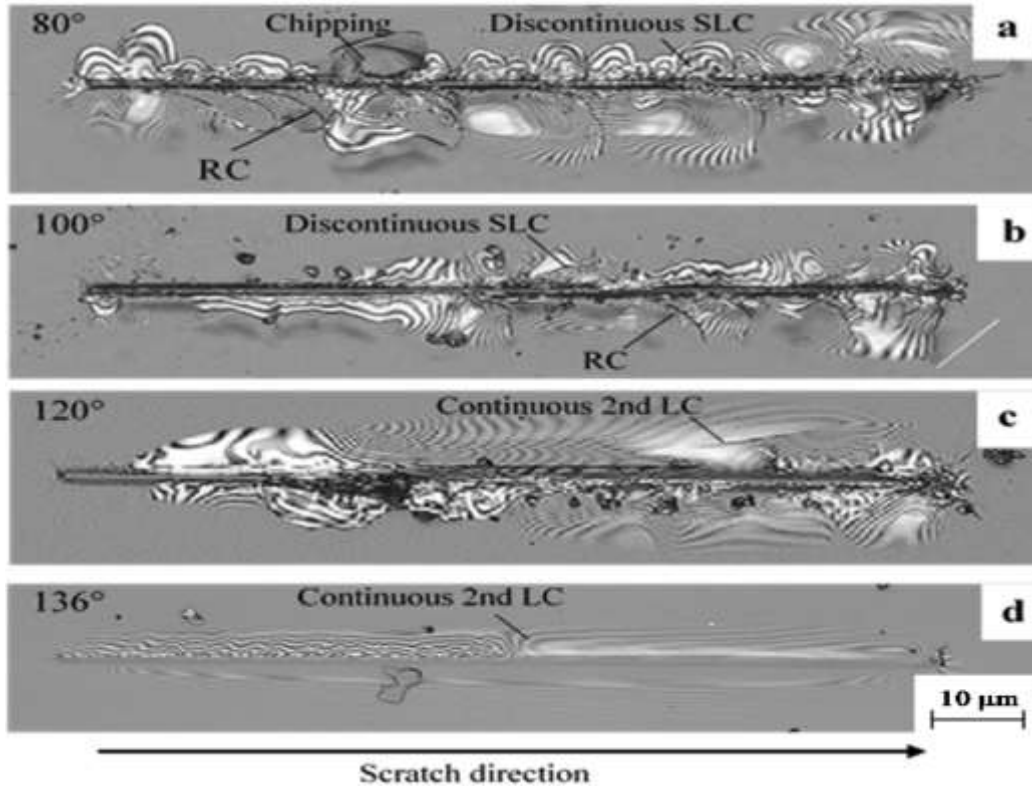


Figure 2.17. Confocal microscopy of single scratches of BK7 glass. For (a) $\alpha=80^\circ$; (b) $\alpha=100^\circ$; (c) $\alpha=120^\circ$; (d) $\alpha=136^\circ$ [190].

2.3.5. Band gap energy

The optical energy band gaps E_g of the films were calculated using the Tauc's relationship as follows [191]. Absorption coefficient (2.5) was calculated and is related to the optical band gap by the relation:

$$\alpha = \frac{k}{h\nu} (h\nu - E_g)^n \quad (2.5)$$

CHAPTER.2 THIN FILMS AND ADHESION

Where k , is a constant, h is Planck's constant, $h\nu$ is the incident photon energy and n is a number which characterizes the nature of electronic transitions between the valance and conduction bands [123 192]. For direct allowed transitions $n=1/2$, and it is known that, ZnS is a direct band gap semiconductor. Therefore, the formula (2.6) used is:

$$\alpha = \frac{k}{h\nu} (h\nu - E_g)^{\frac{1}{2}} \quad (2.6)$$

Figure 2.18 shows the variation of $(\alpha h\nu)^2$ with photon energy $h\nu$. The deposited material exhibit direct type of transition as observed from the linear portion of $(\alpha h\nu)^2$ Vs $h\nu$ curve over a wide range of photon energies [193].

The linear portion of the curve was extrapolated to evaluate the energy gap E_g of the ZnS thin films, indeed, the intercept on energy-axis estimates the band gap energy (3.70 eV) bit higher than that of bulk cubic ZnS (3.54 eV), due to nanocrystalline nature of thin films [194-195].

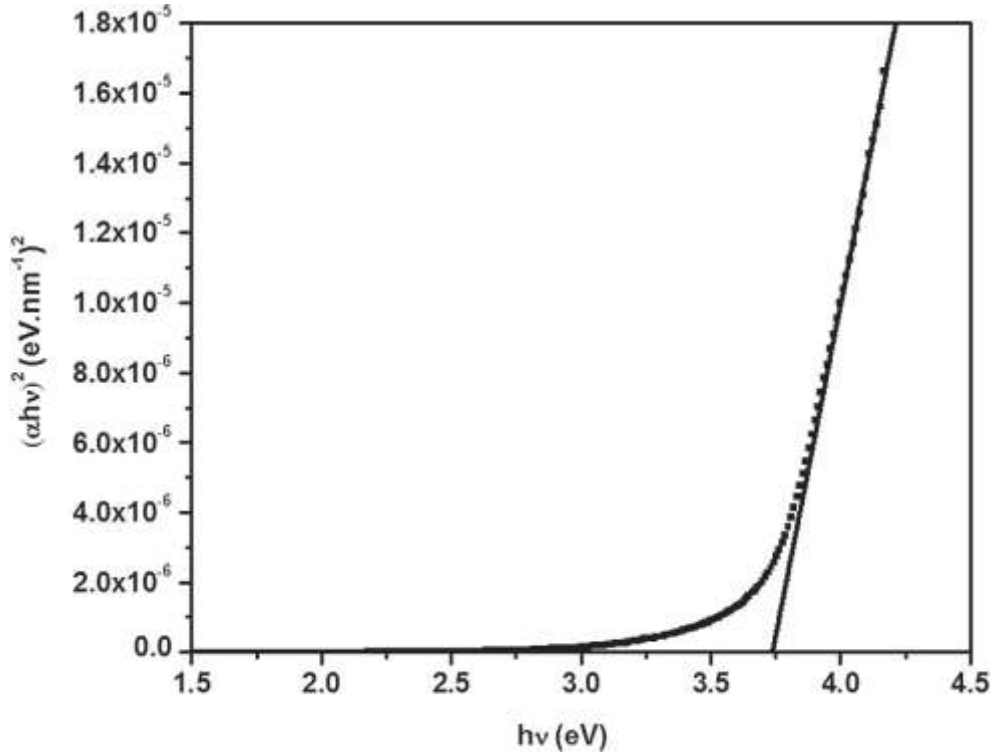


Figure 2.18. Band gap plot of ZnS thin film [195].

2.3.6. Contact angle

The contact angle is the angle, measured through the liquid, at which a liquid–vapor interface meets a solid surface. Junyuan Feng et al [196] have discussed the contact angle quantifies the wettability of the solid by the liquid. Therefore, for a given solid and liquid pressure and temperature, the contact angle has a unique value. In the case of wetting by water all surfaces can be divided onto hydrophilic with water contact angle lower than 90° and hydrophobic with water contact angle

CHAPTER.2 THIN FILMS AND ADHESION

higher than 90°. Wettability in the system vapor-liquid-solid is determined by the Young's equation (2.7):

$$\gamma_{SV} = \gamma_{LV} \cos \theta + \gamma_{SL} \quad (2.7)$$

Where γ_{LV} is the liquid surface tension, γ_{SV} is the solid surface tension, γ_{SL} is the solid-liquid interfacial tension, and θ is the contact angle. Equilibrium between these forces gives the static contact angle of the system, Figure 2.19.

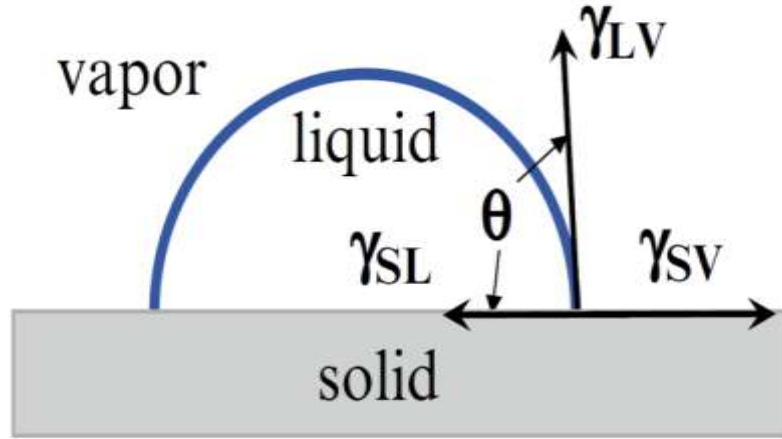


Figure 2.19. Young's Schematic of contact angle measurement [196].

2.3.7. X-ray diffraction

XRD is a standard nondestructive analysis technique for determination of the structure and quality of thin films. It is used for phase analysis, texture, residual stress, lattice parameters or grain size measurements.

In the method, diffraction of X-ray waves on a regular array of the crystal atoms by the elastic scattering leads to producing the diffraction pattern. These X-ray diffraction patterns are determined (2.8) by the Bragg's law:

$$n\lambda = 2d \sin \theta \quad (2.8)$$

Where λ , is the wavelength of the beam, n is any integer, d is the spacing between the diffracting planes and θ is the incident angle [197].

Figure 2.20 illustrates the geometry of a diffraction cone with detection surfaces of a flat 2D detector at two different distances between the sample and the detector (D_i).

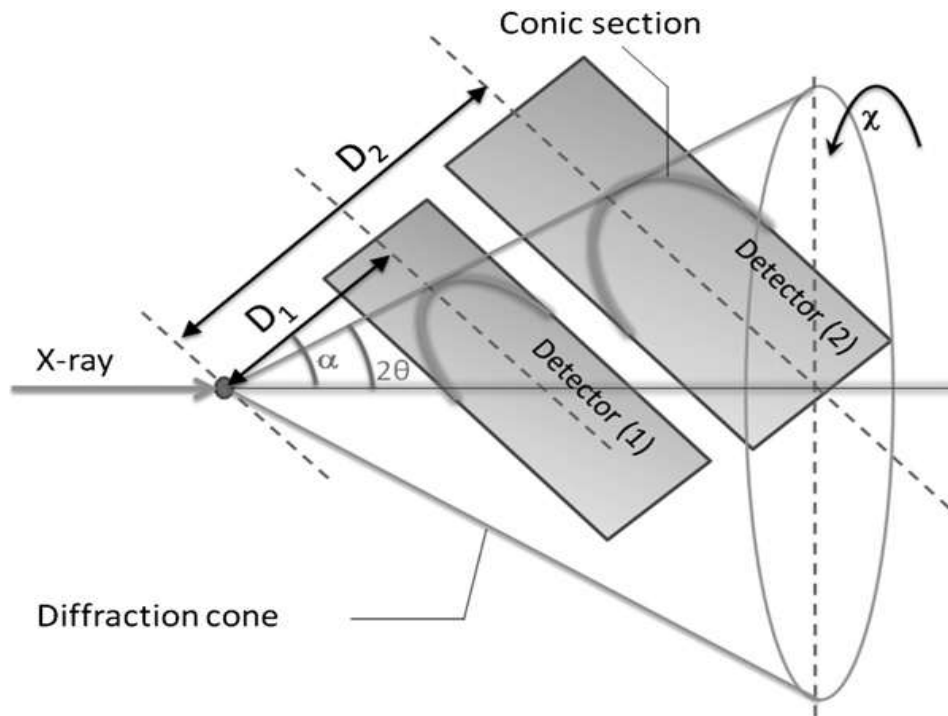


Figure 2.20. XRD schematic of a 2D detector plane with a diffraction cone at two different distances a diffraction cone at two different distances [197].

2.3.8 Scanning electron microscopy

The scanning electron microscope is an electron microscope, which produces images of a sample by scanning it with a focused beam of electrons. The angular resolution of optical microscopes is limited by the wavelength of the visible spectra

The electron beam generated by an electron gun is focused on the sample. Primary electrons interact with the sample material and generate secondary electrons, X-ray radiation, Auger electrons and so on, which can be detected by special detectors. The intensity of these signals strongly depends on the topography of the tested material [198].

The main types of signals that generated and detected during the operation of the SEM [130 199]:

- Secondary electrons
- Reflected electrons
- Electrons passed through the sample
- Electron backscatter diffraction
- X-ray radiation
- Light signal in the case of cathode luminescence

Also, recently reported environmental scanning electron microscope allows working with uncoated samples in a gaseous environment in the specimen chamber, for example Figure 2.21.

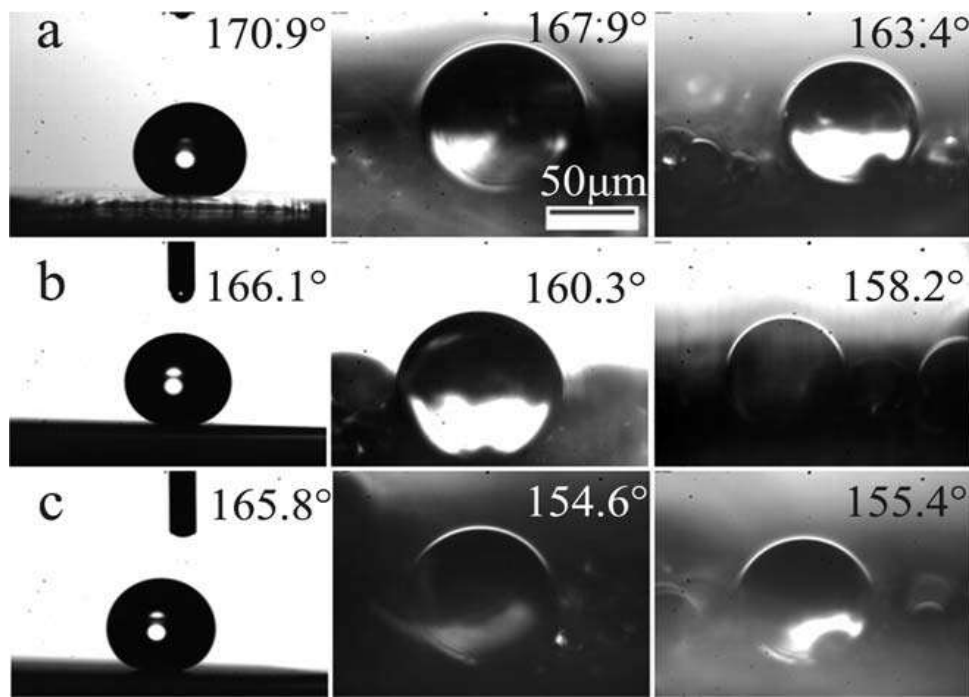


Figure 2.21. SEM image of the water droplet on the superhydrophobic surface[199].

2.4. ADHESION BEHAVIOR

Cohesion is the strength in a single material due to interatomic or intermolecular forces.

Adhesion, also denoted as adhesive force or adhesive strength, is the physical state of a boundary layer which forms between two condensed phases getting into contact with one another [200], as well as between solid state bodies and liquids negligible vapor pressure. Mittal et al [201] have presented the main properties of this state, the mechanical cohesion of the involved phases, are generated by the molecular interactions inside the boundary layer. The forces affecting this mechanical cohesion are not completely studied, for which reason there appear several adhesion theories.

2.4.1. Material Adhesion Mechanism

The adhesion of a film to a surface involves adhesion on the atomic scale as well as the failure of the atomic bonding over an appreciable area on a macroscopic scale.

The origin of the adhesion between two surfaces may be due to several parameters:

Chemical Bonding, Mechanical Bonding, else Stress, Deformation, Failure, and Fracture.

2.4.1.1. Chemical Bonding:

Ionic bonding occurs when one atom loses an electron and other gains an electron, to give the strong coulombic attraction. Covalent bonding occurs when two atoms share two electrons. In ionic and covalent bonding, there are fewer (free electrons) so the electrical conductivity of the material is low, and the material is brittle. Polar covalent bonding occurs when two atoms share two

CHAPTER.2 THIN FILMS AND ADHESION

electrons, but the electrons are closer to one atom than the other, giving a polarization to the atom pair. Metallic bonding occurs when the atoms are immersed in a (sea) of electrons, which provides the bonding. Metallic bonded materials have good electrical conductivity and the material is ductile. In some materials, there is a mixture of bond types [202].

2.4.1.2.Mechanical Bonding:

Adhesion by mechanical means can occur by mechanically interlocking the two surfaces, such that one material or the other must deform or fracture of the materials to be separated. This type of bonding requires that the deposited film be conformal to a rough surface and that there are no voids or poorly contacting areas at the interface [203].

2.4.1.3.Stress, Deformation, and Failure:

Tensile stress occurs when the mechanical stress is applied normal to and away from the interface. Evans et al [204] have developed the shear stress is when the mechanical stress is related parallel to the interface. Compressive stress is when the mechanical stress is concerned normal to and toward the interface [205]. When a tensile stress applies to the surface of a film, the stress that appears at the interface between dissimilar materials will be a complex tensor with both tensile and shear components whose magnitudes depend on the applied stress and the mechanical properties of the materials. The nature of the film failure will differ depending on the relative properties of the film and substrate. For example, a high modulus film, such as an oxide, on a substrate that can elongate or deform easily can have good adhesion, but the film can crack under stress [206]. Deformation of a material requires the input of energy and the deformation may be elastic, plastic, or a mixture of the two. This deformation may occur over a large volume of material or just at the tip of a propagating crack. Elastic deformation occurs when the applied stress causes deformation but, when the force is removed, the material returns to its initial dimensions. Young's Modulus of Elasticity is the ratio of the stress to the strain in the elastic deformation region [207].

2.4.1.4.Fracture:

The loss of adhesion under mechanical stress occurs by the deformation and fracture of material at or near the interface [208].When a fracture surface (crack) advances, energy is needed for the creation of new surfaces and deformation processes that occur around the crack tip. This energy is supplied by the applied stress and the internal strain energy is stored in the film–substrate system (residual film stress). The path of crack propagation is determined by the mechanical properties of the materials and by the resolved tensor stresses at the crack tip. In this case; the crack may progress through the weak material or may be diverted into stronger materials by the resolved stress[209].

CHAPTER.2 THIN FILMS AND ADHESION

In fact, the fracture path depends on the applied tensor stress, the presence of flaws, the interface configuration, (easy fracture paths), and the properties of the materials involved. The fracture path is also determined by the presence of features, which may blunt or change the fracture propagation direction [210].

2.4.2. Surface energy

Surface energy plays a major role in friction, lubrication and wears phenomena in contact materials, and especially in the flow-surface interactions with liquids. Tribology is the science entrusted with evaluating these interactions between surfaces in relative motion. When a solid surface is faced with interfacing materials and environment, a resulting loss of material from the solid surface could take place [211]. This is known as wear and includes abrasion, friction, erosion and corrosion processes. In order to minimize the loss of material in these interaction situations, a modification of the surface properties is performed by applying a coating directly on the surface[212]. Surface energy is defined as the energy associated with the intermolecular forces at the interface between two media and it is also called surface free energy [213]. For solids and liquids, the surface represents a higher energy state in comparison with the bulk.

While the free surface energy characterizes the wetting properties of the material, it is important to know how it correlates with the contact angle.

Various models are used for characterization of the surface energy, for example:

- Zisman model.
- Fowkes model.
- Wu model.
- Owens–Wendt–Rabel–Kaelble (OWRK) model.
- Van Oss, Chaudhury, and Good (VOCG) model.

These models can be divided into one-component (Zisman), two-component (Fowkes, Wu and OWRK) and three-component (VOCG) theories depending on the number of the measured surface energy components. The most useful Wu theory allows to determine not only the polar and dispersive energy components used, but also its contact angle and adhesion force are found using the two liquids with known values of γ^d and γ^p . The values are put into the following equation (2.9), and two equations are solved for γS^d and γS^p [214-215].

$$W_a = \gamma L(1 + \cos \theta) = 4 \frac{\gamma S^d \cdot \gamma L^d}{\gamma S^d + \gamma L^d} + \frac{4(\gamma S^p \cdot \gamma L^p)}{\gamma S^p + \gamma L^p} \quad (2.9)$$

The calculation of the polar and dispersive components, as shown in Table. 2.2 are carried out on the basis of the measuring contact angles, the polar and dispersive components of the surface tension and the total surface tension of two respective liquids [216-217].

CHAPTER.2 THIN FILMS AND ADHESION

	Liquid A Distilled water	Liquid B N-Octane
Measured contact angle	θ_A	θ_B
Polar component	$\gamma_{LA}^P = 51 \text{ mN/m}$	$\gamma_{LB}^P = 0 \text{ mN/m}$
Dispersive Component	$\gamma_{LA}^d = 21.8 \text{ mN/m}$	$\gamma_{LB}^d = 21.4 \text{ mN/m}$
Total	$\gamma_{LA} = 72.8 \text{ mN/m}$	$\gamma_{LB} = 21.4 \text{ mN/m}$

Table 2.2. Polar and dispersive components of surface and total surface tension of two liquids [217].

2.4.3. *Methods of contact angle measurements*

The topic of wetting plays an important role in many industrial processes, such as lubrication, liquid coating, printing, and spray quenching [218]. In recent years, there has been an increasing interest in the study of super hydrophobic surfaces, due to their potential applications in, for example, self-cleaning, nano fluidics and electro wetting[219].

2.4.3.1. *Sessile Drop Method:*

One of the most extensively employed methods for analyzing the contact angle is a direct measurement of the tangent angle at three-phase equilibrium interfacial point using the sessile drop method. For flat surfaces, the wetting property was determined by direct measurement of contact angle by viewing the drop profile [220]. The processes demonstrated that a telescope goniometer was capable to view the liquid drop profile placed over the smooth surface and measure angle formed between three interfacial tensions [221]. An image of the adhering bubble can be projected onto a screen and the outlines traced, thereafter the angle is measured. The graphical representation of the sessile drop technique was presented in Figure 2.22.

CHAPTER.2 THIN FILMS AND ADHESION

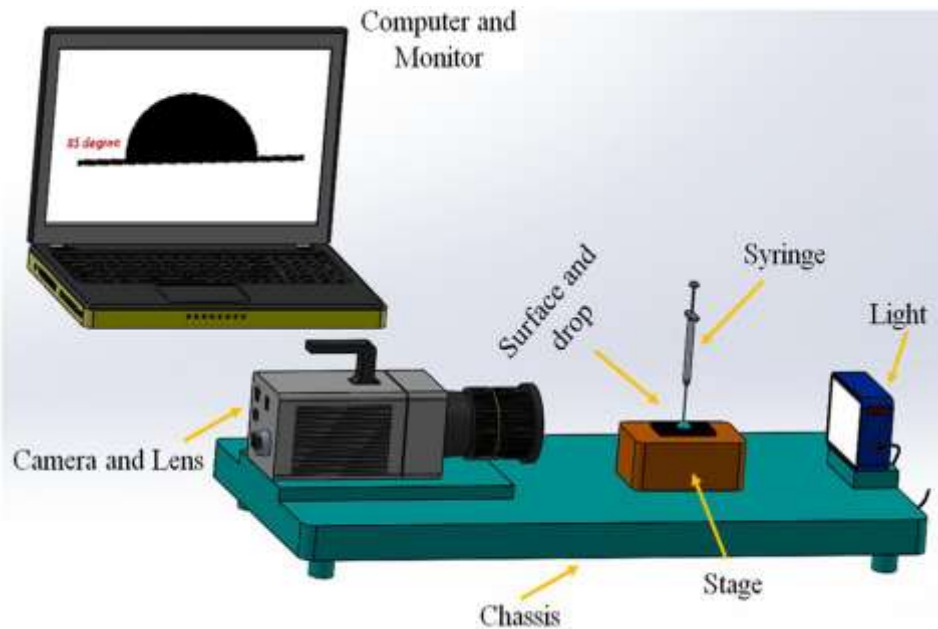


Figure 2.22. Graphical representation of sessile drop method [221].

2.4.3.2. Wilhelmy method:

The Wilhelmy method [222,223] is originally devised for surface tension determination, but it has been found suitable for measuring contact angle between a liquid and a solid and also the interfacial tension between two liquids. The method involves the determination of the force acting on a vertically immersed plate in a liquid [224], as shown in Figure 2.23.

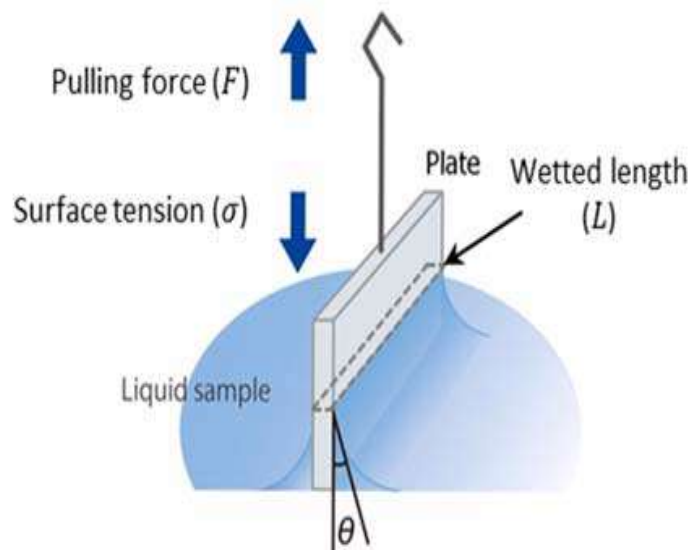


Figure 2.23. Schematic of the Wilhelmy plate measurement method[224].

The plate touches the liquid surface or an interface while it is vertically suspended from a force sensor or tensiometer. The pulling force F that acts on the plate is measured by the tensiometer. By transposing the Wilhelmy equation [225](2.10), the value of the contact angle θ can be obtained as long as the value of the surface tension σ is known.

CHAPTER.2 THIN FILMS AND ADHESION

$$\sigma = \frac{F}{L \cdot \cos \theta} \quad (2.10)$$

Where L, the wetted length, of the plate is equal to its perimeter and must be constant along all the plate to not depend on the immersion depth.

2.4.3.3. Du Nouy ring method:

Another similar method is the Du Nouy ring method [226,227]. As the name suggests, a ring made of platinum is used instead of the plate. The ring that is hanging parallel to the liquid surface has sunk into it [228]. Then, the ring is gradually drawn apart from the surface in a vertical direction, as shown in Figure 2.24.

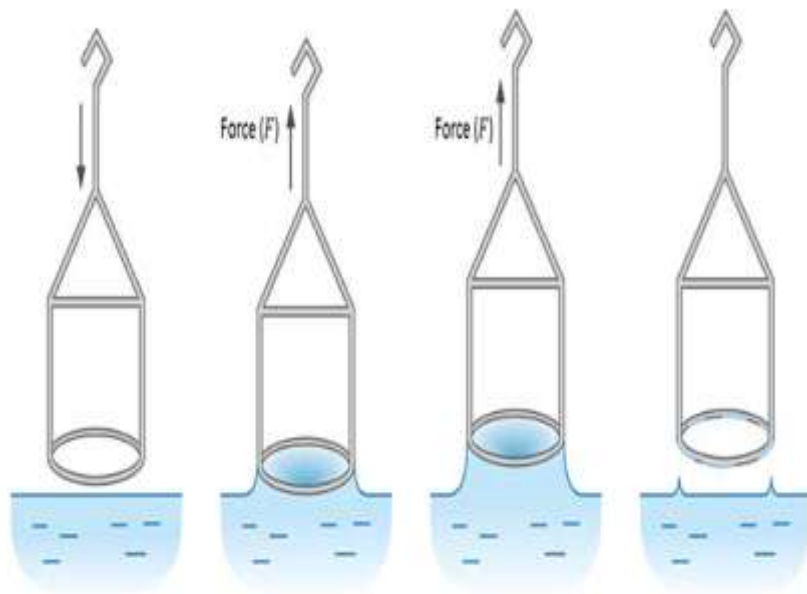


Figure 2.25. Schematic of the measurement process Du Nouy a ring method [228].

In this process, the surface tension of the liquid membrane that is hanging from the ring generates a force on the ring that changes as the ring is drawn farther. The maximum value of the force is used to determine the surface tension by means of an equation (2.11):

$$\gamma = i \frac{F_m}{4\pi R} \quad (2.11)$$

With:

i: correction factors because by removing the ring from the surface.

F_m: is the maximum force of the ring which depends on the voltage.

R (m): radius of the ring.

CHAPTER.2 THIN FILMS AND ADHESION

It is important to highlight that this method needs a measurement correction [228-229], since the weight of the liquid of the plate increases the measured force and also because the force maximum does not occur on the inside and outside of the lamella at the same time.

2.4.3.4.Captive Bubble Method:

As an alternative method to analyze the contact angle of liquid over the flat solid substrate, an air bubble was introduced below the solid sample and is submerged in the liquid (see Figure 2.26). In this technique, contact angle formed by the air bubble in the testing liquid can be directly determined. This method was developed by Taggart et al [230] and is now commonly stated as the (captive bubble method).

This technique has the advantage of ensuring that the solid sample is in equilibrium with atmospheric interfacial tension and also gets the ample time to approach equilibrium with liquid phase. It also reduces the number of contaminations over the solid vapor interface from sources such as air-borne oil droplets [231]. Moreover, in this method, it is possible to investigate the temperature dependence of contact angle studies. The temperature of the testing liquid can be easily monitored compared to sessile drop technique [232].

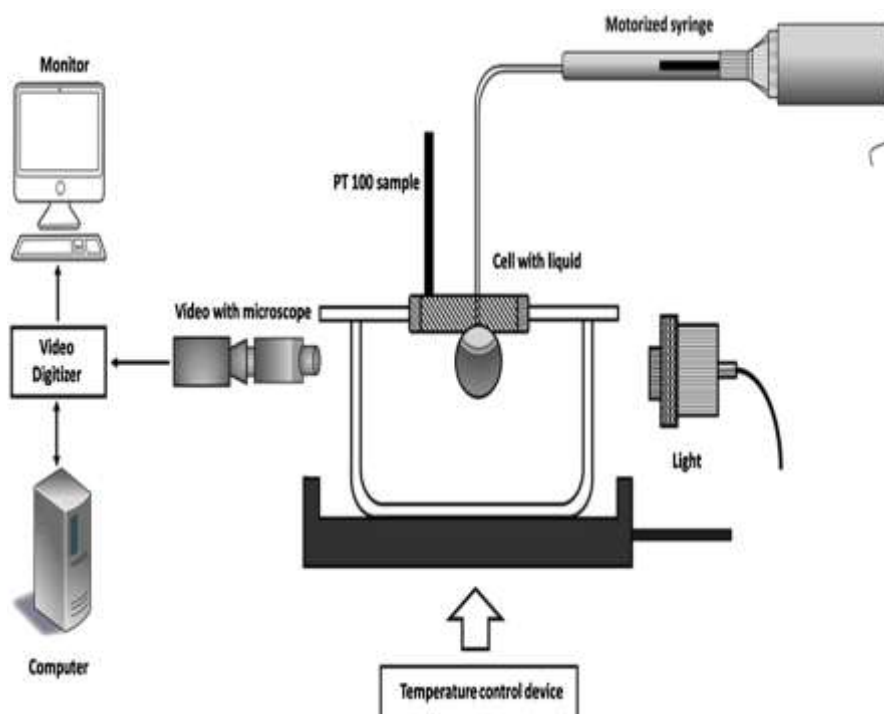


Figure 2.26. Graphical representation of Captive Bubble method [232].

2.4.3.5.Digi Drop method:

DigiDrop shape analysis [233] is an image analysis method for determining the contact angle from a side-view image of a sessile drop. The method consists of acquiring an image of a drop placed on a solid surface from side-view commonly by means of a camera. The drop in contact with the solid surface assumes a spherical shape [234].

CHAPTER.2 THIN FILMS AND ADHESION

The interaction of drop profile with membrane surface was detected with a microscope and the contact angle was analyzed with a goniometer. By this method, advancing contact angle can be measured by enhancing the drop volume and angle reducing the drop volume [235]. Figure 2.27 represented the contact angle instrument and representative image.



Figure 2.27 Measurement technique of Digi Drop[235].

2.5. SURFACE ROUGHNESS EFFECT ON ADHESION BEHAVIOR

Roughness has important effects in many physical phenomena, such as wettability super-hydrophobic surfaces. In adhesion science, it is empirically known that roughness can either decrease or increase adhesion (structural adhesives on materials).

In the first case, the first research [236,237] involved modeling the contact between a solid-elastic surface and a surface with random roughness. However, the composition of the material must be taken into account to understand how energy is dissipated during the detachment. This study [238,239] showed that the adhesion between a cylinder with a random roughness and a surface may be maximum depending on the amplitude of the roughness [240].

The effect of roughness on wettability has often been studied from a theoretical point of view on the basis of physics and thermodynamics. Studies have been carried out on surfaces whose geometry is created and controlled. However, these studies are difficult to transpose to real surfaces. In fact, they involve computable parameters, considering the geometrically organized surface [241]. On the actual surface, the value of the angle of contact was measured. The relations obtained from the variation of the angle of contact as a function of Sq (Root mean square height (Sq)) are different

CHAPTER.2 THIN FILMS AND ADHESION

according to the material concerned. They show that the material, implying surface chemistry, influences the contact angle.

In another case, common surfaces such as metals, glasses or ceramics due to their strong chemical bonds (metallic, ionic or covalent) usually show very high values of surface energy and are completely wetted by water. In comparison, surfaces of polymers with low-energy forces (for ex. Van der Waals forces) show very low surface energy, and therefore are not wetted by water.

It is important to note that roughness of the solid plays an important role in the surface

Wettability [242]. This influence was described by Robert N. Wenzel (2.12) using a simple formula:

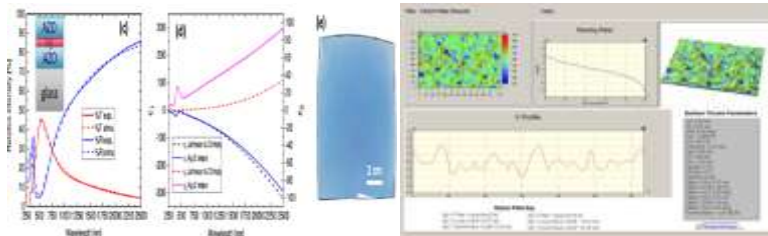
$$\cos \theta^* = r \times \cos \theta \quad (2.12)$$

Where θ^* is the measured contact angle, θ is the measured contact angle for a smooth surface and, r is the roughness factor of the true area of the solid surface of the apparent area.

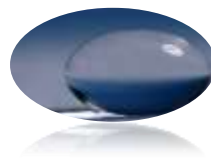
$$r = \frac{\text{actual surface area}}{\text{projected surface area}} \quad (2.13)$$

The roughness factor (r) increases the contact angle for hydrophobic surfaces and decreases its value for hydrophilic surfaces, so a rough hydrophobic material becomes more hydrophobic while a hydrophilic one becomes more hydrophilic. This equation shows the importance of the material roughness control for comparison of the wettability of different materials [243].

CHAPTER. 3



PRACTICAL STUDY



CHAPTER.3PRACTICAL STUDY

3. PRACTICAL STUDY

3.1. SUBJECT

This study aims to study the storage duration, environment and the roughness on the thin film's adhesion behavior.Indeed, storage conditions and surface quality, can have an effect on the optical materials and their performances and then can influences the adhesion of the thin films very used in the optical filed.

For that, storage duration of optical materials and their surface quality were investigated, as well as the adhesion behavior of Zinc Sulfide and Silica thin films.

Consequently, optical materials were treated and stored, then they were characterized.

3.2. MATERIALS AND DEVICES

In order to carry out our study we used several means and materials in this a study:

- Optical materials type: Flint ,Crown (Dense Flint SF2 and Fluorite Crown FK),Borosilicate Crown BK7 supplier (SHOTT GMBH),Poly Methyl Methacrylate PMMA, Soda lime glass (SL), B270,polycarbonate (PC).
- Solvents: distilled water, N-octane, Tin dioxide(SnO_2), Titanium dioxide(TiO_2).
- Alumina abrasive grains: 80, 60, 14, and 3 μm .
- Cerium oxide Abrasive grains: 1 μm .
- Silica Abrasive grains :60 nm.
- Polishes: Polyurethane.
- Ultrasonic cleaning apparatus.
- Lapping and polishing machine.
- Abbe Refractometer .
- Optical profilometry .
- AFM instrument.
- Infrared Absorption Spectra (FTIR).
- Raman spectroscopy.
- Digi Drop instrument.
- Scratch test instrument.
- UV-visible spectrophotometer.
- Optical interferometer.
- Total integrated scattering(TIS) instrument.
- Photoluminescence spectroscopy.

CHAPTER.3PRACTICAL STUDY

3.3. STORAGE EFFECT ON THE OPTICAL MATERIALS

3.3.1. *Experimental procedure*

3.3.1.1. *Samples preparation:*

For the SF2, FK, BK7, and PMMA we have prepared cylindrical samples (ϕ 22 mm \times 15 mm). All the samples were lapped using free alumina abrasive grains (80, 60, 14, and 3 μ m successively). Then, a number of SF2 and FK samples were polished using 60 nm silica and 1 μ m cerium oxide slurries. Indeed BK7, PMMA, SL, B270, and PC were polished using 1 μ m cerium oxide slurry. SF2, FK, BK7, and PMMA substrates were polished for fourteen minutes (optimal polishing time) by step of two minutes.

After polishing, the material surfaces were cleaned using an ultrasonic cleaner for 15 minutes in acetone and distilled water solutions. The last operation was the storage of the optical materials, firstly the SF2 and FK were stored in the Colloidal Silica premixed solution (CMP solution), and also the storage of BK7 and PMMA was in special solution (diamond solution) in the same conditions for 3 years. Finally, SL, B270, and PC samples were stored in the air.

The storage solutions of the CMP and Diamond are abbreviated in Table 3.1.

CMP solution	CK solution
Diamond solution	PEG solution

Table 3.1. Abbreviations of the used solutions.

3.3.1.2. *Characterization procedure:*

3.3.1.2.1. SF2 and FK

The surface roughness ((Sq) root mean square height) of the stored glasses was measured for each polishing time using the optical profilometry (ZDotTM Zeta-20). The surface topography was visualized using the AFM (Nanotech Electronic Mod Cervantes). The used glasses were characterized by the measurement of both optical and physical properties. Thus, Abbe number and the refraction index were measured by Abbe Refractometer (Novex –Holland. Model 98.490).

3.3.1.2.1. 1. Optical profilometry:

The ZetaTM -20 is a fully integrated optical profiling microscope that provides 3D metrology and imaging capability in a compact. Simultaneously collects high-resolution 3D roughness and waviness on smooth to very rough surfaces, with a transparent film thickness from 30nm to 100 μ m, and capture defects greater than 1 μ m.

3.3.1.2.1. 2. AFM intstrument:

The AFM verified the surface topography, with fast extended-range is 5-20 \times , and features large 100 μ m X-Y & 12 μ m Z ranges.

CHAPTER.3PRACTICAL STUDY

3.3.1.2.1. 3. Abbe Refractometer:

The instrument is equipped with a built-in thermometer and water connection to control fluid temperatures. Equipped with a Brix and a Refraction Index (RI) scale and supplied with a test plate with 0.5 ml calibration liquid, with Range(n_D): 1.30000-1.70000 , resolution of 0.00001, and temperature Range (Min. 0.1°C).

3.3.1.2.2. BK7 and PMMA

The Roughness (R_q) root mean square and topography of the substrates were measured using two techniques; TIS(Total integrated scattering) and the optical interferometer instrument (Leica Map DCM 7.3.7904) used before and after the storage in PEG solution. Optical material transmittance was measured by UV–visible spectrophotometer(Carl Zeiss Spectroscopy GMBH). Thus, the refraction index and Abbe number were measured by Abbe Refractometer (Novex –Holland. Model 98.490).

3.3.1.2.2.1. Storage effect on the roughness (R_q):

The samples were characterized by TIS technique to measure the roughness (R_q), and their surfaces were visualized by optical Interferometry.

A. *TIS technique*

Total integrated scattering (TIS) technique was established according to the Experimental setup consists of a light source. It is an area-integrating method that uses the total integrated light scatter for calculating the square roughness (R_q) measurements of the samples (BK7 and PMMA) before and after storage.

Usually He-Ne laser of wavelength $\lambda = 632.8$ nm, the laser beam is directed at an angle $\theta = 8.36^\circ$ spatially filtered , enlarged by the objective of microscope, and the converging lens is divided by the beam splitter into two beams of equal intensity. The first beam crosses the cube and it is measured by a photodiode detector giving the incident intensity I_i . The second beam falls at normal incidence on the sample surface that reflects specularly a portion of this beam, it is measured by the detector giving the reflected intensity I_r and the other part is scattered, collected by the integrating sphere and measured by the detector giving the scattered intensity I_d presented in Figure 3.1.

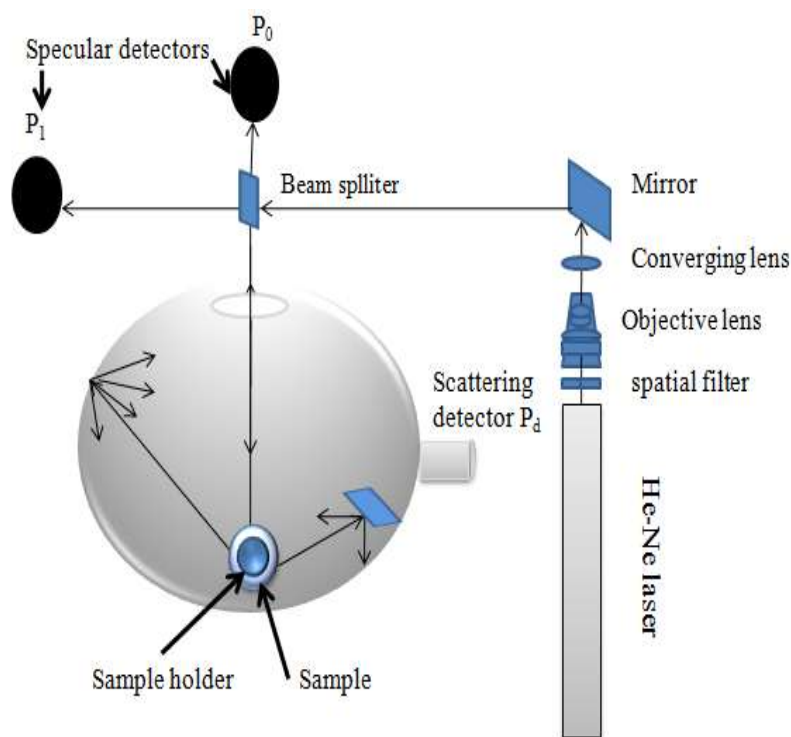


Figure 3.1. Experimental setup of total integrated scattering (TIS).

B. Optical Interferometry

Optical interferometry uses the interference of electromagnetic waves with wavelengths λ in the range of visible light or nearby. The wavelength range is approximately located between 10^{-7} and 10^{-6} m.

3.3.1.2.2.2. UV–visible spectrophotometer:

With the UV–visible spectrophotometer, transmission and reflection measurements can be carried out quickly and with high accuracy in spectral range 400-800 nm (visible range). By measuring the light transmission, the quality of an adhesive bond or the transparency of a laminate can be determined and described, and conclusions can be drawn about the resistance of the materials to external influences.

3.3.1.3. Preparation of the solution:

3.3.1.3.1. Silica sols Preparation

For the thin film deposition, Silica solutions were readied. Indeed, they were prepared by hydrolysis and polymerization reactions of TEOS by mixing the precursor materials (EtOH: Ethanol, H₂O: distilled water and TEOS: tetraethoxysilane) in the molar ratio with different concentrations:

EtOH: H₂O:(20%)TEOS = 13:5:1 ; PH=1.45

EtOH: H₂O: (30%)TEOS = 8:3:1; PH=1.5

EtOH : H₂O: (40%)TEOS = 5:2:1 ; PH =1.6

CHAPTER.3PRACTICAL STUDY

EtOH : H₂O: (60%)TEOS = 3:1:1 ;PH=1.67

A pre-mixing of the solutions was done in a magnetic stirrer at 26 °C of temperature during 30 minutes. Then, mixing was continued for each solution in the same conditions to obtain its gelation state determined using the Infrared Absorption Spectra (FTIR) technique. In fact, different times were obtained for every solution, i.e. 96 hours for 20%, 44.5 hours for 30%, 48.5 hours for 40% and 59 hours for 60%, the last concentration (60%) was obtained in a solid state then it was not used in deposition.

The different solutions of the Silica sol-gel with different concentrations are abbreviated in Table 3.2.

Silica concentration 20%	SG20
Silica concentration 30%	SG30
Silica concentration 40%	SG40
Silica concentration 60%	SG60

Table 3.2. Abbreviations of the prepared Silica sol-gel solutions.

3.3.1.3.2. Zinc Sulfide preparation sols

Solution of Na₂S with 25ml volume and (1 M) molar mass added to 25 ml (0.5 M) zinc acetate solution drop by drop with continuous stirring. The solution was then mixed and heated to 90°C forever 1 hours using a hot plate with a temperature controlled chemical bath deposition method (CBD), six dips of 30 min duration were given to the substrate. The used molar ratio with different concentrations:

(20%) Zn: Na₂S = 1:4 ;PH=4.79

(30%) Zn: Na₂S = 3:7 ;PH=5.12

(40%) Zn: Na₂S = 2:3 ;PH=5.83

The different Zinc Sulfide solutions concentrations are abbreviated in Table 3.3.

CHAPTER.3PRACTICAL STUDY

Zinc Sulfide concentration 20%	ZnS20
Zinc Sulfide concentration 30%	ZnS30
Zinc Sulfide concentration 40%	ZnS40

Table3.3. Abbreviations of the prepared Zinc Sulfide solutions.

Then, the two concentrations of ZnS 30 and ZnS40 were got in a solid state, and then they were not used in deposition.

3.3.1.4. Digi Drop measurement:

The measurement of the contact angle was done via the falling drop method, where a Digi Drop device was used (Krüss Easy Drop Standard). A droplet about 2 μ l of the prepared sol-gel solutions (SG20 and SG30) was deposited on the optical glass surfaces (SF2 and FK). The SG20 and SG30 solutions were deposited both on the glasses polished using Silica and cerium oxide polishing slurry. In fact, the used solvents: distilled water, N-octane, Tin dioxide(SnO_2), and Titanium dioxide(TiO_2) were deposited on the glasses substrates (SL, B270, and PC) with the Digi Drop technique .

3.3.1.5. Thin film used:

3.3.1.5.1. Silica thin film

The thin films were prepared using deep coating methods. The FK and SF2 optical glass substrates of 1mm thickness were introduced in the solution at 2mm/min of deep speed. After one minute of maintaining, the samples were raised up out of the bath in the same speed. Then, the annealing process was performed in a furnace where the heating temperature was fixed at 450°C (optimal temperature for the sol-gel solutions) obtained by the 21°C/min of heating speed. The samples were maintained for one hour at 450°C then cooled with the same speed (21°C/min).

After deposition, the thin film quality was controlled by morphological and surface roughness characterization using optical profilometry (ZDotTM Zeta-20) and AFM (Nanotech Electronic Mod Cervantes).

3.3.1.5.2. Chemical structural properties

The chemical structural properties of the deposited thin films were verified using the Raman Spectroscopy and the FTIR (Fourier Transform Infrared Spectroscopy). The used Raman device was Renishaw InVia equipped with green Argon laser (532nm). Its optical resolution was about 1 μ m and its objective magnification was about 100 \times . The Infrared Absorption Spectra of the Silica

CHAPTER.3PRACTICAL STUDY

sol-gel were obtained using a Perkin-Elmer FTIR spectrometer (Model Spectrum BX (USA)).The analysed spectrum was fixed between 600 and 4000 cm^{-1} , and was working in the Attenuated Total Reflectance (ATR) mode. Ten scans were measured for each sample, subtracting the baseline in all cases.

3.3.1.5.3. Coating adherence behavior

The coating adherence was verified by scratch test, where a Universal Indentation and Scratch Tester Model device (APEX-1) was used. A Rockwell diamond indenture of 200 μm diameter was displaced on the thin film surface, loaded by variable nominal force from 0.22 N to 44 N with speed 2mm/min. The test was repeated five times for each sample.

3.3.1.5.4. Zinc Sulfide thin film

The Zinc Sulfide thin film was prepared using chemical bath deposition technique, and after each dip the BK7and PMMA sample was taken out and washed with distilled water and dried. After six dips the substrates were dried in a vacuum oven at 85 $^{\circ}\text{C}$ for 2h.

For the band gap of ZnS were measured by photoluminescence spectroscopy (Leica) successfully. The liquid of surface tension measured with Digi Drop ($\gamma_{lv}\text{ZnS20}=1.672\text{N/m}$).

3.3.1.6. Adhesion and cohesion measurement:

In order to study the Spreading coefficient effect (S) of the deposited liquids (distilled water, N-octane, Tin dioxide(SnO_2), Titanium dioxide(TiO_2)on the optical materials,Soda lime glass(SL), polycarbonate (PC),and B270 .The samples used were storage for 4 years in our institute, the adhesion and cohesion forces were determined on the basis of the superficial tensions for each liquid given in the following table 3.4.

Liquid	Distilled water	TiO_2	N- octane	SnO_2
Superficial tension(N/m)	72×10^{-3}	1.05	21.8×10^{-3}	1.4
Density(g/ml)(25 $^{\circ}\text{C}$)	0.9970	4.23	0.6979	6.99
Molar mass(g/mol)(25 $^{\circ}\text{C}$)	18	79.87	114.23	150.70

Table 3.4. Superficial tension of deposited liquids.

The parameters of the energies W_{ad} (3.1), W_{co} (3.2) and S(3.3) are calculated by the following relations[244]:

$$W_{ad} = \gamma_{sv} - (\gamma_{sl} + \gamma_{lv}) = \gamma_{lv}(1 + \cos\theta) \quad (3.1)$$

$$W_{co} = 2\gamma_{lv} \quad (3.2)$$

$$S = W_{ad} - W_{co} \quad (3.3)$$

CHAPTER.3 PRACTICAL STUDY

With:

W_{ad} : The adhesion force.

W_{co} : The cohesion force.

γ_{sv} : The solid- vapor superficial tension.

γ_{lv} : The liquid – vapor superficial tension.

γ_{sl} : The solid- liquid superficial tension.

S: Spreading coefficient with: $S \geq 0$: Good adhesion and $S < 0$: Bad adhesion.

3.4. RESULTS AND DISCUSSION

3.4.1. Storage effect on the sample's optical proprieties

Optical proprieties of the stored samples are summarized Table 3.5. It was found that there is a difference between the properties of the optical materials, which will be due to the changes caused by storage duration and its environment.

Glass	$V_d(\text{supplier})$	$V_d(\text{measured})$	$n_d(\text{supplier})$	$n_d(\text{Measured})$	Observation
SF2	34.440	34.5454 ± 0.12	1.6178	1.6656 ± 0.15	Storage in CK solution
FK	61.250	61.3543 ± 0.11	1.4551	1.4725 ± 0.18	Storage in CK solution
BK7	64.170	64.3242 ± 0.114	1.5248	1.5364 ± 0.17	Storage in PEG solution
PMMA	58.014	58.2535 ± 0.123	1.4891	1.5123 ± 0.14	Storage in PEG solution
SL	63.454	63.5153 ± 0.13	1.5234	1.5345 ± 0.17	Air storage
B270	58.532	58.6227 ± 0.14	1.5228	1.5351 ± 0.15	Air storage
PC	30.213	30.4432 ± 0.15	1.5871	1.5942 ± 0.14	Air storage

Table 3.5. Refractive index and Abbe number of the used samples.

According to the results in Table 3.5, a difference was noticed between the optical materials properties, probably related to their chemical compositions, changed by the molecule effect of the liquids used, also the superficial layer of optical materials. In addition, the storage time and nature

CHAPTER.3PRACTICAL STUDY

of solutions were elucidated by the difference to two decimal places between the measured and the - supplied values.

3.4.2 .Silica sol-gel solution characterization

The results of the FTIR spectrum were illustrated in Figures 3.2-3.5, to analyze the gelation state during the Silica sol-gel solutions preparations.

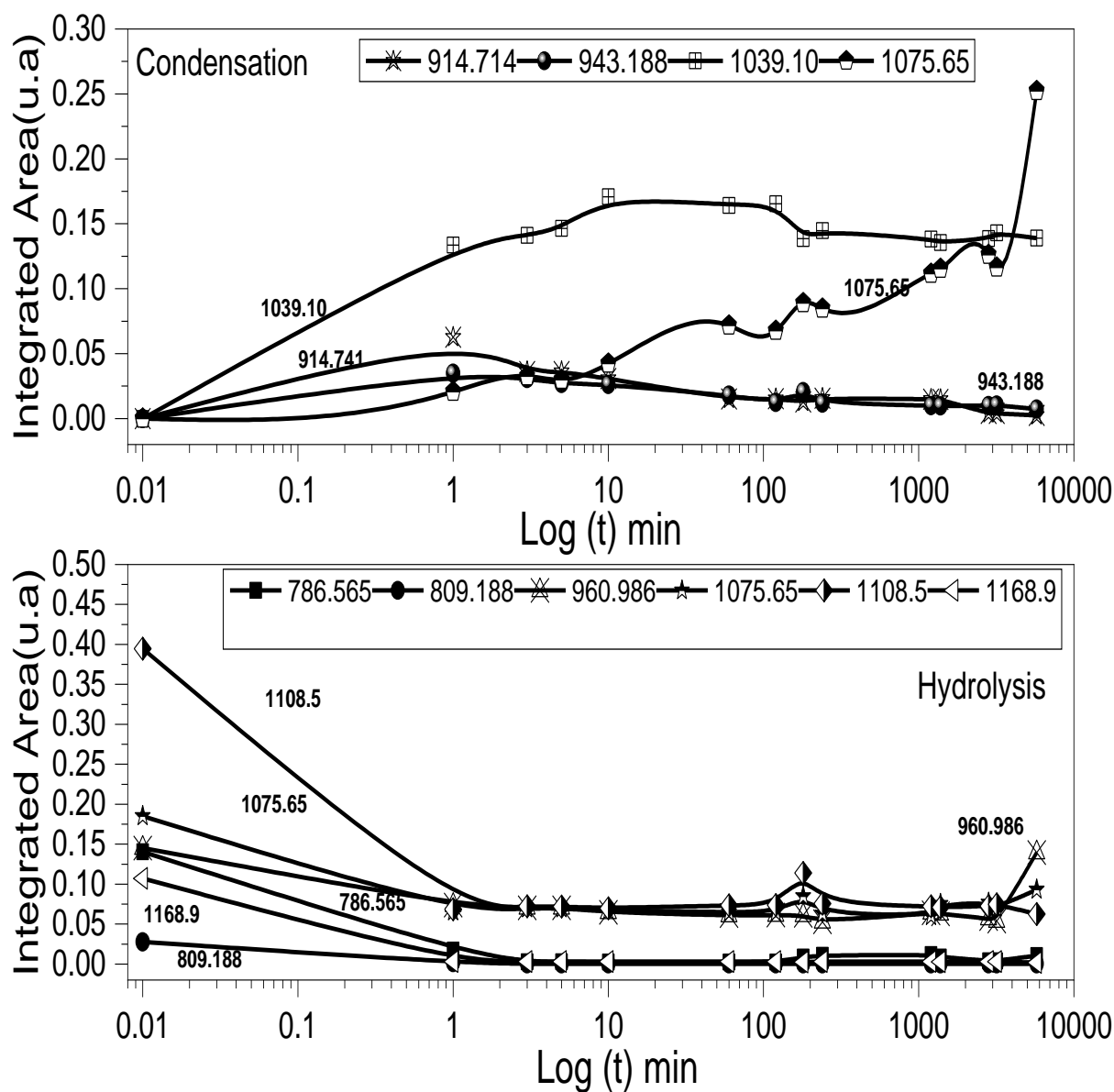


Figure 3.2. FTIR spectrum of the SG20 concentration.

CHAPTER.3PRACTICAL STUDY

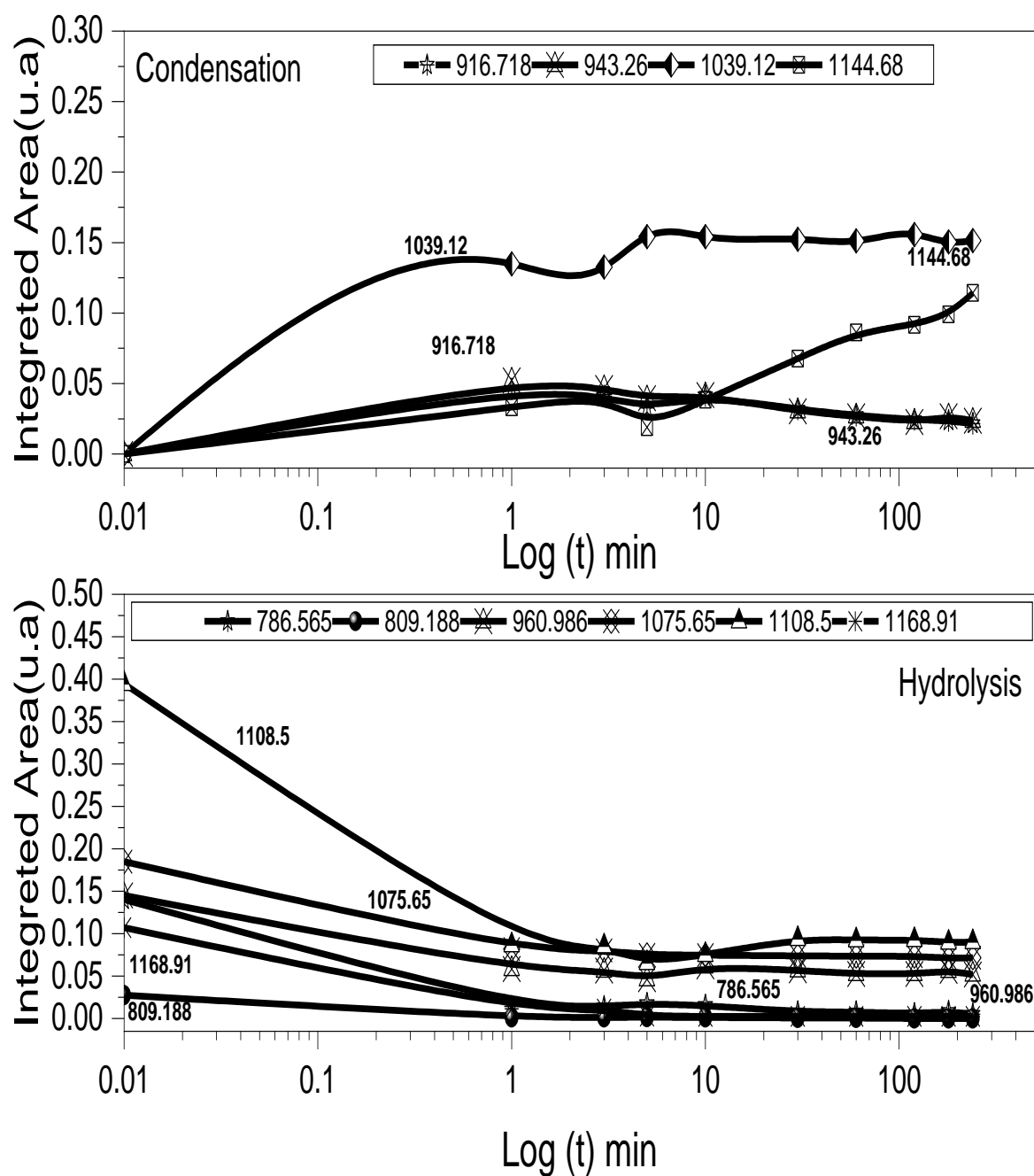


Figure 3.3. FTIR spectrum of SG30 concentration.

CHAPTER.3PRACTICAL STUDY

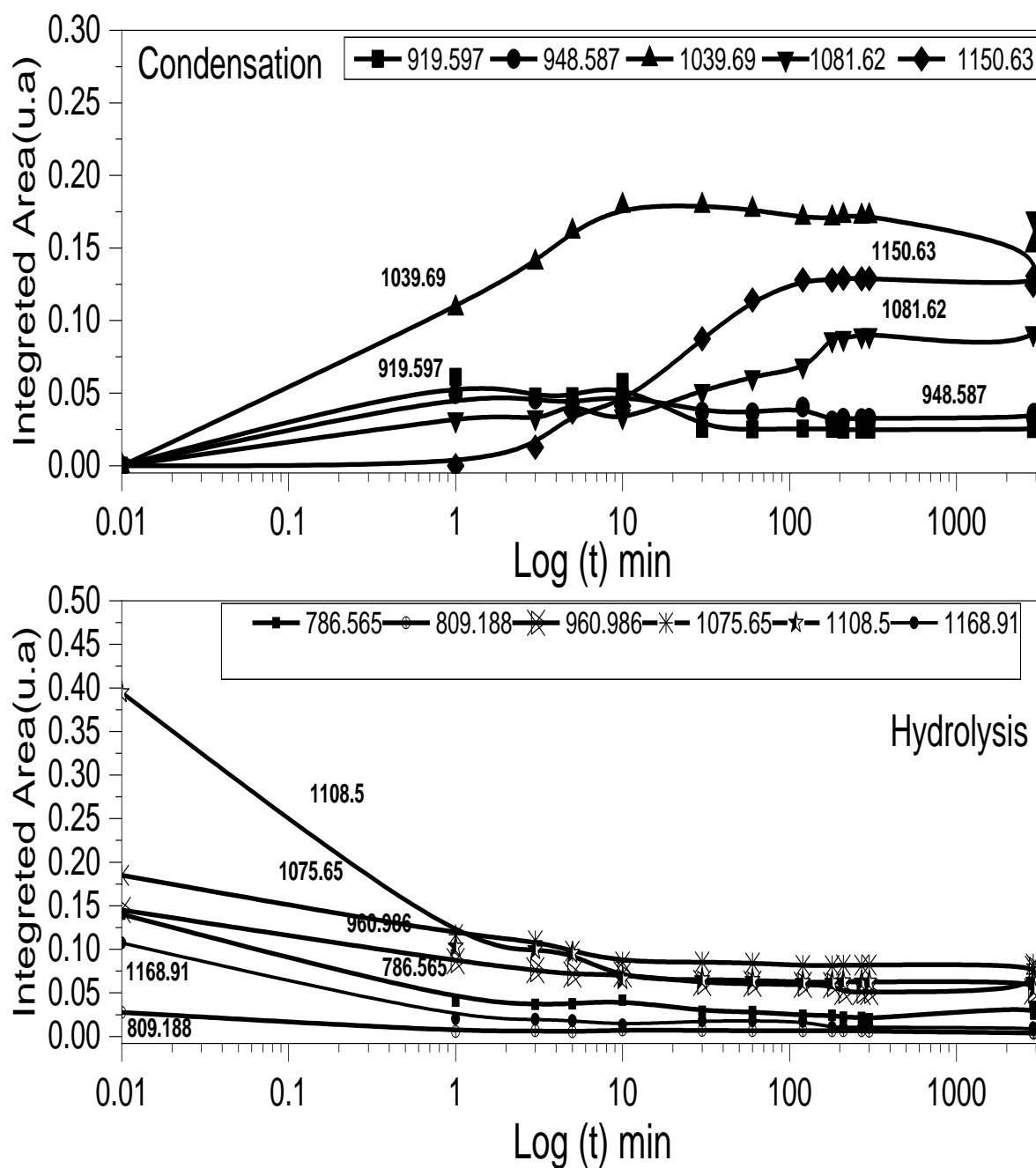


Figure 3.4.FTIR spectrum of SG40 concentration.

CHAPTER.3PRACTICAL STUDY

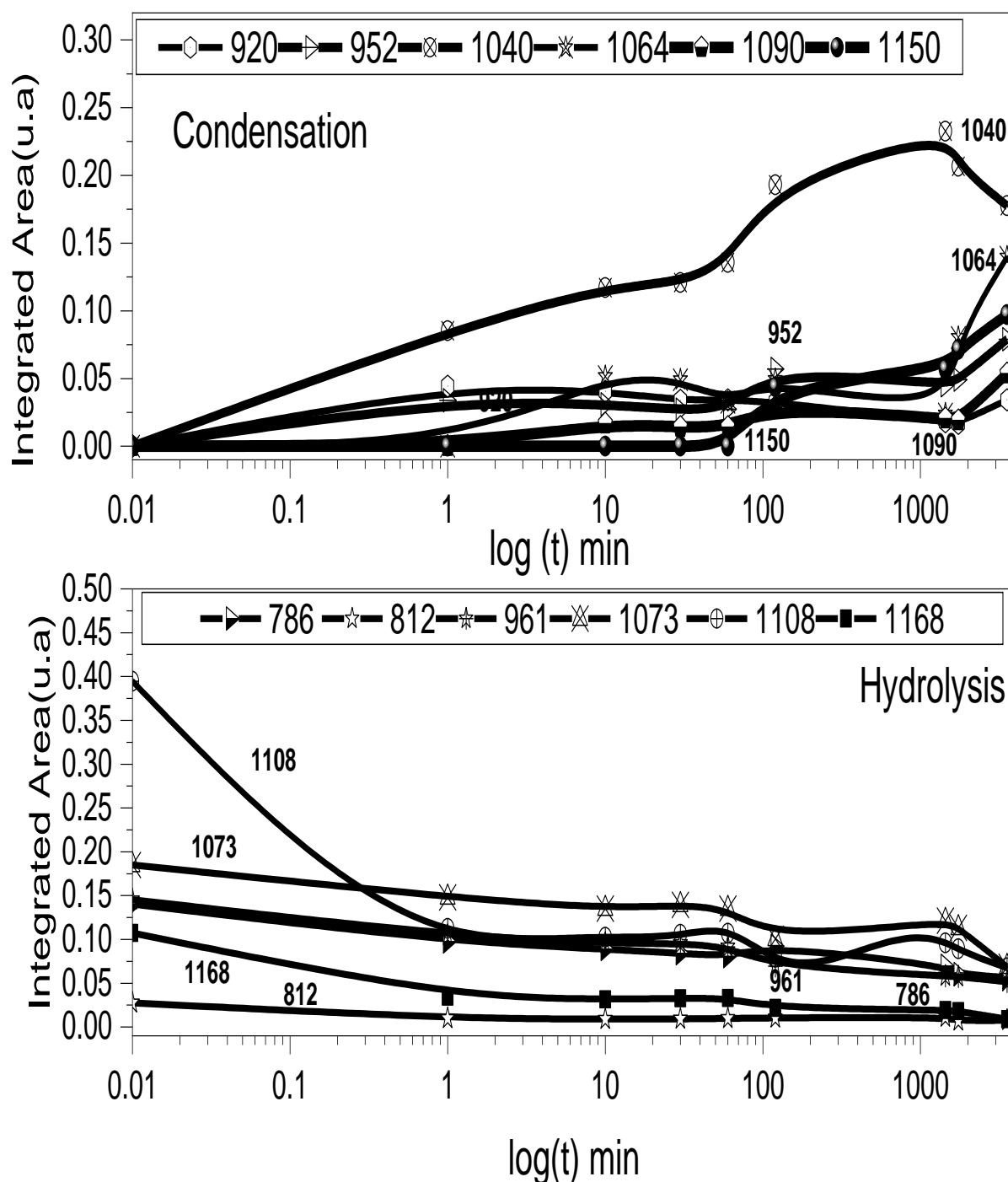


Figure 3.5. FTIR spectrum of SG60 concentration.

On the hydrolysis curves (see Figures 3.2- 3.5) of TEOS (Tetraethoxysilane) for SG20, SG30, SG40, and SG60 it is illustrated that the bands of TEOS decreased with time and a reaction between TEOS and H₂O occurs. When the TEOS particle was totally hydrolysed, all bands have reached zero value. In this case, only two bands have reached zero: 809 and 1168 cm⁻¹. At the similar positions of the TEOS bands, there are other bands of (Siloxane) Si-O-Si bonds that appear simultaneously. Therefore, the bands at 786, 960, 1075, and 1108 cm⁻¹ are due to both TEOS and

CHAPTER.3 PRACTICAL STUDY

Si-O-Si bond. Afterward, when the TEOS bands must decrease due to the hydrolysis, new Si-O-Si bonds are being formed. Similar results were obtained in previous studies [245-246].

On the condensation plots, Si-OH (Orthosilicic acid) groups SG20, SG30, SG40, and SG60 were formed from TEOS hydrolysis. These bands appeared at 914, 920, 943, 952, 961, 1039, 1063, 1081, and 1150 cm^{-1} . However, there are also Si-O-Si bands at 786, 960, 1075 and 1108 cm^{-1} , the positions of which are not the same. The OCH_2CH_3 band of TEOS at 786 cm^{-1} and the SiO_4 band of Silica at 800 cm^{-1} are very close because of their relation to the same vibration Si-O₄ but, in one case, the O atom is bonded to CH_2CH_3 groups and, in the other case, it is too attached to other Si atoms. A similar explanation occurs for the 952 and 960 cm^{-1} bands; the 952 cm^{-1} band of Si-O CH_2CH_3 (Tetraethyl orthosilicate) of TEOS overlapped with the 960 cm^{-1} band of Si-OH groups. For the evolution of the Si-O-Si bands, the 920 cm^{-1} corresponded to Si-(OH)₂ groups, the 952 cm^{-1} to Si-OH groups, the 1039 cm^{-1} to Si-O-Si bonds in linear or even planar configuration, the 1063 cm^{-1} to Si-O-Si bonds in planar or three-dimensional setups, and both the 1081 and 1150 cm^{-1} bands could be attached to Si-O-Si bonds in three-dimensional configurations, but one consists of symmetric vibrations and the other one is an anti-symmetric vibrations, so that the 1039 and 1063 cm^{-1} bands have anti-symmetric vibrations. However, they overlap with those of 1081 and 1150 cm^{-1} symmetric vibration. Consequently, the Si-OH bonds (952 and 1039 cm^{-1} bands at 1 minute) demonstrate that the hydrolysis of TEOS forms Si-OH groups but not all of them are bonded to form Si-O-Si bonds.

Moreover, the 952 cm^{-1} band remained constant between 1 to 100 minutes and the 1039 cm^{-1} band increased. This indicates that when the Si-OH groups are formed, they rapidly react to form Si-O-Si bonds. However, not all Si-OH groups reacted; they rather remained in the solution until they found other Si-OH groups and then reacted to form Si-O-Si bonds.

The band at 1063 and 1081 cm^{-1} appeared in the 10th minute but their evolution was slow until the 1000th minute. This showed that the Si-OH bonds are reacting to form Si-O-Si bonds in the three-dimensional structure and that 1000 minutes are necessary for growing such 3D structures.

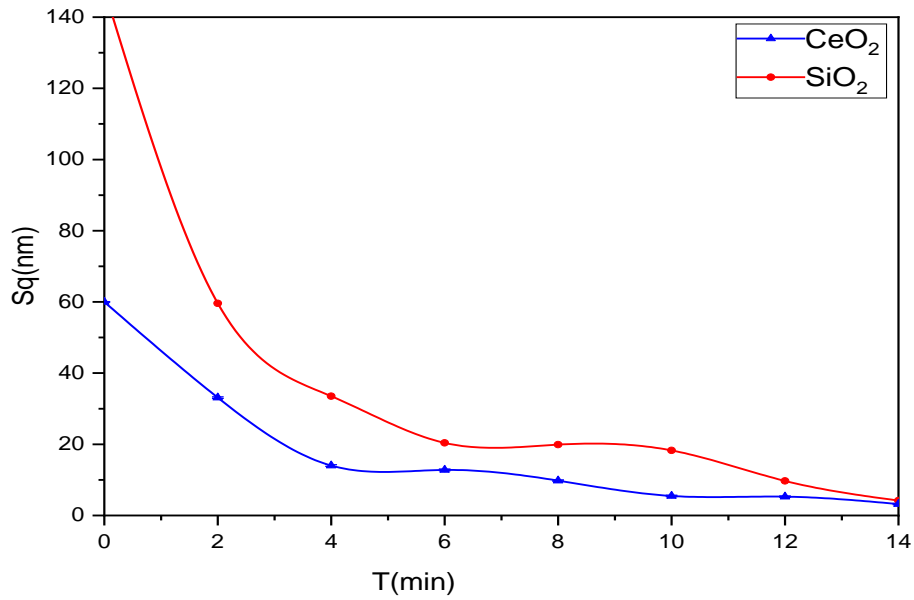
3.4.3. Surface roughness

The results illustrate a clear impact of the polishing time on the surface roughness via its decreasing when the polishing time increases. This is closely related to the removal of surface defects by the abrasive grains during the process (as the time is longer), the fact that contributes to the roughness reduction. It should be noted that the surface finish depends considerably on the nature of the polished glass and the slurry abrasive grain size. Effectively, FK glass seems to be easily polished than the SF2 with Silica slurry (see Figure 3.6 (a) and (b)), but the inverse is observed when using

CHAPTER.3PRACTICAL STUDY

the cerium oxide slurry. This can be related to the slurry composition, nature and the glasses behavior after storage.

(a)



(b)

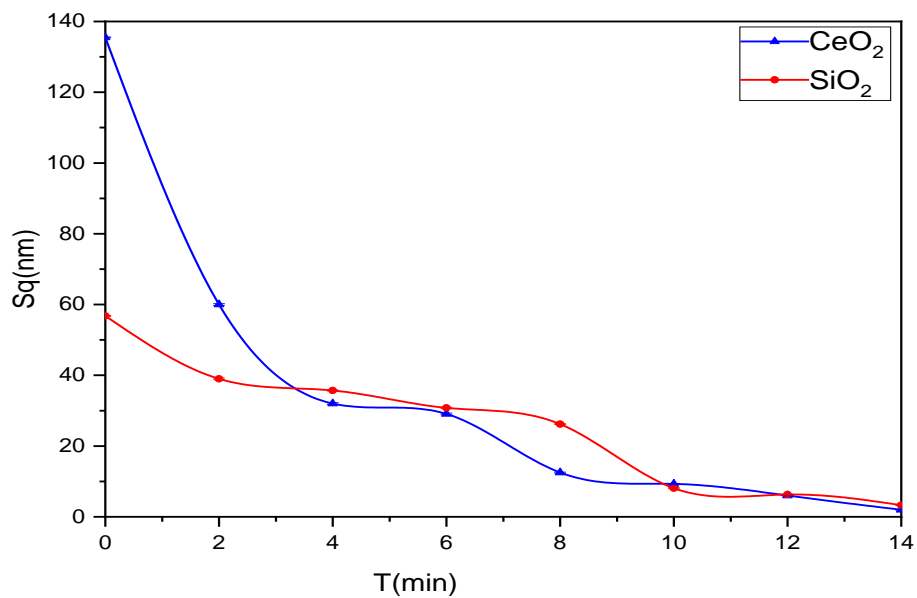


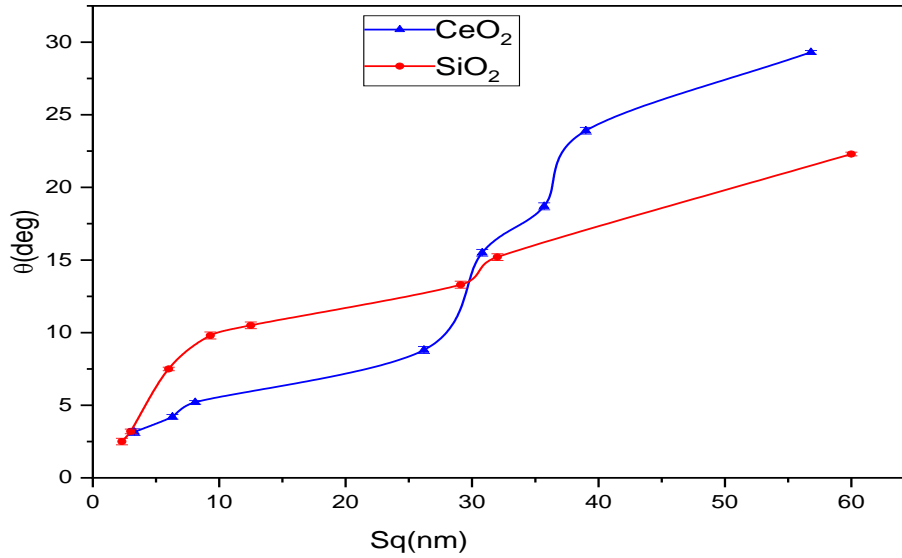
Figure 3.6. Variation of the surface roughness vs. polishing time of the glass surfaces: (a)SF2 and (b) FK.

CHAPTER.3PRACTICAL STUDY

3.4.4. Surface roughness Effect on the contact angle

The Figure 3.7 demonstrates the effect of the surface roughness on the contact angle. In this case, although FK and SF2 glasses don't have the same values. For the two types of studied glasses the curve shape indicates that the contact angle decreased when the surface roughness was lower.

(a)



(b)

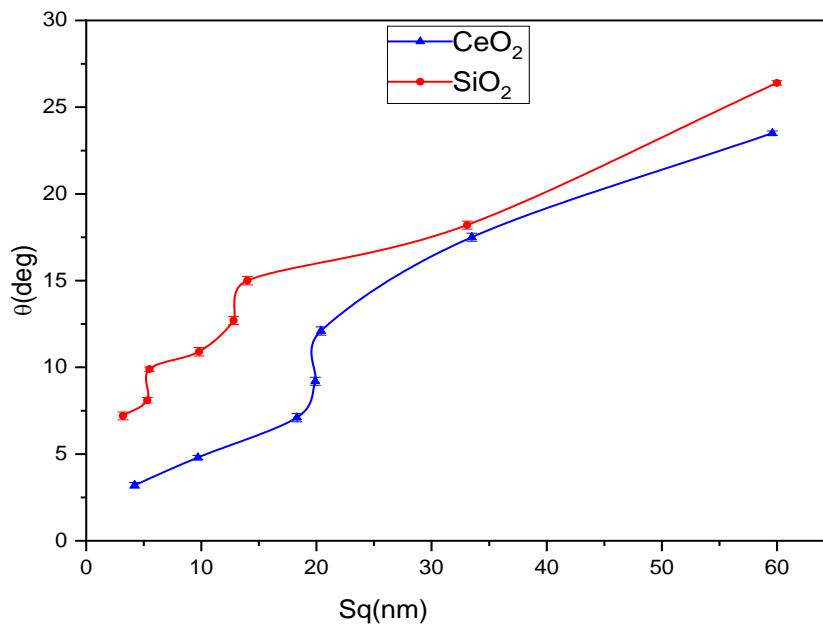
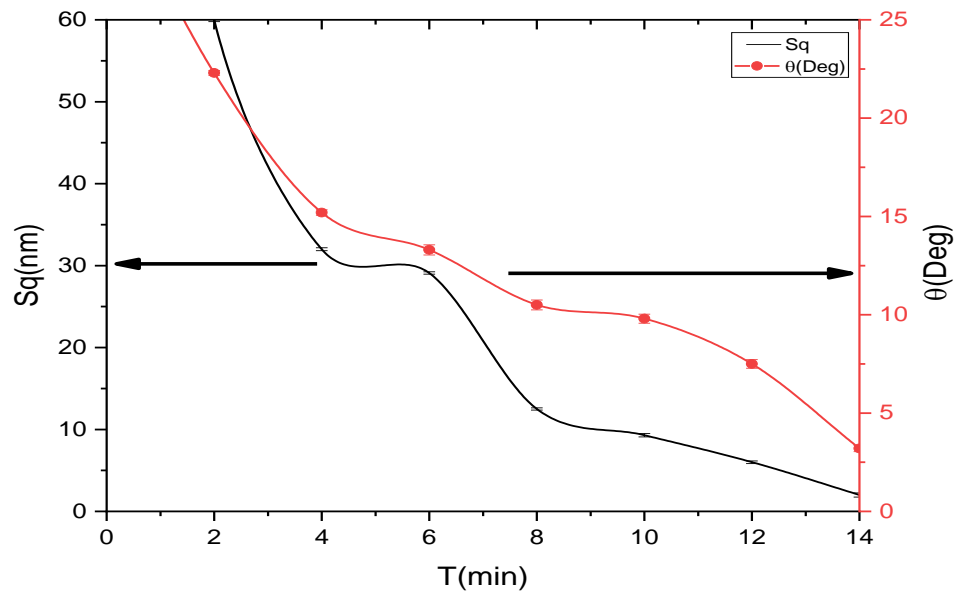


Figure 3.7. Variation of the contact angle vs. (Sq) root mean square height: (a) FK and (b) SF2. The correlation between the contact angle and the surface roughness can easily establish the effect of the surface quality on the adhesion, as shown in Figures 3.8 to 3.11.

(a)



(b)

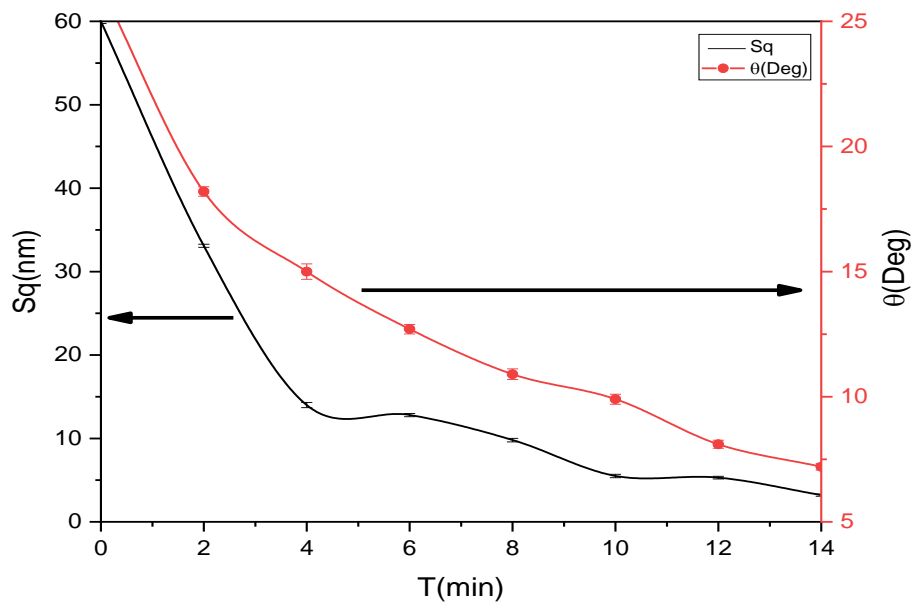
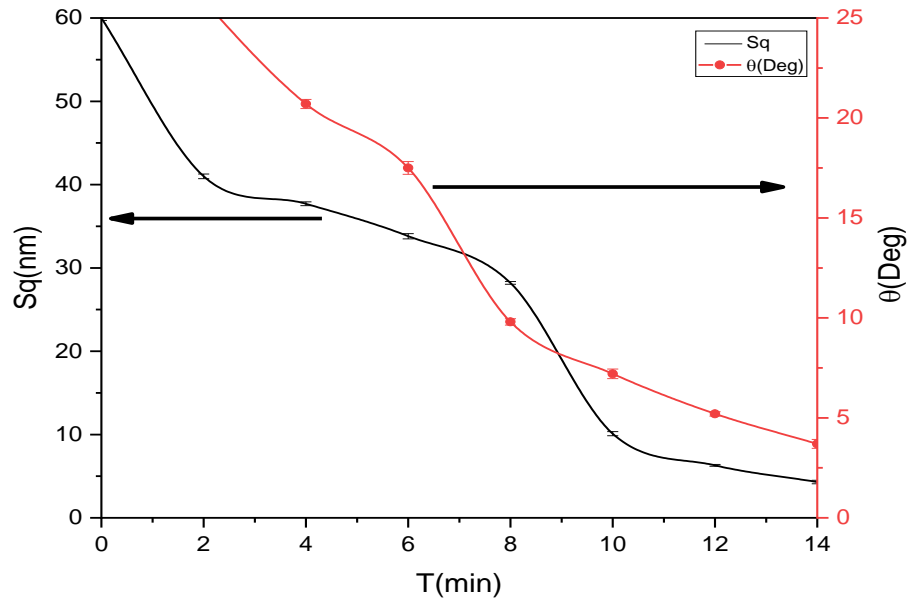


Figure 3.8. Correlation between the contact angle and the surface roughness for the SG30 concentrated on optical glass: (a) FK and (b) SF2 polished by cerium oxide slurry.

(a)



(b)

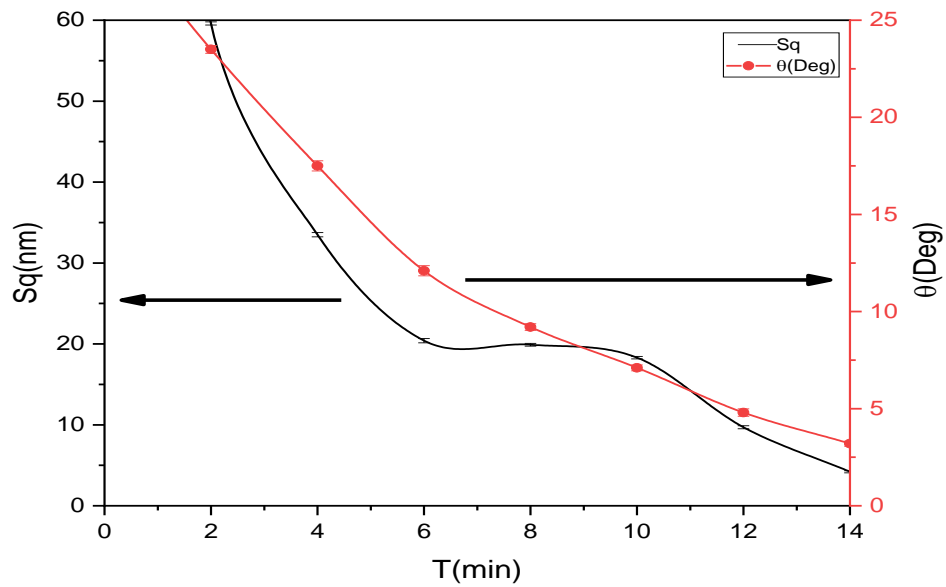
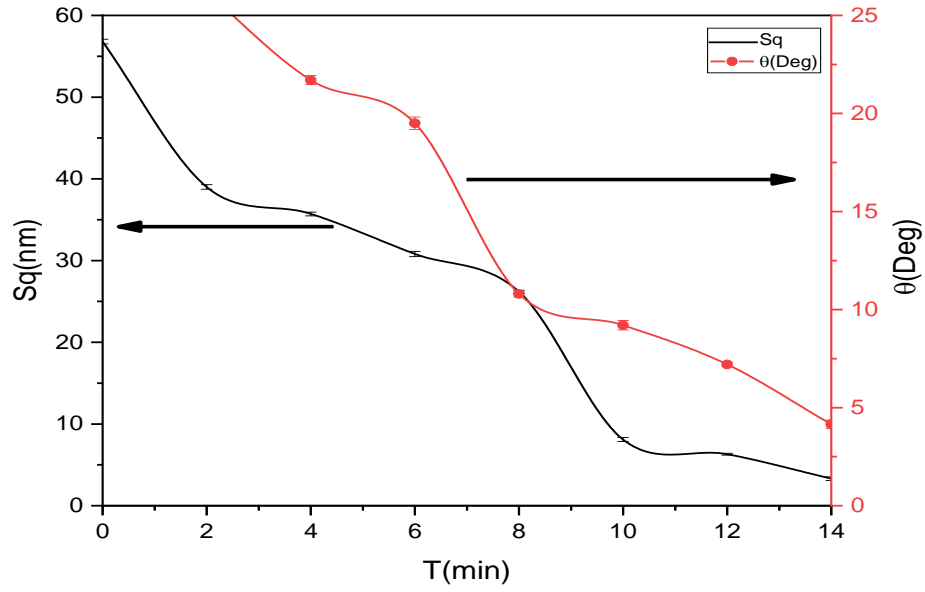


Figure 3.9. Correlation between the contact angle and the surface roughness for the SG20 Concentrated on optical glass: (a) FK and (b) SF2 polished by silica slurry.

(a)



(b)

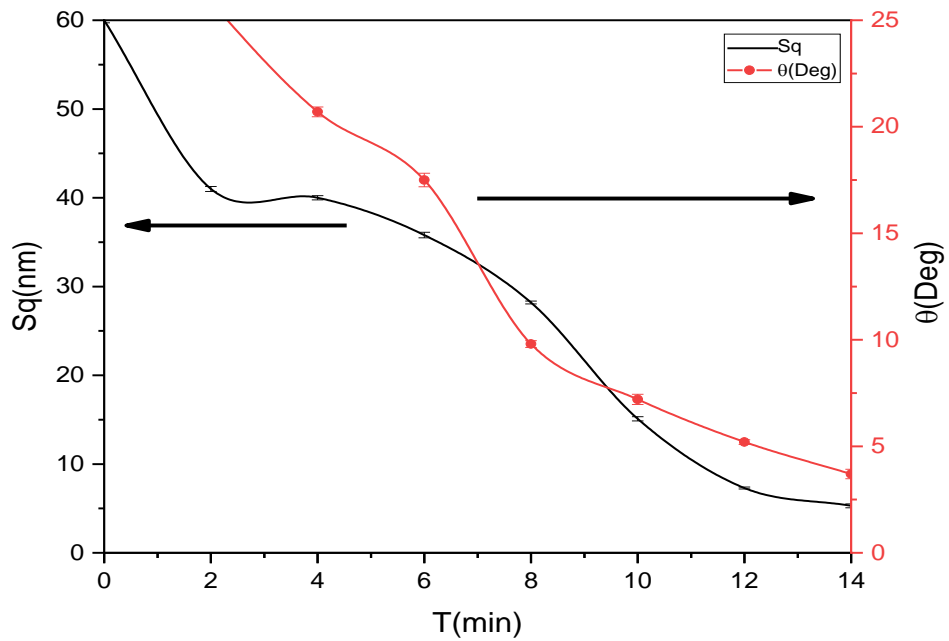
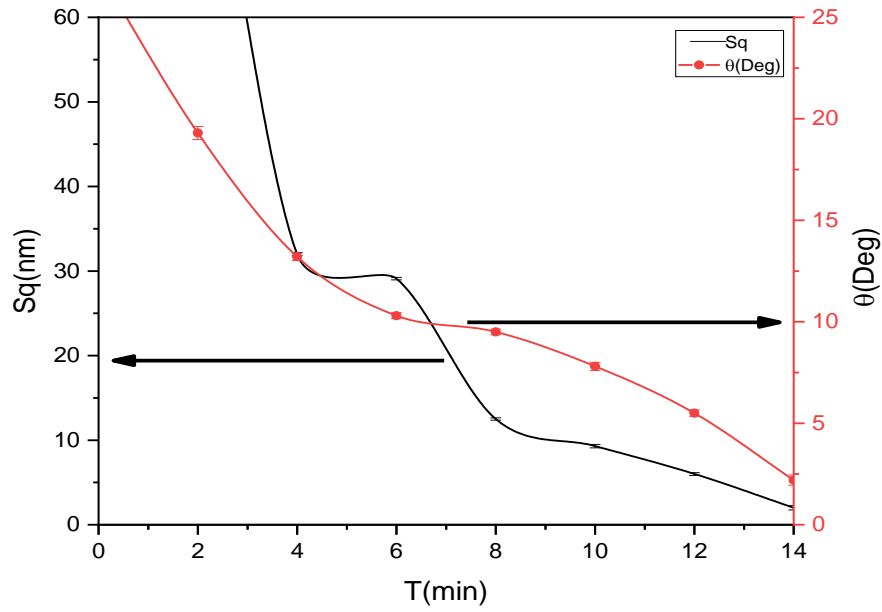


Figure 3.10. Correlation between the contact angle and the surface roughness for the SG30 Concentrated on optical glass: (a) FK and (b) SF2 polished by silica slurry.

(a)



(b)

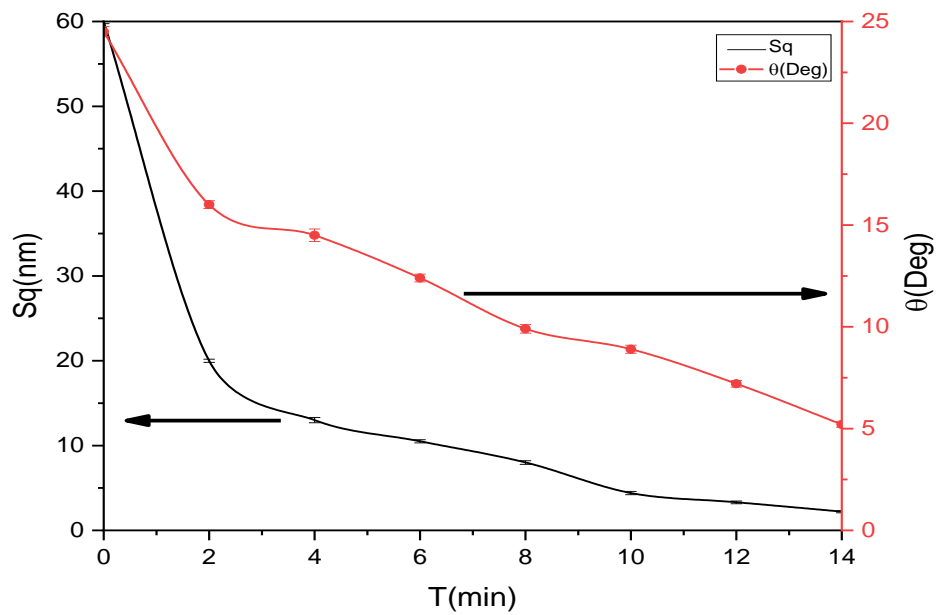


Figure 3.11. Correlation between the contact angle and the surface roughness for the SG20 concentrated on optical glass: (a) FK and (b) SF2 polished by cerium oxide slurry. The contact angle is proportional to the roughness, independently to the optical glass finishing and the used slurries. The difference may be significant in magnitude between the two types of glass.

CHAPTER.3PRACTICAL STUDY

Otherwise, it was found that the hydrophilic of the SG20 solution is better than SG30 one for the SF2 and FK.

Figures 3.12-3.13 show the variation of the contact angle during the Digi drop technique depending on the glass nature ,surface roughness, and the deposited solution.





<p>(a)</p>  <p>$Sq=5.6\pm0.25nm$ FK surfaces polished for 14min by CeO_2 slurry (SG30), before storage.</p>	<p>(b)</p>  <p>$Sq=3\pm0.2nm$ FK surfaces polished for 14 min by CeO_2 slurry, stored in CK solution (SG30)(After storage).</p>
<p>(c)</p>  <p>$Sq=5.3\pm0.2nm$ SF2 surfaces polished for 14min by CeO_2 slurry (SG30), before storage.</p>	<p>(d)</p>  <p>$Sq=2.2\pm0.2nm$ SF2 surfaces polished for 14min by CeO_2 slurry, stored in CK solution (SG30) (After storage).</p>

Figure 3.12. Effect of the glass nature: (a), (b),(c) and(d) on the contact angle of SG30.

CHAPTER.3PRACTICAL STUDY





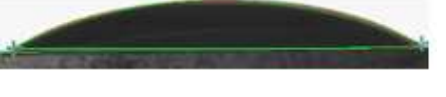

<p>(a)</p>  <p>$Sq=29.4\pm0.26$ SF2 surfaces polished for 6min by silica slurry (SG20), after storage.</p>	<p>(b)</p>  <p>$Sq=25.8\pm0.32nm$ FK surfaces polished for 6min by silica slurry (SG20), after storage.</p>
<p>(c)</p>  <p>$Sq=13.3\pm0.15nm$ SF2 surfaces polished for 10min by silica slurry (SG20), after storage</p>	<p>(d)</p>  <p>$Sq=7.1\pm0.24nm$. FK surfaces polished for 10min FK polishing with silica slurry (SG20), after storage.</p>
<p>(e)</p>  <p>$Sq=4.0\pm0.13nm$ SF2 surfaces polished for 14min by silica slurry (SG20), after storage.</p>	<p>(f)</p>  <p>$Sq=3.3\pm0.22\mu m$ FK surfaces polished for 14min FK by silica slurry (SG20), after storage.</p>

Figure 3.13. Effect of storage time :(a), (b),(c), (d),(e) and (f) on the contact angle of SG20 .

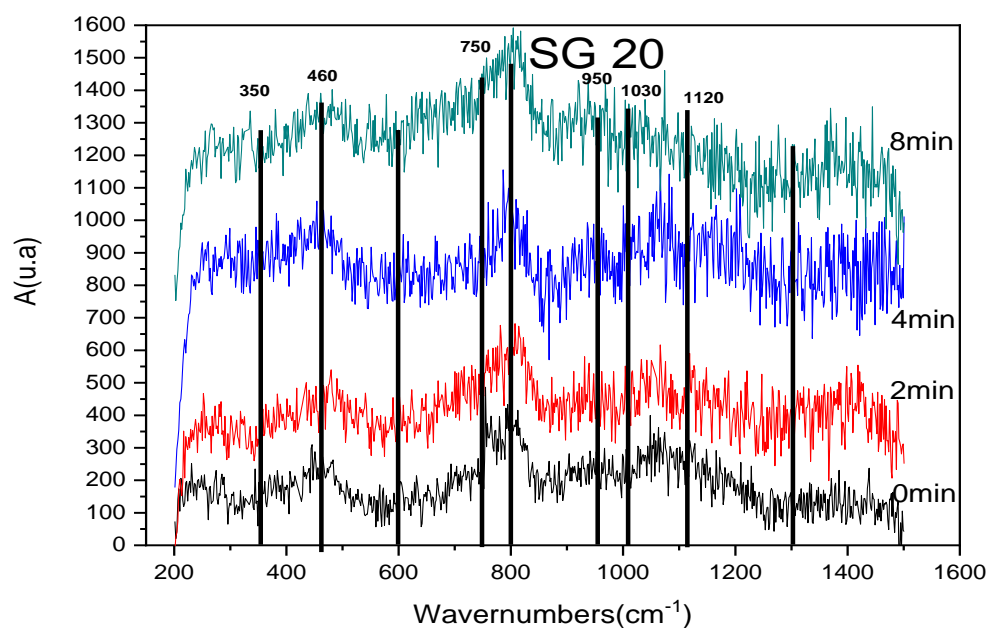
The results obtained show that the storage time of the optical glasses in the CK solution affects both the optical and the mechanical behavior of the optical glasses. This may be due to compliance with the storage conditions of the glasses and their high quality during their production. Furthermore, it was noted that there is a close relationship between the surface roughness of the polished optical glasses and the adhesion of the sol-gel solutions, and between the solution concentration and their adherence (see Figures3.12-3-13).

CHAPTER.3PRACTICAL STUDY

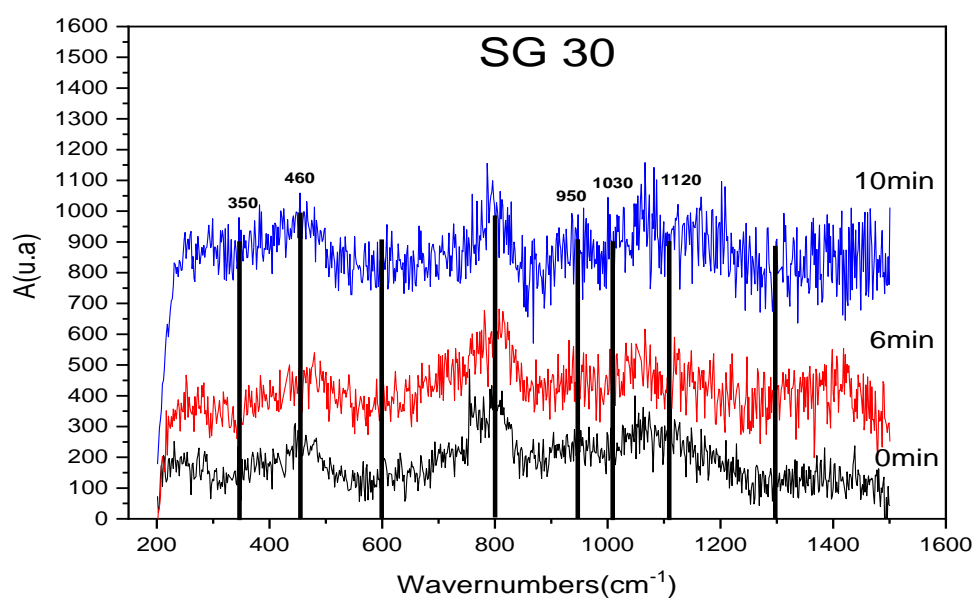
3.4.5. Coating Silica characterization

Raman diagrams are represented in Figures3.14 and3.15.

(a)



(b)



CHAPTER.3PRACTICAL STUDY

(c)

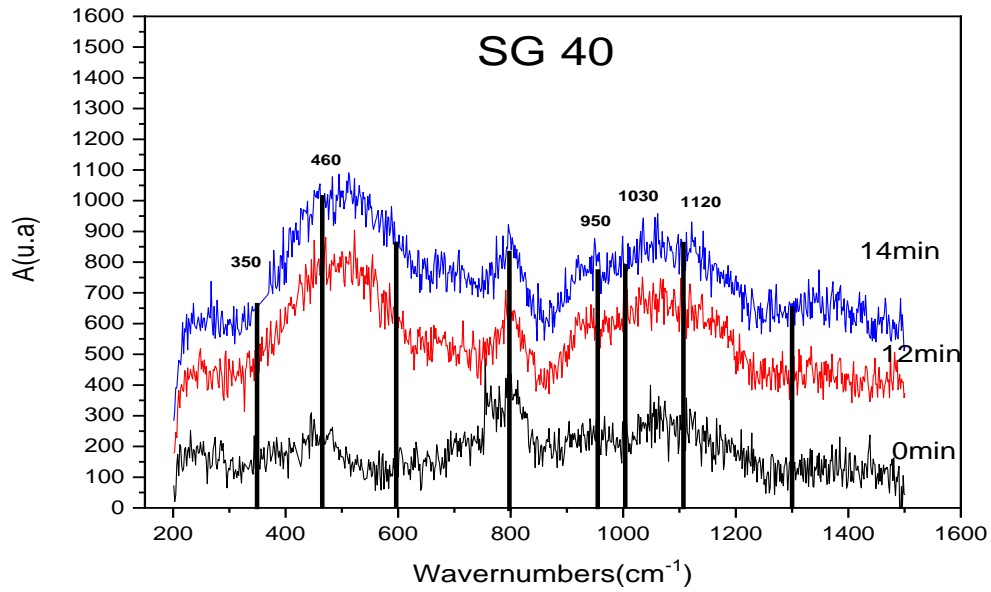
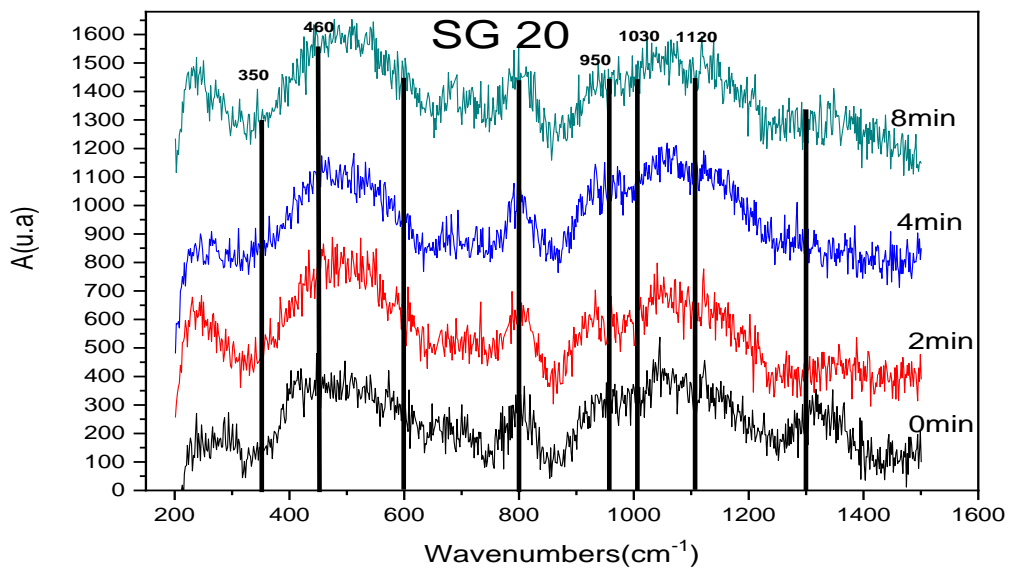


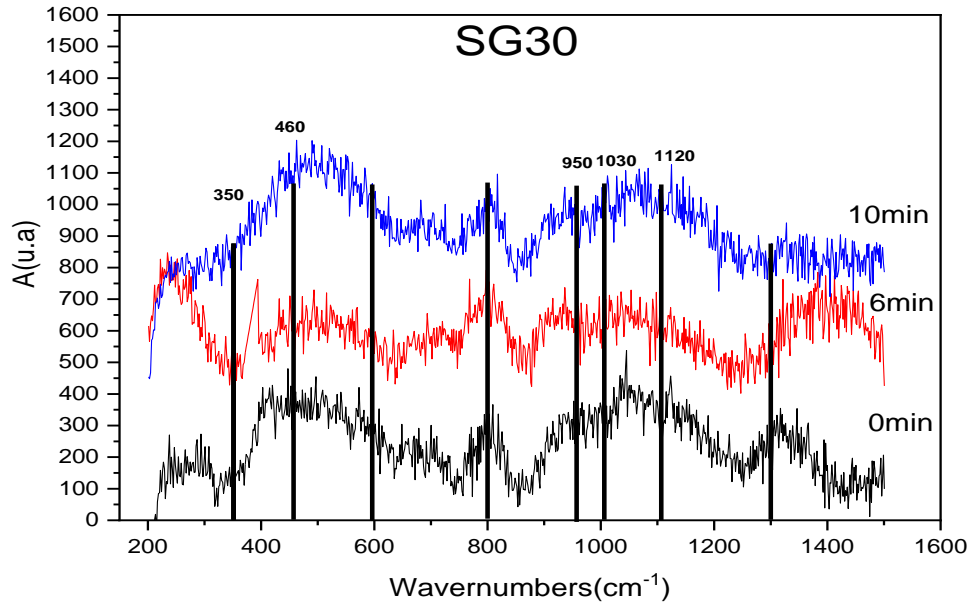
Figure 3.14. Raman Spectra of the different coating of SiO_2 . (a) SG20,(b) SG30,(c) SG40 are used in this study as function polishing time (FK).

(a)



CHAPTER.3PRACTICAL STUDY

(b)



(c)

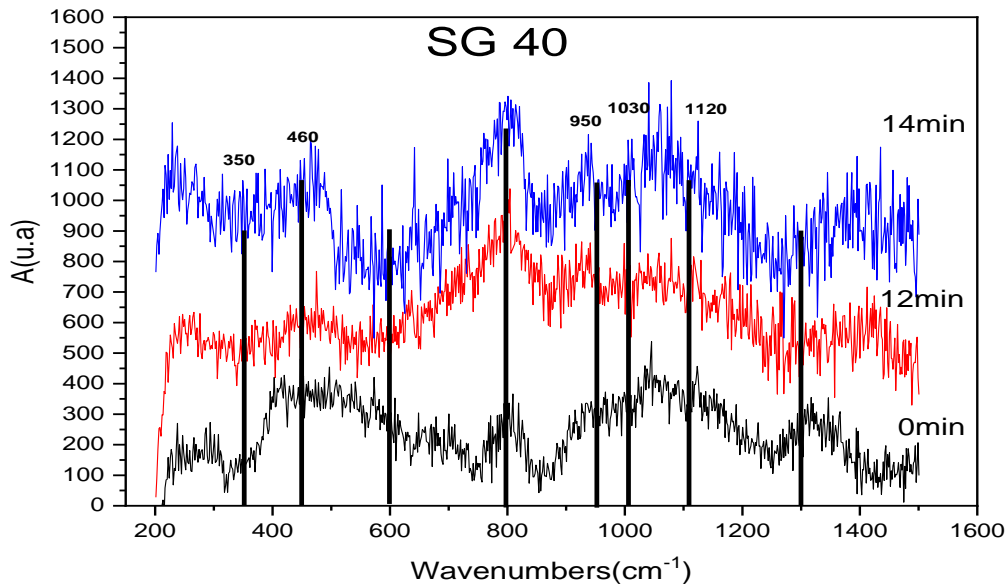


Figure 3.15. Raman Spectra of the different coating of SiO₂. (a) SG20, (b) SG30, (c) SG40 are used in this study as function polishing time (SF2).

The results indicated in Figures 3.14 and 3.15, a certain resemblance between the two glasses. For the FK glass, there were peaks at 460, 800, 950 and 1100 cm⁻¹, mainly due to Si-O-Si bonds, whereas peaks at 960 cm⁻¹ are probably due to Si-OH bonds or Si-O-B bonds. This latter

CHAPTER.3 PRACTICAL STUDY

assumption could be associated with the peak close to 750 cm^{-1} which also appeared due to B-O-B bonds.

When this glass was coated with a Silica sol for different times and concentrations, it was observed that the SG20 coating was very thin in the aforementioned peaks. The same conclusion appeared for the SG30 coating, but in this case, the B-O-B band at 750 cm^{-1} tends to disappear, indicating that the Silica gel has reacted with such bonds or has coated the glass surface. For the SG40 concentration, an important change appeared where the intensity increasing of the $350\text{-}600\text{ cm}^{-1}$ band and indicating that the Si-O-Si bonds of the Silica gel are mainly on the glass surface, i.e., the Silica sol is coating the glass surface. The 750 cm^{-1} band also disappeared, indicating that the B-O-B bonds of the glass are coated with the Si-O-Si bonds. In all cases, the reaction time seems to be affected in the 750 cm^{-1} band that disappears more quickly when the time increases.

For the SF2 glass, the same results appeared and the same conclusions are to be drawn, except that the effect of the coating is less important; the peak at 750 cm^{-1} did not appear. For both glasses, the bands between 900 and 1200 cm^{-1} are composed with at least 3 peaks which are due Q2, Q3 and Q4 Silica units. When glass compositions are taken into account, the Raman peak at 780 cm^{-1} is due to B-O-B bonds that are typical of boroxol units. This peak is in both glasses (SF2, FK) because both had B_2O_3 in their compositions. The Raman band at about 950 cm^{-1} could be due to both Si-O-B bonds and Si-O- (non-bridging oxygen = NBO) bonds. The NBO bonds are produced by the reaction of K_2O and SiO_2 because K_2O breaks the Si-O-Si bonds to give Si-O- ones. The bands at about 1030 and 1120 cm^{-1} are due to Si-O-Si bonds in Q3 and Q4 units which must be assigned to Si-O-Si (it is Q4) or Si-O-X (where $\text{X}=\text{B}, \text{Zn}, \text{Al}$; it is Q3) bonds.

The band at about 1300 cm^{-1} must be assigned to B-O-B bonds, similarly to the one at 780 cm^{-1} . But in such case (1300 cm^{-1}), it corresponded to the B-O bond, while the 780 cm^{-1} is related to the boroxol unit. The wide Raman bands between 300 and 600 cm^{-1} are due to Si-O-Si bonds.

3.4.6. Silica Adhesion

Micrographics of the treated surfaces are shown in Figures 3.16 to 3.21. AFM topography of some surfaces, after film deposition are shown in Figure 3.22-3.25.

The results of Figures 3.16-3.17 clearly show that the thin films obtained by the solution SG40 are of bad quality since several cracks are observed on the surface. Furthermore, the other solution concentrations (SG20 and SG30) have produced good thin films, as illustrated in the Figures 3.18 to 3.21 and demonstrated in the falling drop tests.

It is to be noticed that the quality of the thin films of every concentration can be related to the glass surface roughness. Indeed, in the Figures 3.22-3.25, it is clear that the topography of the two types

CHAPTER.3PRACTICAL STUDY

of glass is different for every roughness and the surface waviness is also different. Consequently, the final surface quality of the deposited thin film is different too.

(a) $S_q = 3.2 \pm 0.3$ nm

(b) $S_q = 2 \pm 0.25$ nm

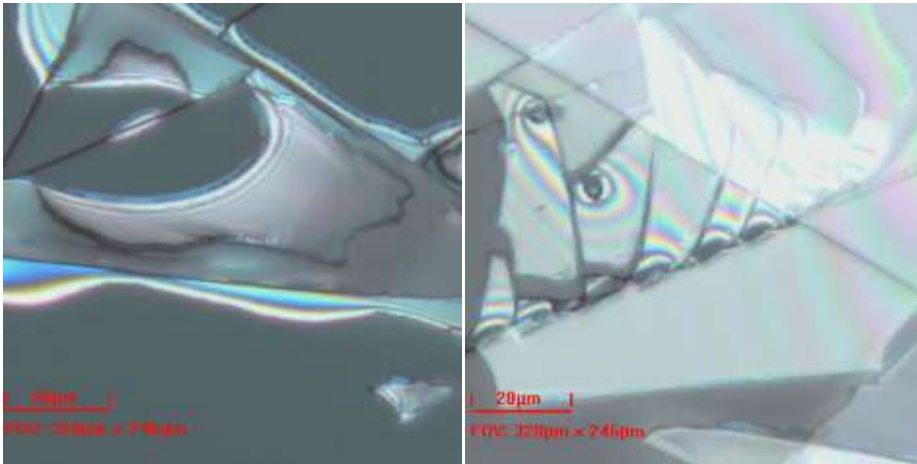


Figure 3.16. Micrographs of the deposited thin films using the SG40 on the optical glasses

(a) SF2 and (b) FK polished by cerium oxide slurry (x100).

(a) $S_q = 4.3 \pm 0.16$ nm

(b) $S_q = 3.4 \pm 0.24$ nm

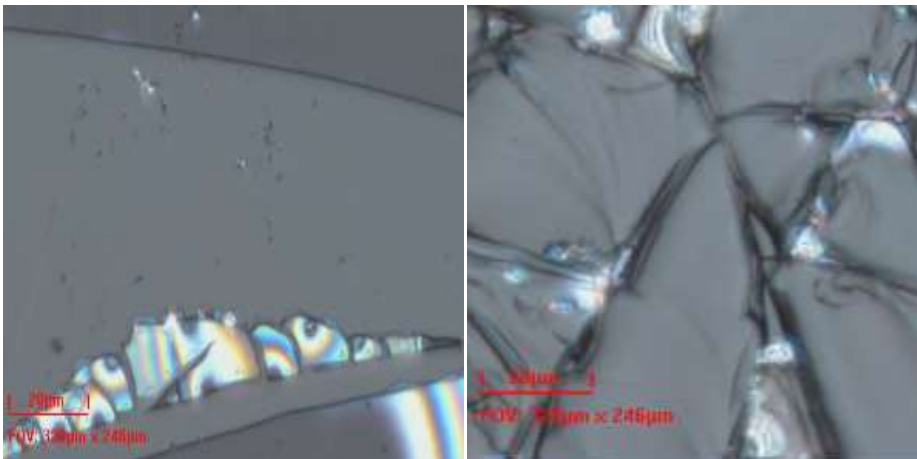


Figure 3.17. Micrographs of the deposited thin films using the SG40 on the optical glasses:

(a) SF2 and (b) FK polished by silica slurry (x100).

CHAPTER.3PRACTICAL STUDY

(a) $Sq=5.5\pm0.2nm$

(b) $Sq=9.3\pm0.2nm$

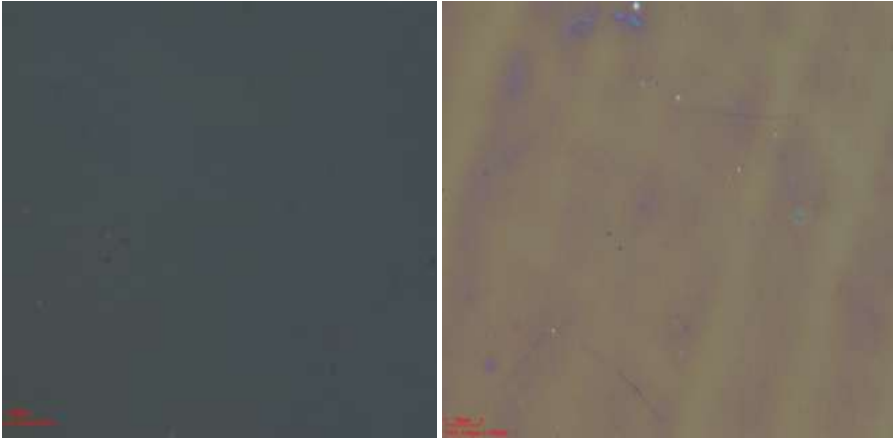


Figure3.18. Micrographs of the deposited thin films using the SG30 on the optical glasses:

(a) SF2 and (b) FK polished by cerium oxide slurry (x100).

(a) $Sq=4.5\pm0.14nm$

(b) $Sq=3.5\pm0.17nm$

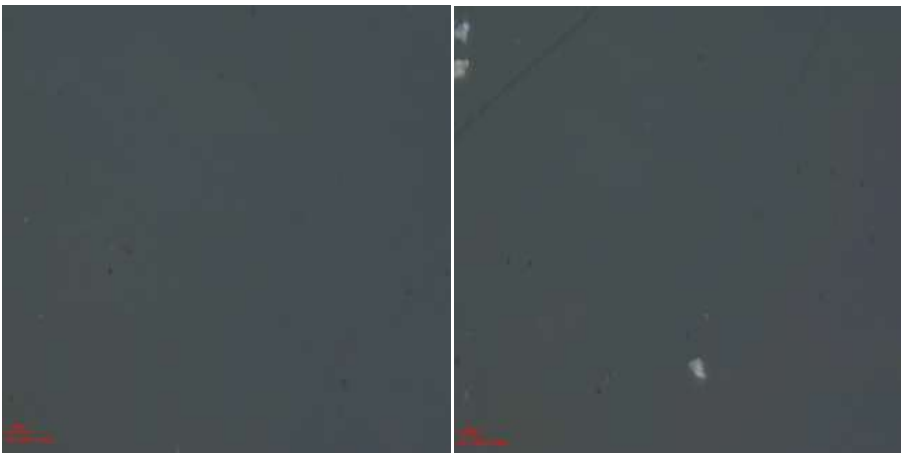


Figure 3.19. Micrographs of the deposited thin films using the SG30 on the optical glasses: (a) SF2 and (b) FK polished by silica slurry (x100).

CHAPTER.3PRACTICAL STUDY

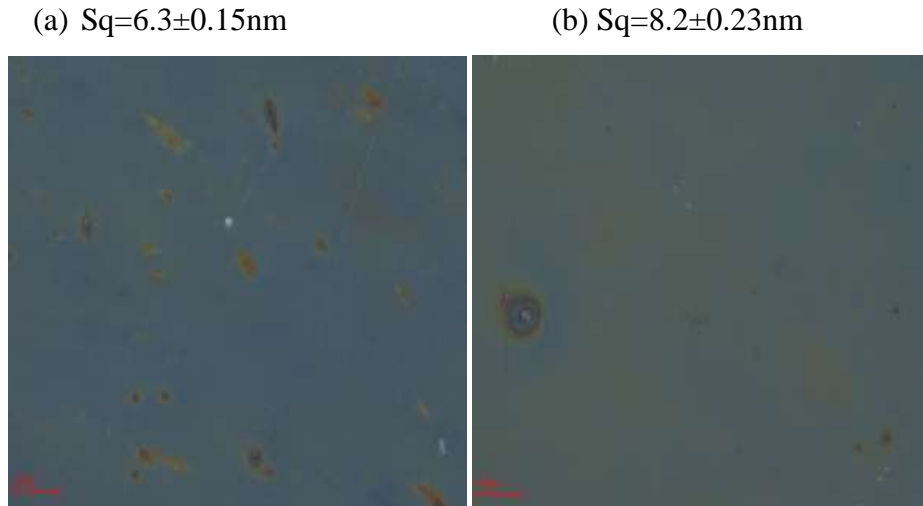


Figure3.20. Micrographs of the deposited thin films using the SG20 on the optical glasses: (a) SF2 and (b) FK polished by cerium oxide slurry (x100).

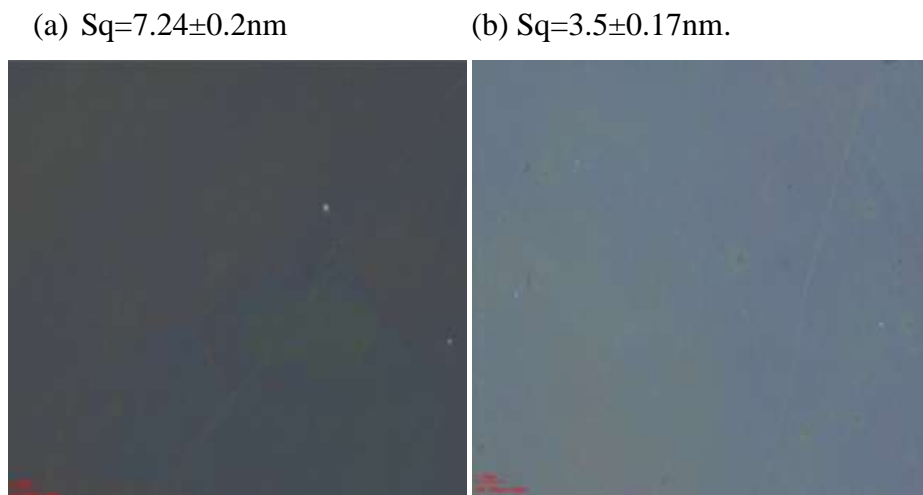


Figure 3.21. Micrographs of the deposited thin films using the SG20 on the optical glasses: (a)SF2 and (b) FK polished by silica (x100).

CHAPTER.3PRACTICAL STUDY

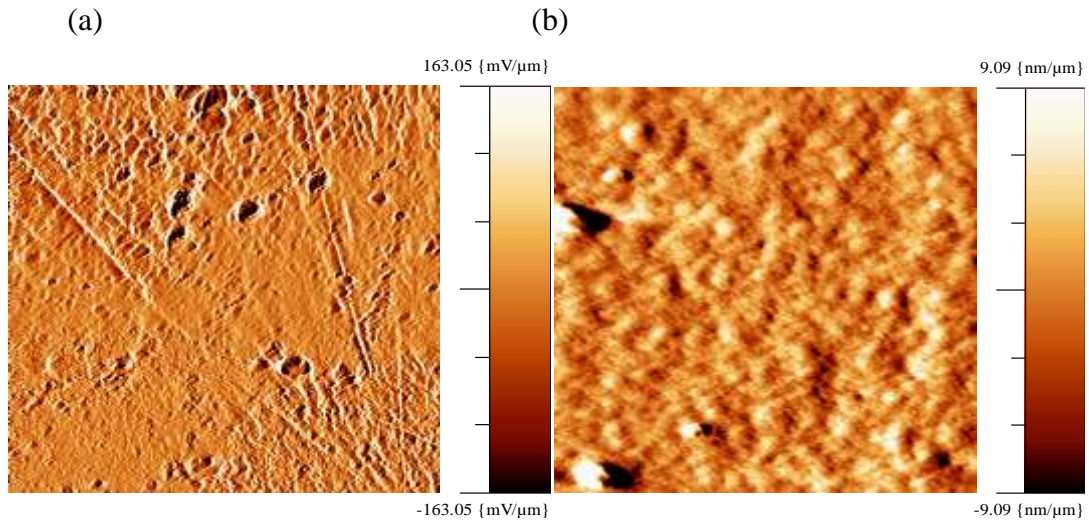


Figure 3.22. 3D AFM of the thin films using the SG30 on the FK optical glass polished by cerium oxide slurry ((a) without coating and (b) with coating).

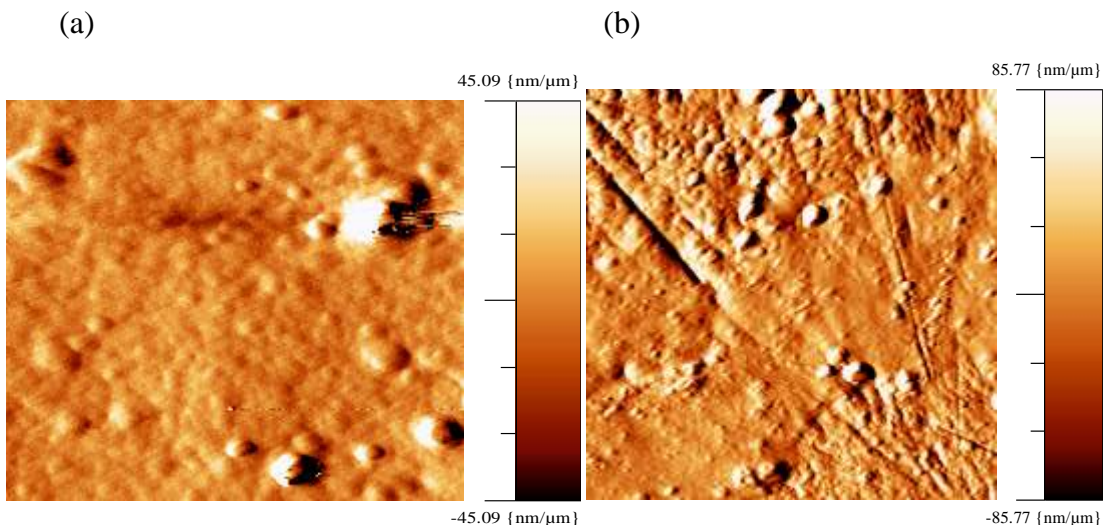


Figure 3.23. 3D AFM images films using the SG20 on the FK optical glass polished by cerium oxide slurry ((a) Without coating and (b) with coating).

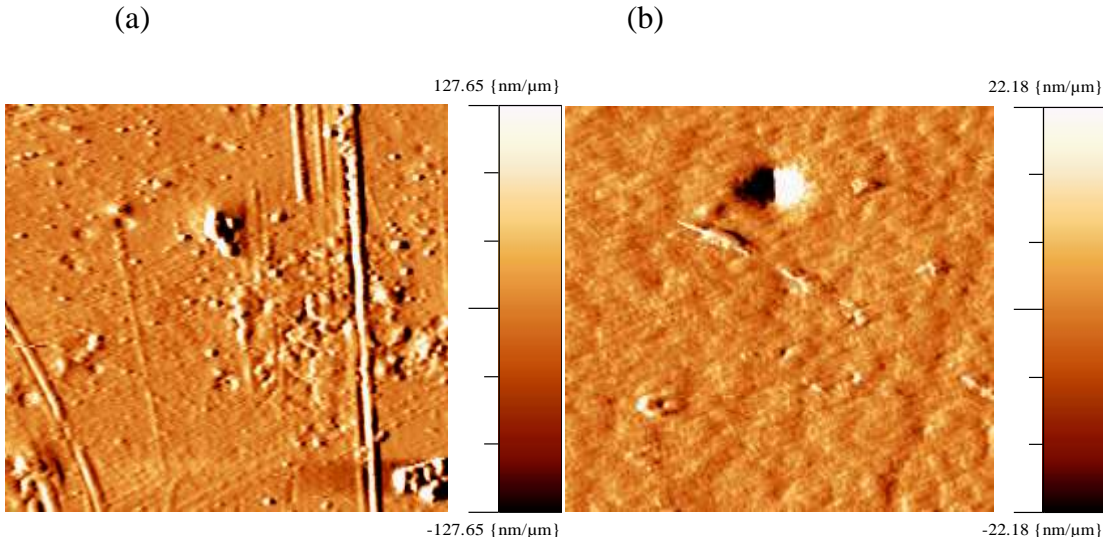


Figure 3.24. 3D AFM of the thin films using the SG30 on the SF2 optical glass polished by cerium oxide slurry ((a) without coating and (b) with coating).

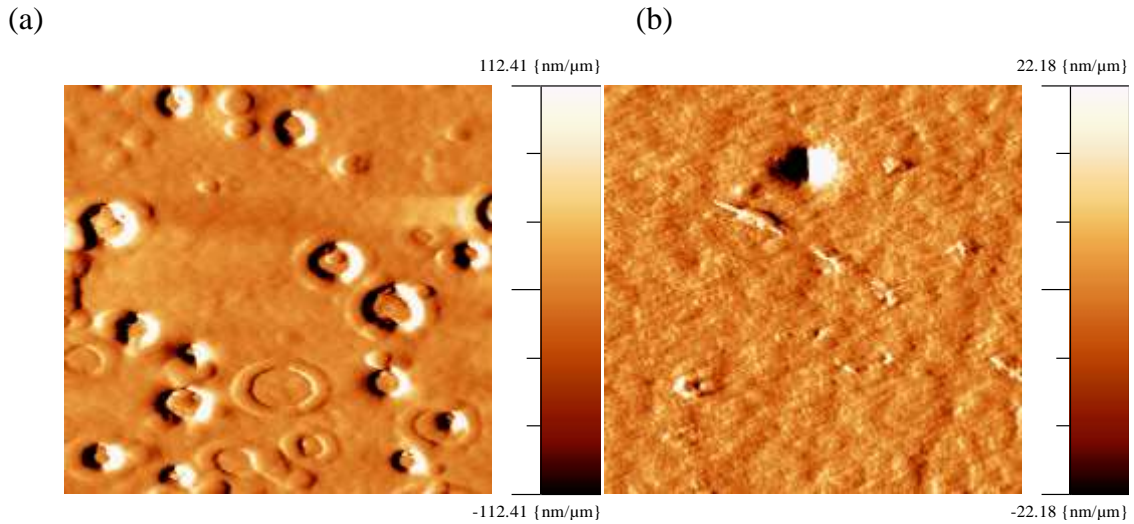


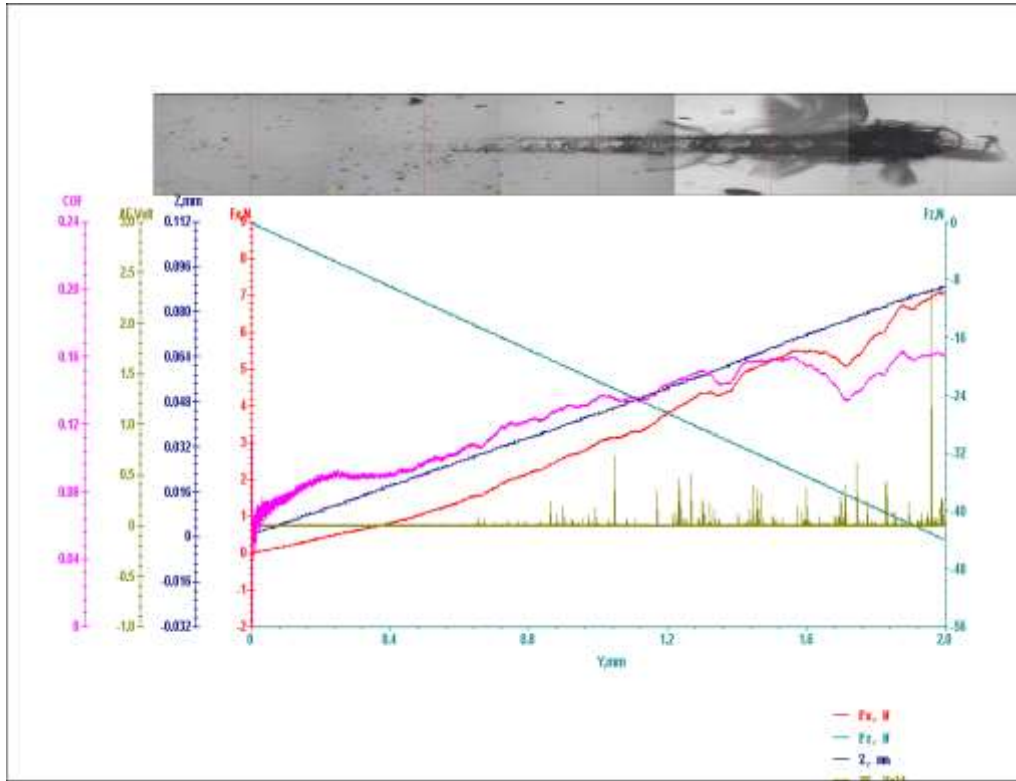
Figure 3.25. 3D AFM of the thin films using the SG20 on the SF2 optical glass polished by cerium oxide slurry ((a) without coating and (b) with coating).

3.4.7 .Scratch test of Silica thin films

Because of its importance, adhesion of thin films [247] was studied by the falling drop test before deposition and when thin films were deposited scratch test was used. The process was performed in progressive mode with a controlled variation of the normal force where acoustic emission, penetration depth and friction coefficient were measured. Figure 3.26 illustrates scratch test results of the SG20 obtained thin films.

CHAPTER.3PRACTICAL STUDY

(a) SF2 : $Sq=14\pm0.31nm$



(b) FK : $Sq = 12.5 \pm 0.14nm$

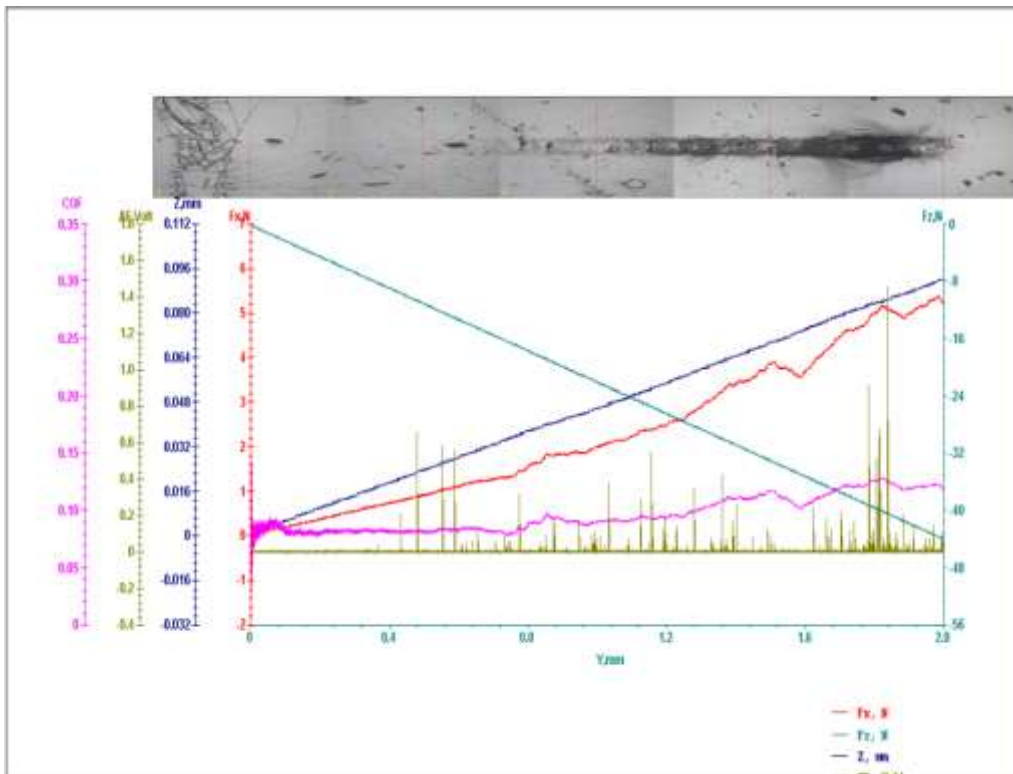


Figure 3.26. Scratch test results of the SG20 thin films on optical glasses (SF2 and FK) polished by SiO_2 slurry.

CHAPTER.3 PRACTICAL STUDY

Concentration	Surface roughness		Friction coefficient	
	SF2	FK	SF2	FK
SG20	12±0.21nm	15.1 ±0.16nm	0.08	0.10
SG30	5.5 ±0.20nm	5.4±0.21 nm	0.07	0.09
SG40	6.13±0.2 nm	6.23±0.2 nm.	0.16	0.21

Table 3.6. Friction coefficient results of the SG20, SG30, and SG40 thin films deposited on optical glasses (FK and SF2) polished by CeO₂ slurry.

Concentration	Surface roughness(Sq)		Friction coefficient	
	SF2	FK	SF2	FK
SG20	14±0.31nm	12.5 ±0.14nm	0.09	0.14
SG30	8.5 ±0.21nm	4.3±0.25 nm	0.08	0.012
SG40	7.2±0.3 nm	5.13±0.32 nm.	0.18	0.25

Table 3.7. Friction coefficient results of the SG20, SG30, and SG40 thin films deposited on optical glasses (FK and SF2) polished by SiO₂ slurry.

According to the results are presented in Tables 3.6 to 3.7, FK and SF2 optical glass, polished by Silica slurry, demonstrate a better adherence than the surfaces polished by cerium oxide of the relatively thin films. For the first glass (SF2), the layer had its first crack after application of a normal force about 1 N, this crack is obtained by higher normal force when the roughness is lesser (14 nm). At the same time, the penetration depth and the friction coefficient were different. These values indicate that the roughness has an influence on the adhesion. It also affects the adhesion positively when it is lower. The same remarks were noticed for the other type of glass. However, it must be noted that the value is not the same and the scratch tests reveal that the thin films obtained by the SG20 solution with high surface quality of the FK glass seem to be those with high adhesion.

3.4.8. Adhesion behavior

The adhesion behavior has been studied by calculation of the adhesion strength via the measured surface tension [248] of the different prepared sols using the relation (3.4). The results are presented in Figures 3.27-3.29.

$$W_{ad} = \gamma l v (1 + \cos \theta) \quad (3.4)$$

CHAPTER.3PRACTICAL STUDY

With:

θ : The contact angle (deg).

γ_{lv} :The liquid of surface tension measured with Digi Drop ($\gamma_{lv}\text{SiO}_2$ (SG20)=0.118 N/m ,and $\gamma_{lv}\text{SiO}_2$ (SG30)=0.165N/m).

W_{ad} : The adhesion strength (force) (N/m)

The results indicate that the increasing of the surface roughness decreases the adhesion strength.

This highlights the effect of the roughness surface on the quality of the thin films.

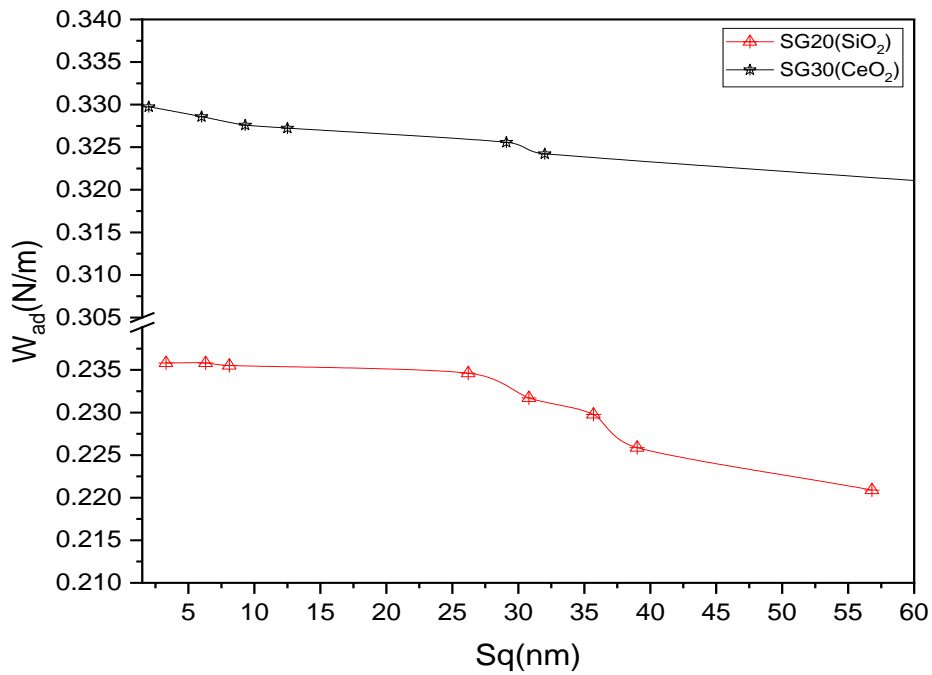


Figure 3.27. Variation of the coating adhesion strength on the FK glass using SG20 and SG30 solutions vs. root mean square height (Sq).

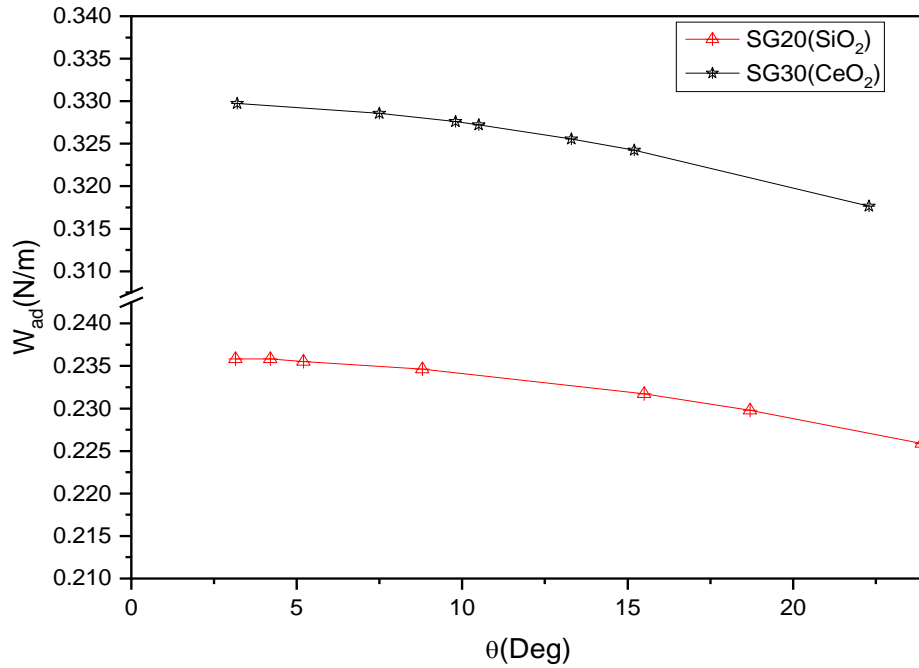


Figure 3.28. Variation of the coating adhesion strength on the SF2 glass using SG20 and SG30 solutions vs. root mean square height(Sq)

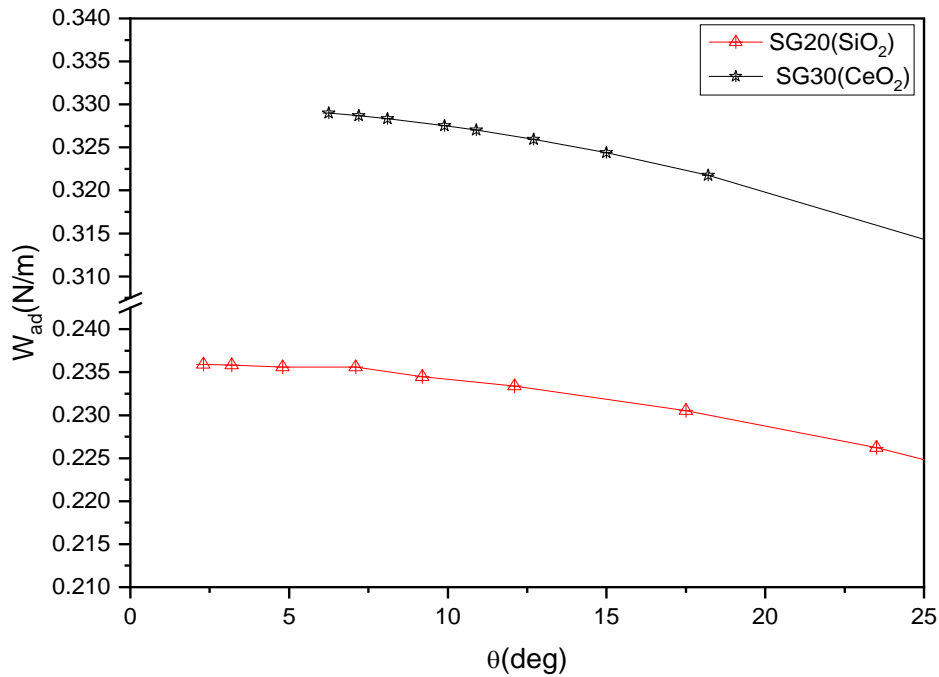


Figure 3.29. Variation of SF2 adhesion strength of coating SG20 and SG30 vs. contact angle (θ).

The storage in the CK solution has affected the glass properties as demonstrated in Figures 3.27-3.29, especially the surface quality that has induced different spread of the droplet. This phenomenon may be due to the removal of micro and nano- asperities, leaving a very fine surface

CHAPTER.3PRACTICAL STUDY

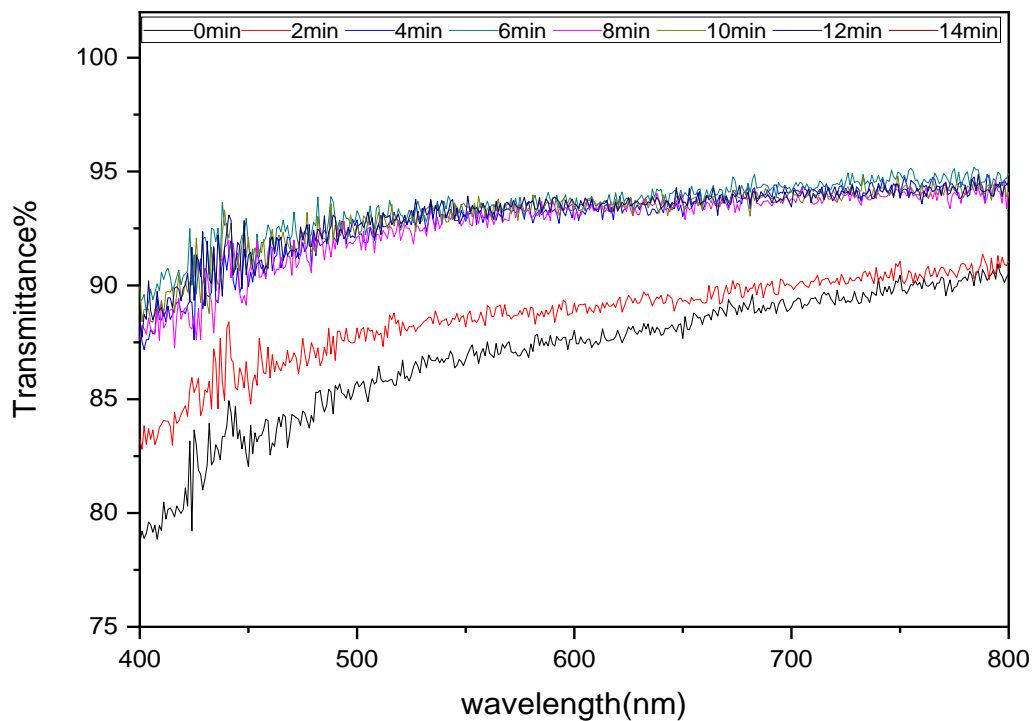
which decreases the contact surface and increases the adhesion, easily notable by the hydrophilic increasing in SG20 than in SG30. Indeed, the CK solution where the optical glasses (SF2 and FK) were stored has condensed the glass surface; the cations diffused inside and induced transformation into the surface. This deterioration of the surface can improve the optical and mechanical properties of the layers, such as surface roughness, adhesion, and hardness and abrasion resistance.

3.4.9. Influence of polishing on the transmission of stored materials

In order to understand the effect of the two parameters, storage and surface quality on optical materials, we performed the characterization of the transmission and surface roughness of two samples a mineral that is BK7 and a polymer that is PMMA.

Results of the Transmission spectra obtained for the stored substrates (BK7 and PMMA) in the PEG solution are shown in Figure 3.30-3.31.

(a)



CHAPTER.3PRACTICAL STUDY

(b)

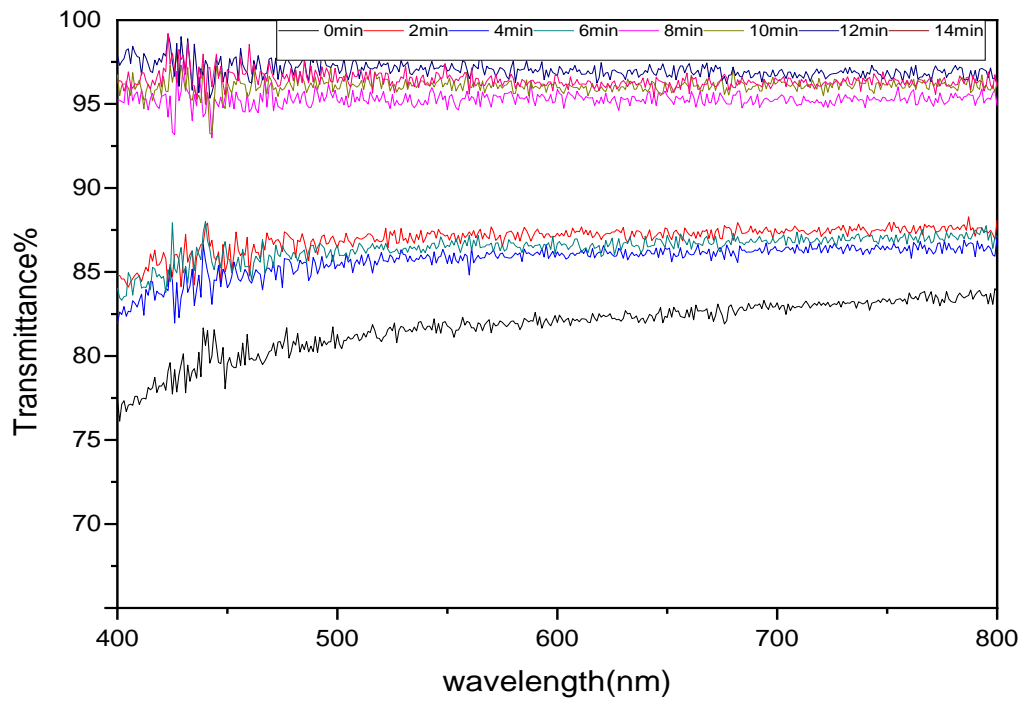
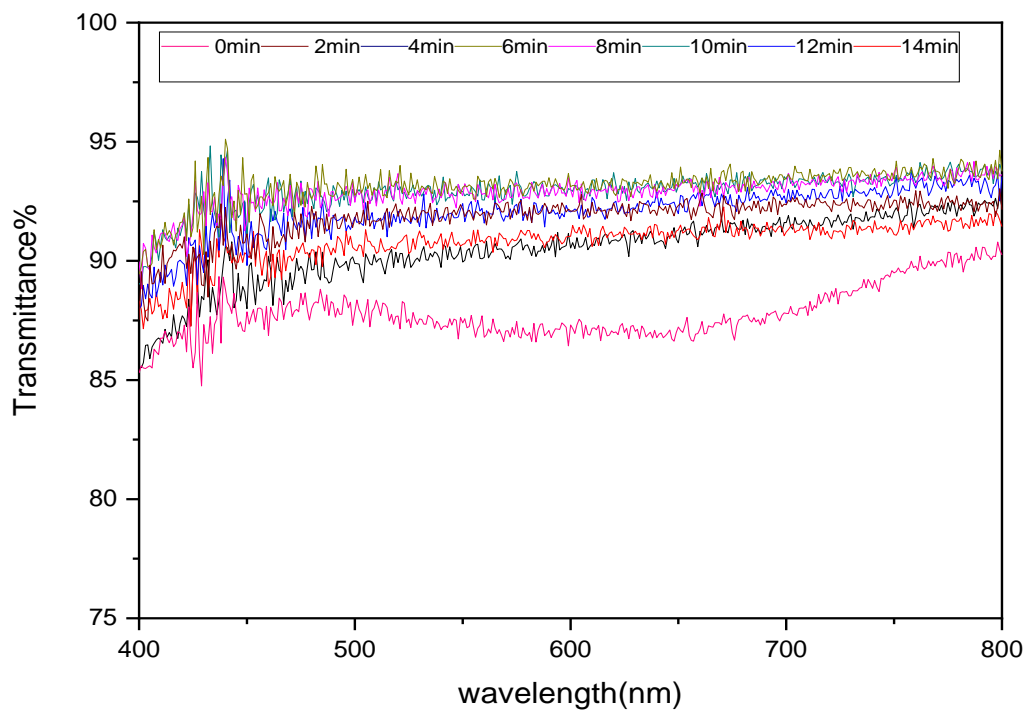


Figure 3.30. Optical transmittance spectral values of BK7 ((a)before and(b) after storage).

(a)



(b)

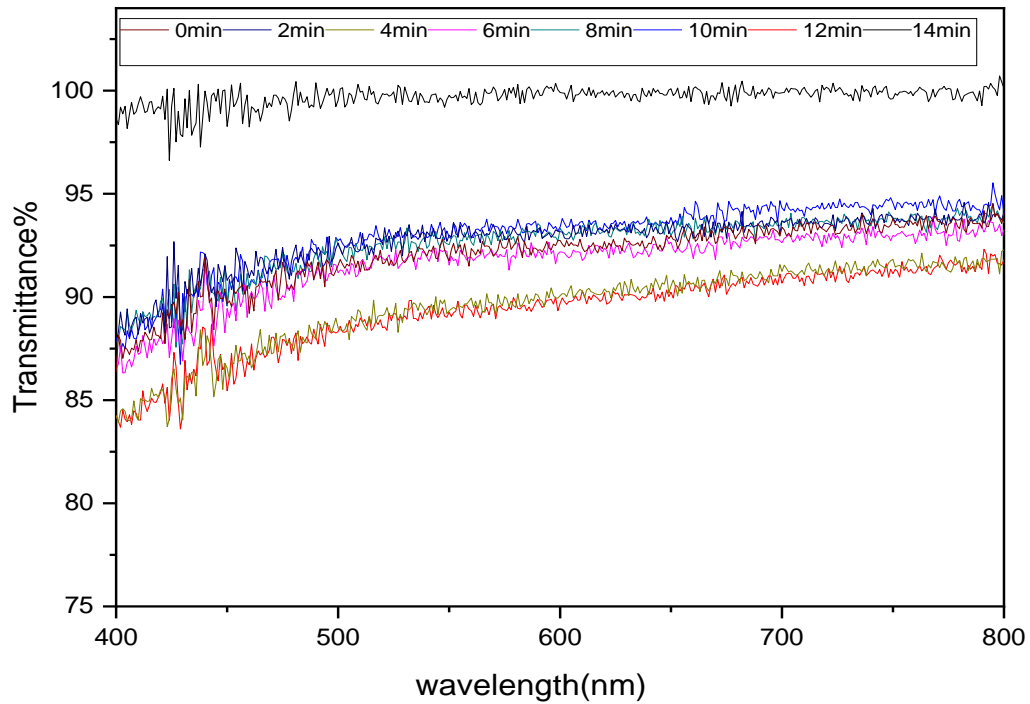


Figure 3.31. Optical transmittance spectral values of PMMA ((a) before and(b) after storage)

BK7 and PMMA transmission values increase versus polishing time as shown in Figure 3.30-3.31, but the values are specific for each type of sample because of its nature, behavior during the polishing process and storage effect.

The curve in Figure 3.32- 3.33 showed the storage effect of the BK7 and PMMA samples on the roughness variation R_q .

CHAPTER.3PRACTICAL STUDY

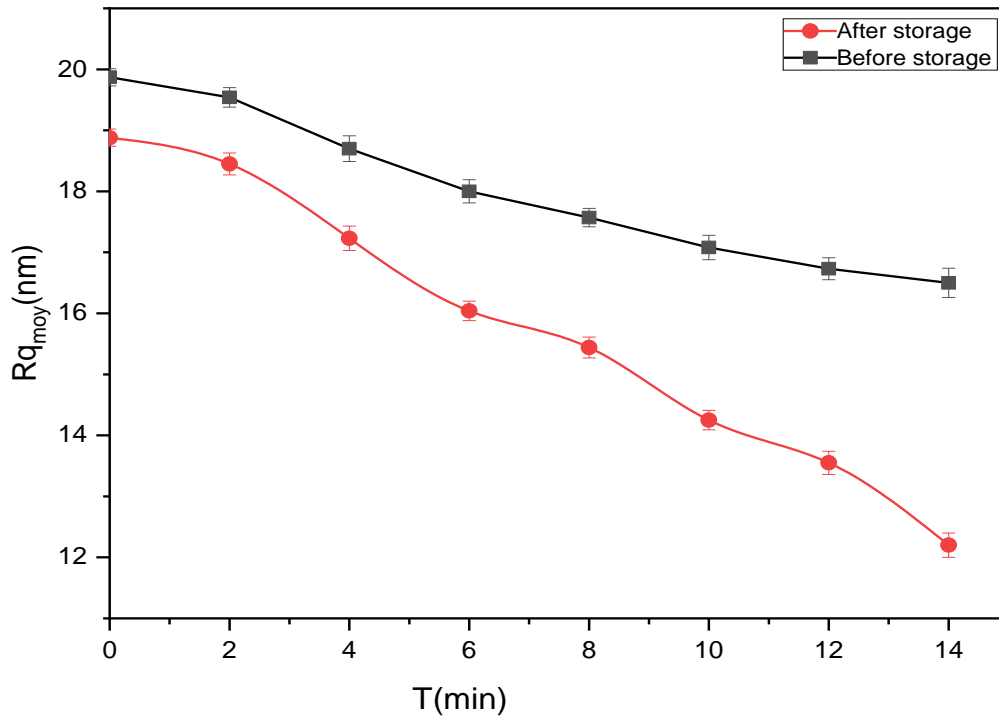


Figure 3.32.Storage effect on the R_q variation of BK7 vs. polishing time.

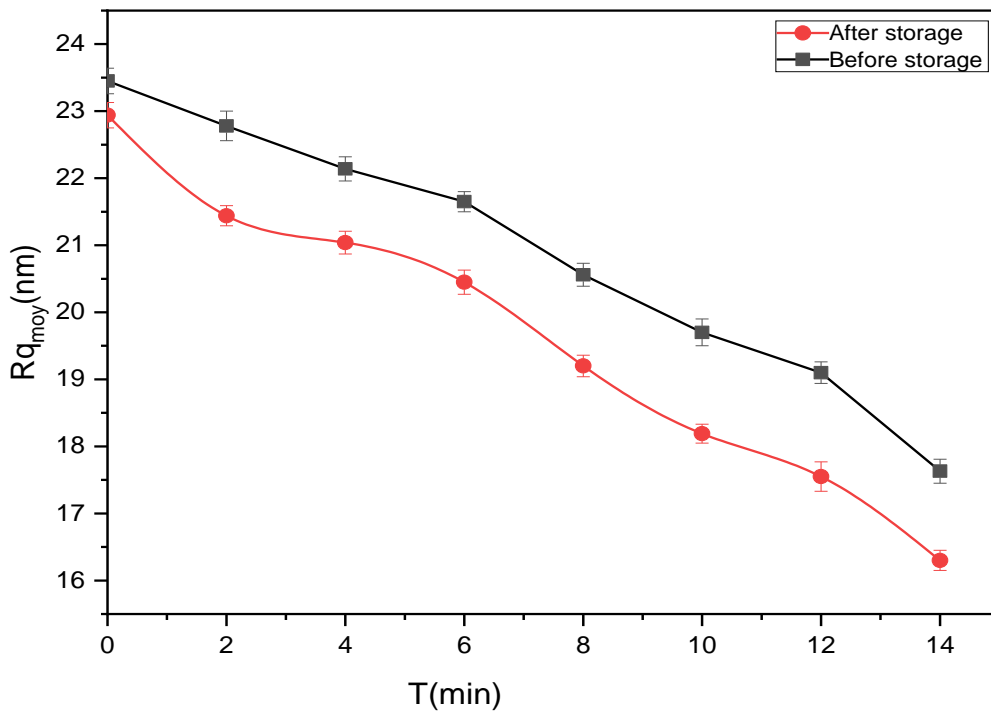


Figure 3.33.Storage effect on the R_q variation of PMMA vs. polishing time.

Surfaces morphology visualized by Optical interferometry is illustrated by the micrographics of Figures 3.34 and 3.35.

CHAPTER.3PRACTICAL STUDY

(a) $R_q=17.5\text{nm}\pm0.14$

(b) $R_q=16.55\text{nm}\pm0.16$

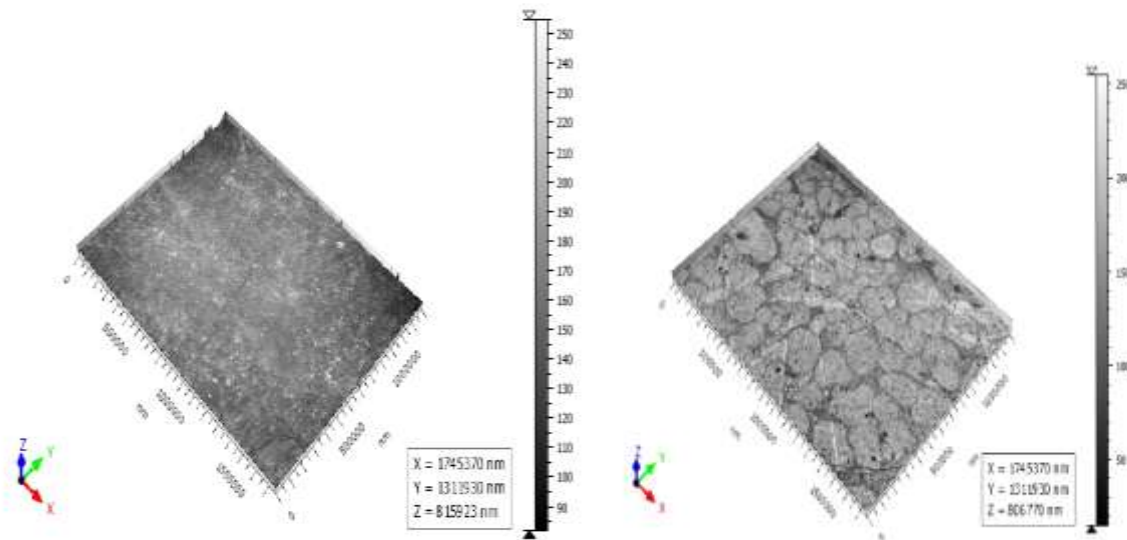


Figure3.34. Interferometric 3D image of BK7 samples :(a) Before storage and (b) After storage on PEG solution .

(a) $R_q=19.9\text{nm}\pm0.2$

(b) $R_q=17.5 \text{ nm}\pm0.22$

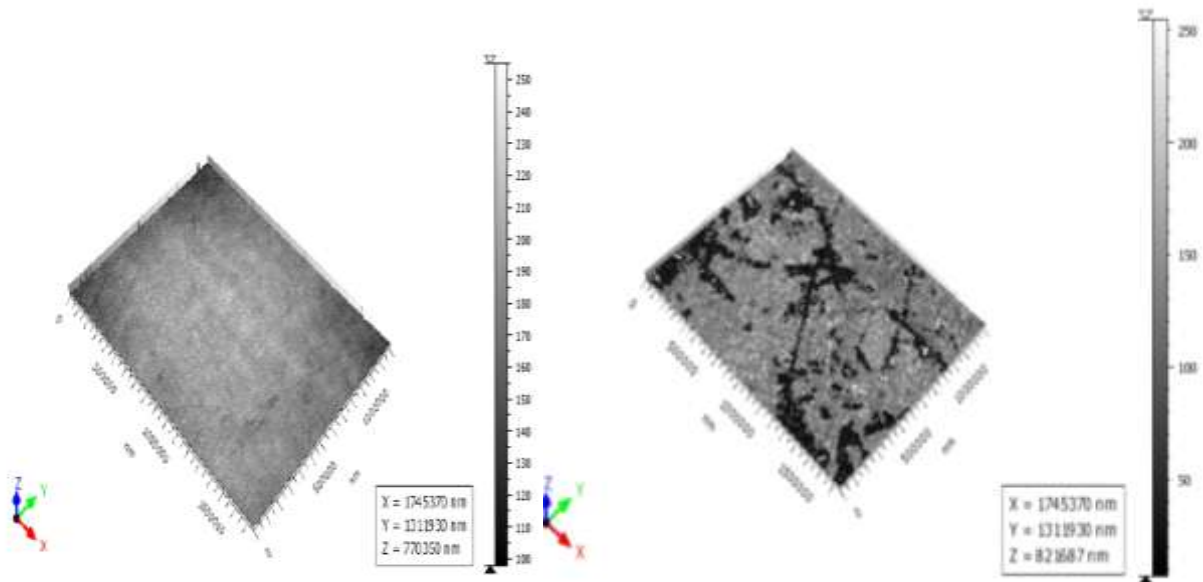


Figure3.35. Interferometric 3D image of PMMA samples :(a) Before storage and (b) After storage on PEG solution .

Based on these results, the optical materials mean that the roughness changes according to the type of used materials, storage effect, and the duration. Therefore, it can be noted that the roughness

CHAPTER.3PRACTICAL STUDY

decreased and then the surface quality is improved after storage in the PEG solution of both types of optical materials (BK7, PMMA).

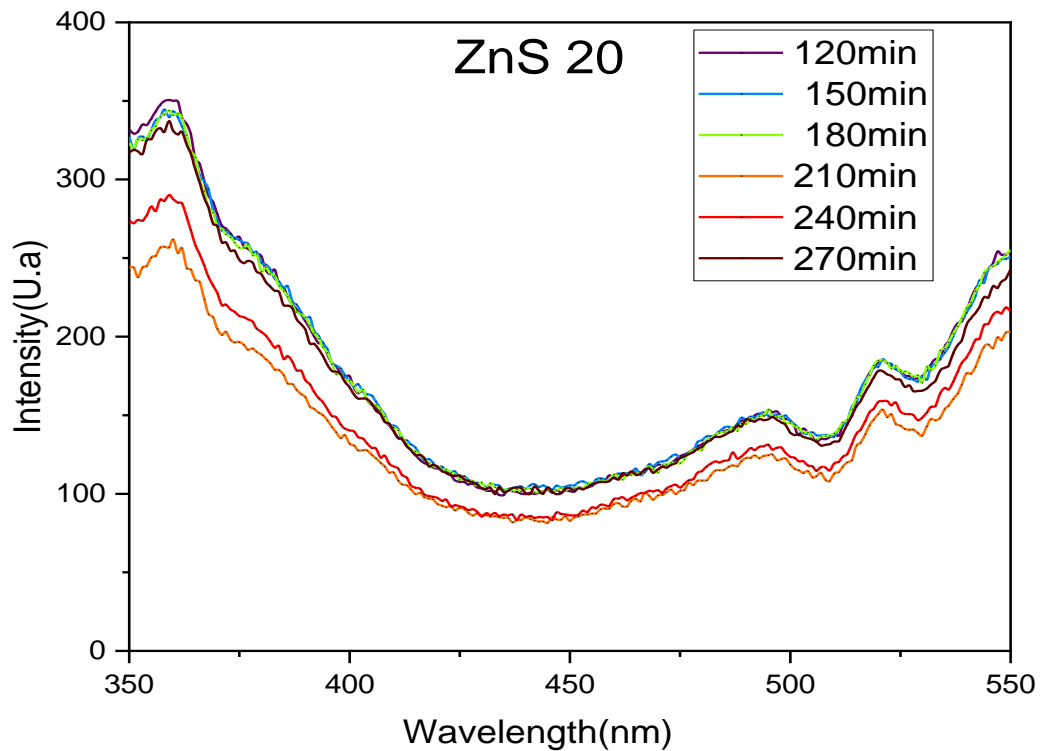
3.3.10.Behavior of stored samples on the thin film deposition

3.3.10.1. Thin films solution characterization:

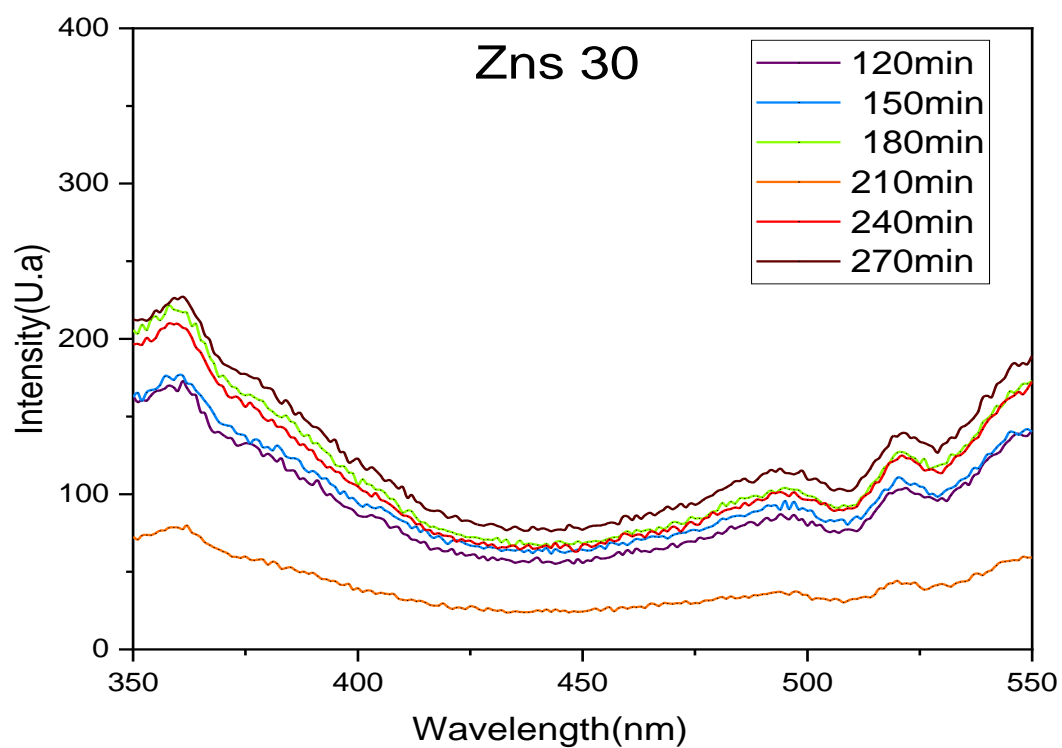
In order to show the storage effect and roughness parameters, we proceeded to deposit the ZnS thin films in order to see the adhesion behavior.

The graphs in Figure 3.36 show the photoluminescence of ZnS solutions with different concentrations (20,30,40%).

(a)



(b)



(c)

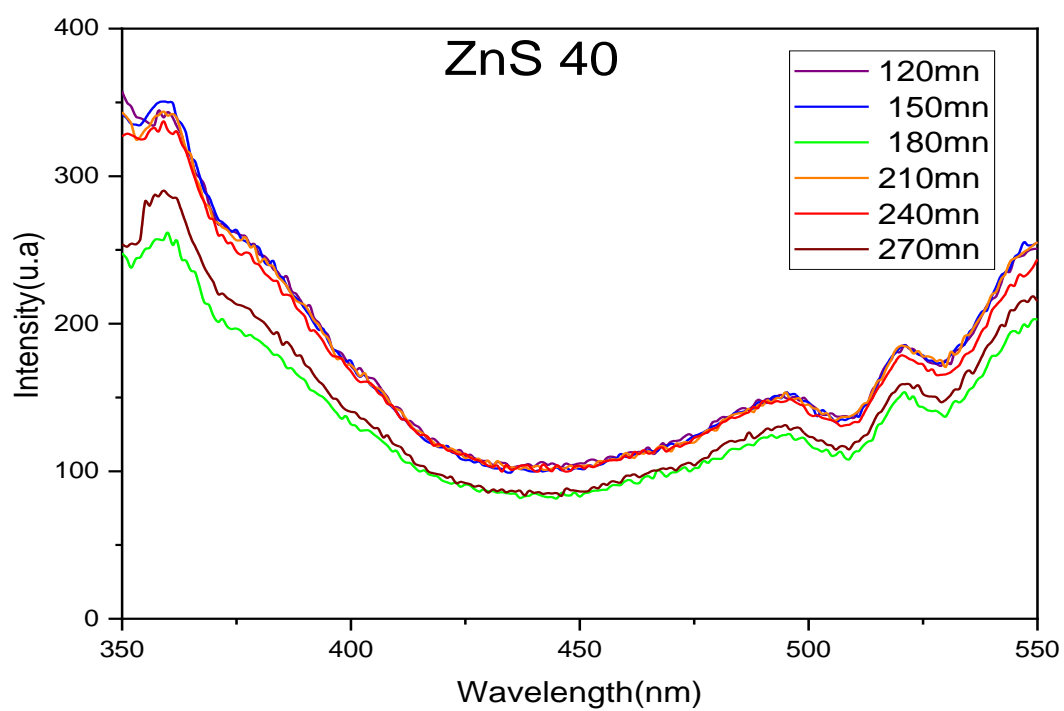
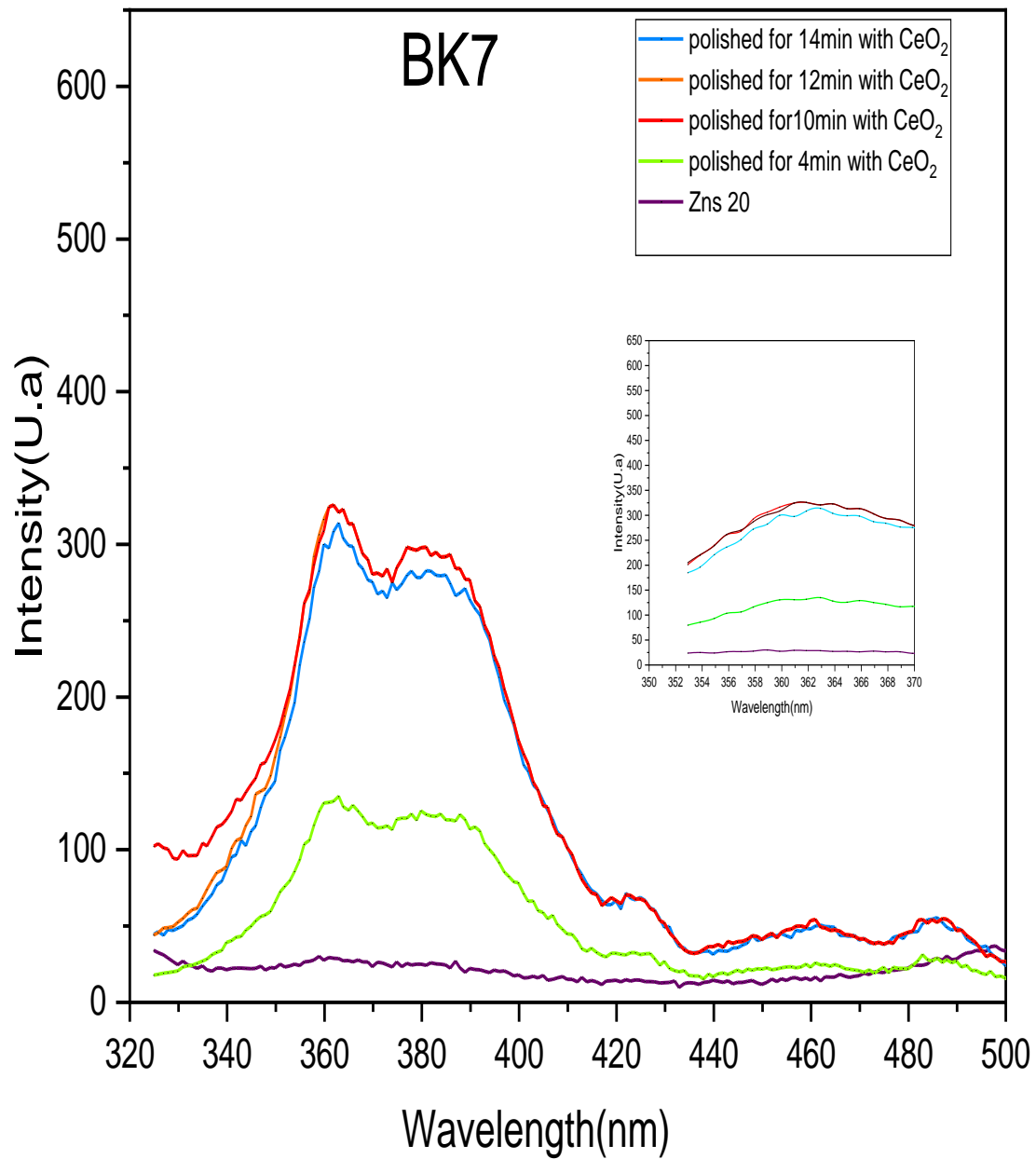


Figure3.36. Photoluminescence spectra of ZnS solutions with different concentrations
(a) 20%,(b) 30% ,and (c) 40%.

CHAPTER.3PRACTICAL STUDY

For the preparation of the ZnS thin films,the photoluminescence of ZnS20 thin films deposited obtained on optical materials (BK7and PMMA) with a polishing time (see Figure 3.37).

(a)



(b)

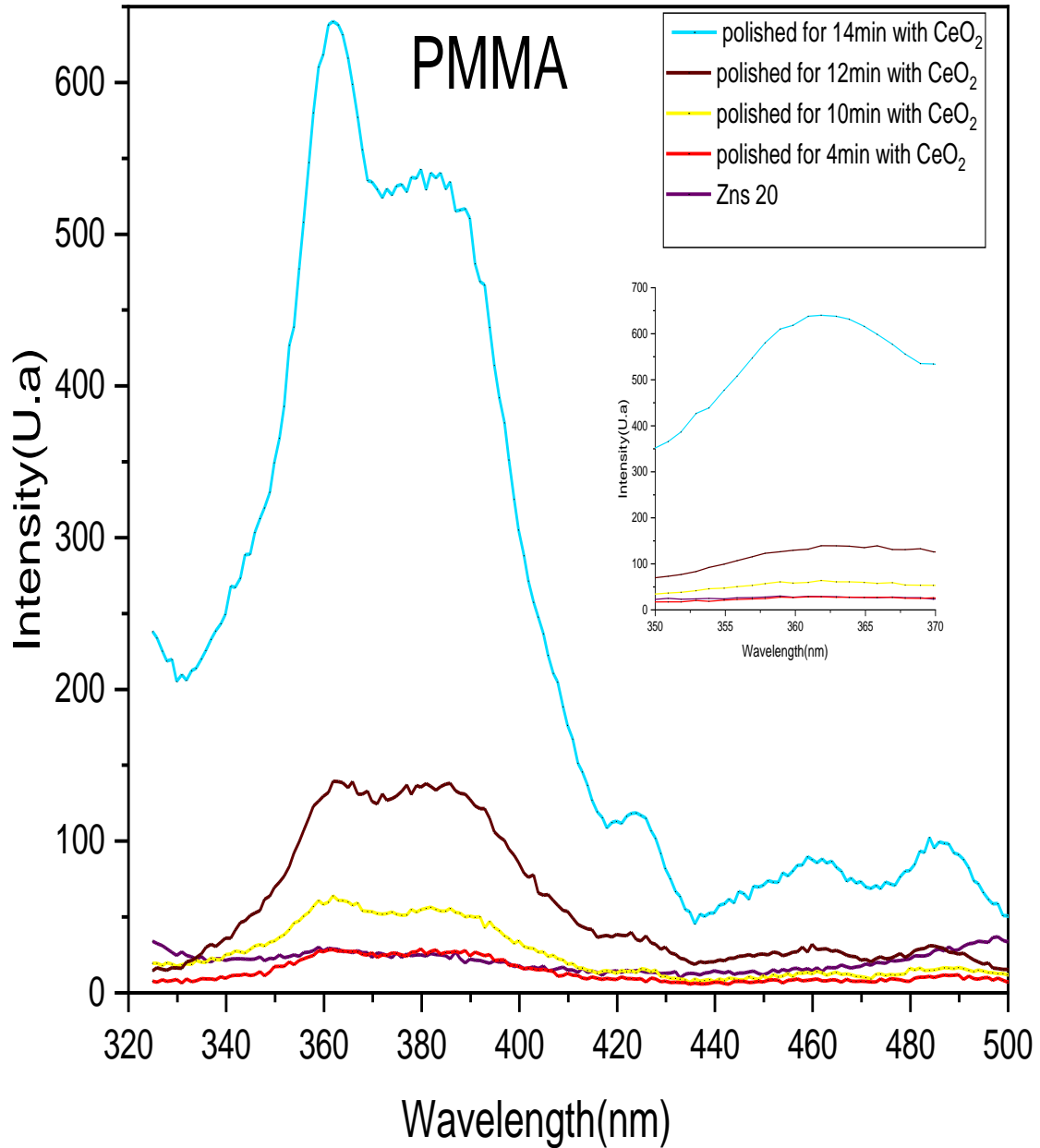


Figure 3.37. Photoluminescence spectra of ZnS20 film vs. polishing time: (a)BK7,(b)PMMA.

Luminescence can be generally divided into band edge emission, including excitonic emission, and trap state emission. In ZnS thin films, different types of structural and surface defects such as zinc and sulfur vacancies or interstitials give a various emission mechanisms resulting from there combination of photo generated electrons and holes. The room temperature photoluminescence spectra of as-grown ZnS thin films were recorded with an excitation wavelength (λ_{exc}) of 320nm under identical conditions. The Photoluminescence spectra of ZnS solutions with different

CHAPTER.3PRACTICAL STUDY

concentrations (20%, 30% and 40%), shown in Figure 3.36, exhibited different luminescence intensities. In fact, the luminescence peak was observed at energy lower than the optical band gap for all the films, indicating impurity states in the mid-band-gap region. Several workers have attributed this type of luminescence to the emissions associated with the vacancy sites. Semiconductor nanoparticles exhibit the luminescence from excitonic emissions as well as trapped emissions and the photoluminescence properties are limited by the large surface to volume ratio and surface defects of nanosized particles, which leads to the reduced excitonic emission via non radiative surface recombination. Hence, a few reports are available on the excitonic emission of ZnS nanoparticles due to the prevalence of trap-state emission [249,250]. The PL spectra in Figure 3.36 shows that the band edge emission of ZnS solutions 20%, 40% is more intense than the 30% ZnS solution. For that, the preparation of the ZnS thin films was made from the ZnS (20%) on optical materials (BK7 and PMMA) with a polishing time of (04, 10, 12 and 14min) (see Figure 3.37).

In Figure 3.37 (a) and (b), all the layers deposited of ZnS (20%) on BK7 and PMMA samples at different polishing time exhibit a sharp UV emission peak in all the graphs. The luminescence peaks located around 357.5 nm ($E_g = 3.47$ eV), 359.9 nm ($E_g = 3.45$ eV) and 360.7 nm ($E_g = 3.44$ eV) are associated with the zinc vacancies and the emissions located at 352.3 nm ($E_g = 3.52$ eV) and 355.5 nm ($E_g = 3.49$ eV) can be attributed to the interstitial sulfur [251].

The observed variation in the luminescence's intensity clearly indicated the influence of surface area of the grains on the luminescence. It well known that the luminescence intensity depends on the particle diameter, where it increases with the increase of the density of surface states due to large surface to volume ratio for the smaller crystallites [252]. Hence, the materials with smaller crystallites showed higher luminescence intensity compared to the crystallites of larger diameter. We obtained an ideal reaction in photoluminescence spectrum of ZnS20 of BK7 at 10 min, but an ideal reaction well defined from PMMA at 14 min. It is worthy to mention that the ZnS (20%) made on PMMA samples exhibit PL emission intensity approximately twice as high as that of ZnS (20%) made on BK7 samples. Besides the PL intensity observed for the different samples is almost similar in emission behavior.

The sharp peak's bandwidth recorded in UV range becomes narrow with increasing the time of polishing.

CHAPTER.3PRACTICAL STUDY

3.3.11. Adherence behavior

The results in Figure 3.38-.3.39 demonstrate that the decreasing of the contact angle and the increasing of the adhesion of ZnS20 is proportional to the storage time, and the roughness.

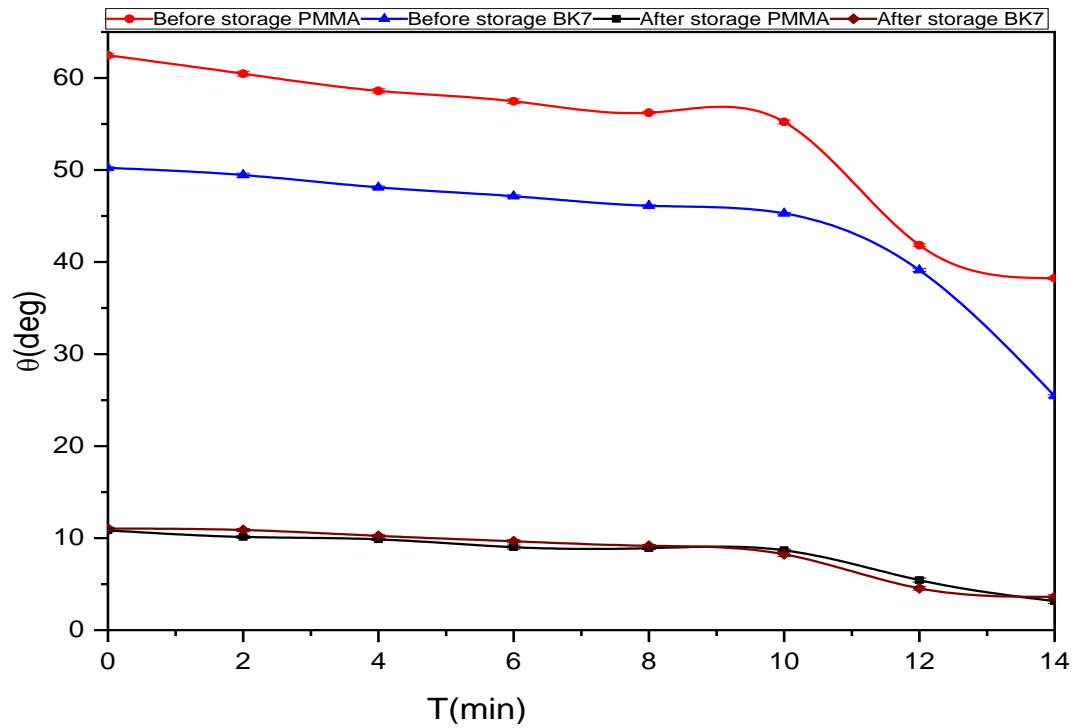


Figure 3.38. Variation of the contact angle vs. polishing time of BK7 and PMMA substrates.

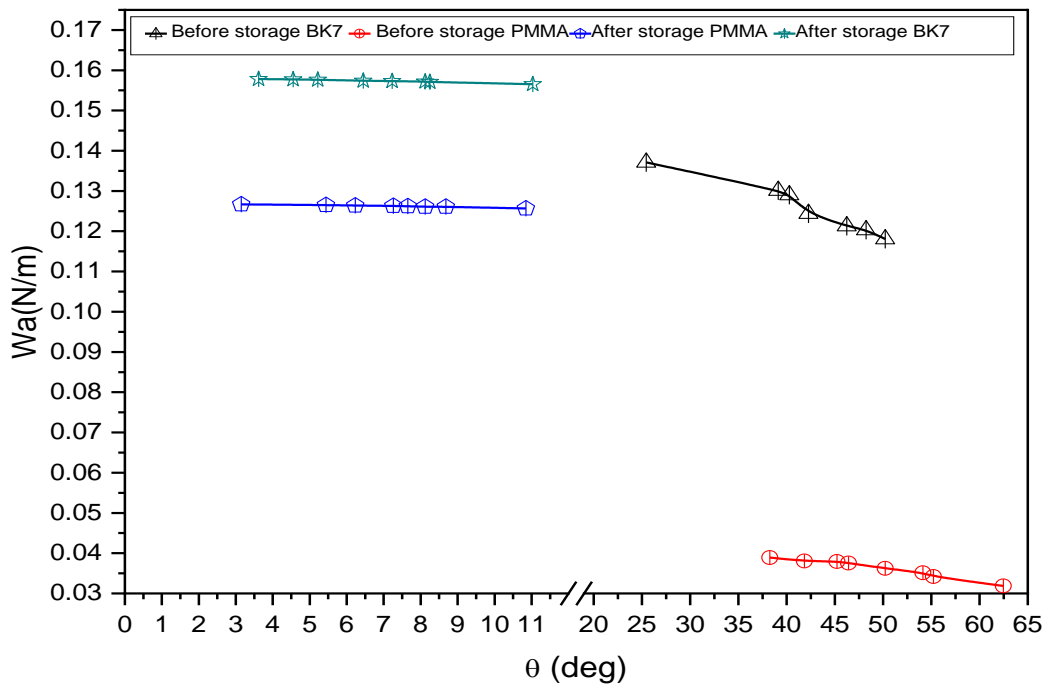


Figure 3.39. Variation of the adhesion strength of BK7 and PMMA vs. contact angle (ZnS20).

CHAPTER.3PRACTICAL STUDY

The results obtained in the Figure 3.38-3.39 show that the effect of the surface condition has an influence on the adhesive behavior of the ZnS20 solution. Indeed, this improvement in the surface's condition is accompanied by a decrease in the contact angle. However, another experimental parameter influences the adhesion, namely the wettability of the liquid. This parameter manages the spreading characteristics of the deposited solutions.

3.3.12.Adhesion and cohesion behavior

The results for several liquids (distilled water, N-octane, Tin dioxide(SnO_2), Titanium dioxide (TiO_2)) are presented in Figures 3.40-3.42.

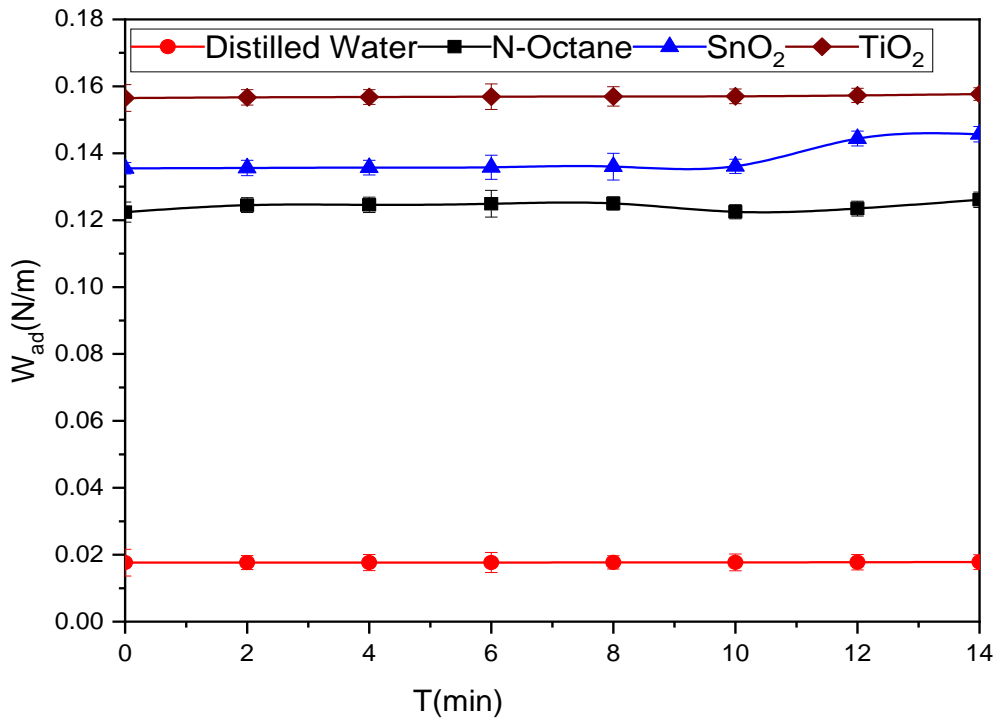


Figure 3.40. Variation of adhesion strength vs. polishing time of SL.

CHAPTER.3PRACTICAL STUDY

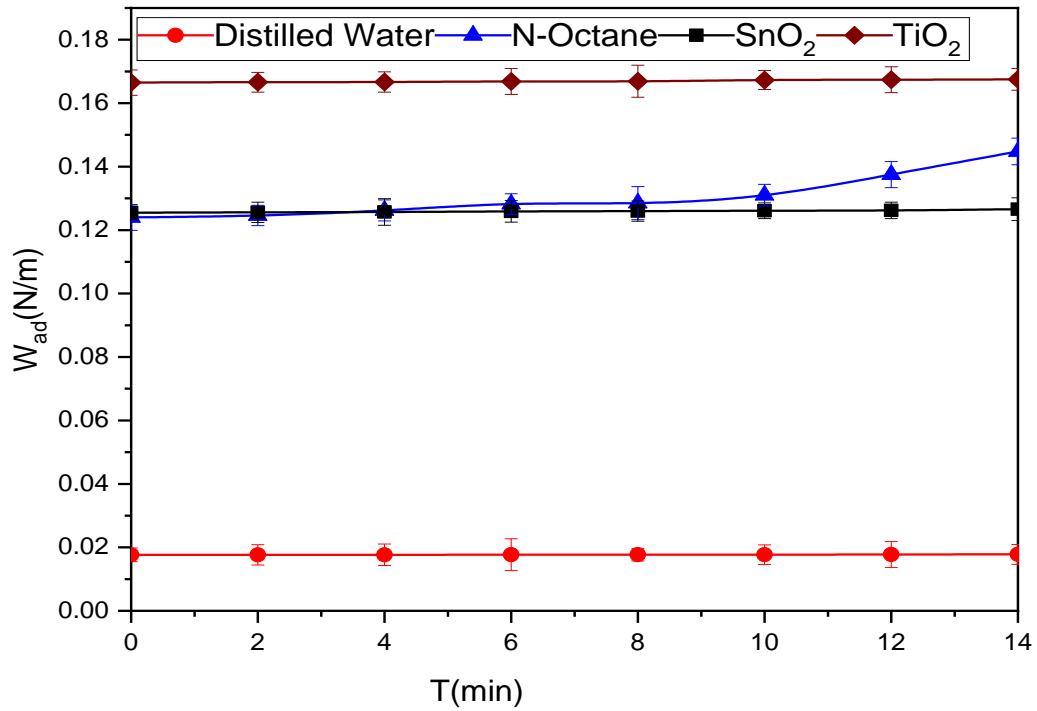


Figure3.41. Variation of adhesion strength vs. polishing time of B270.

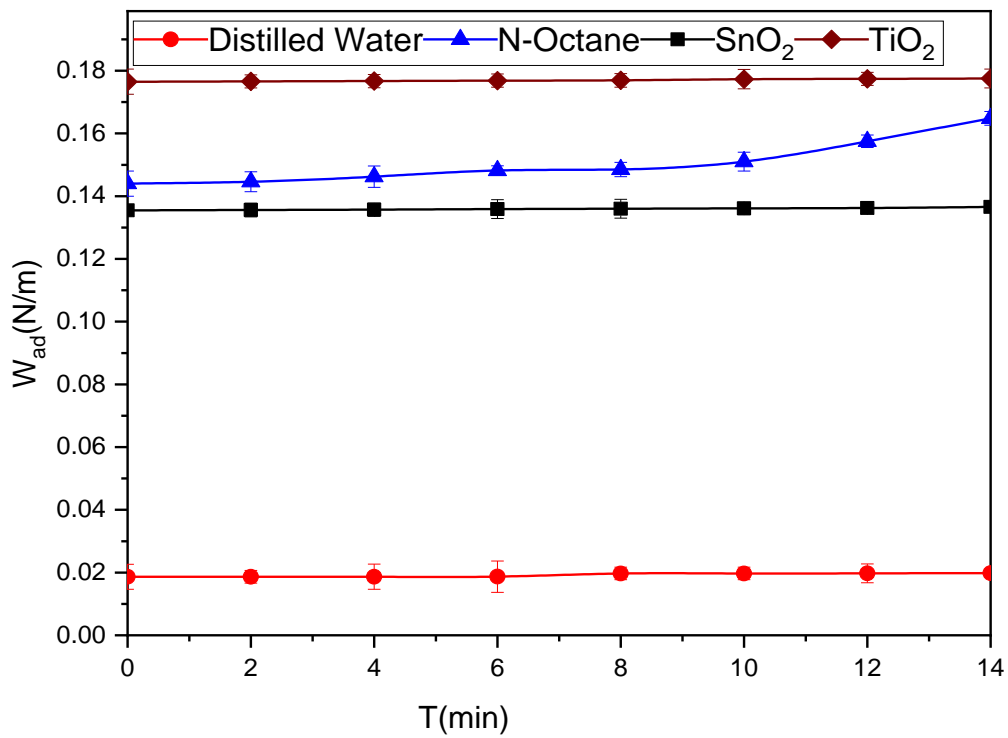


Figure3.42. Variation of adhesion strength vs. polishing time of PC.

The following diagrams in Figures 3.43-3.45 represent the liquids adhesion force according the contact angle.

CHAPTER.3PRACTICAL STUDY

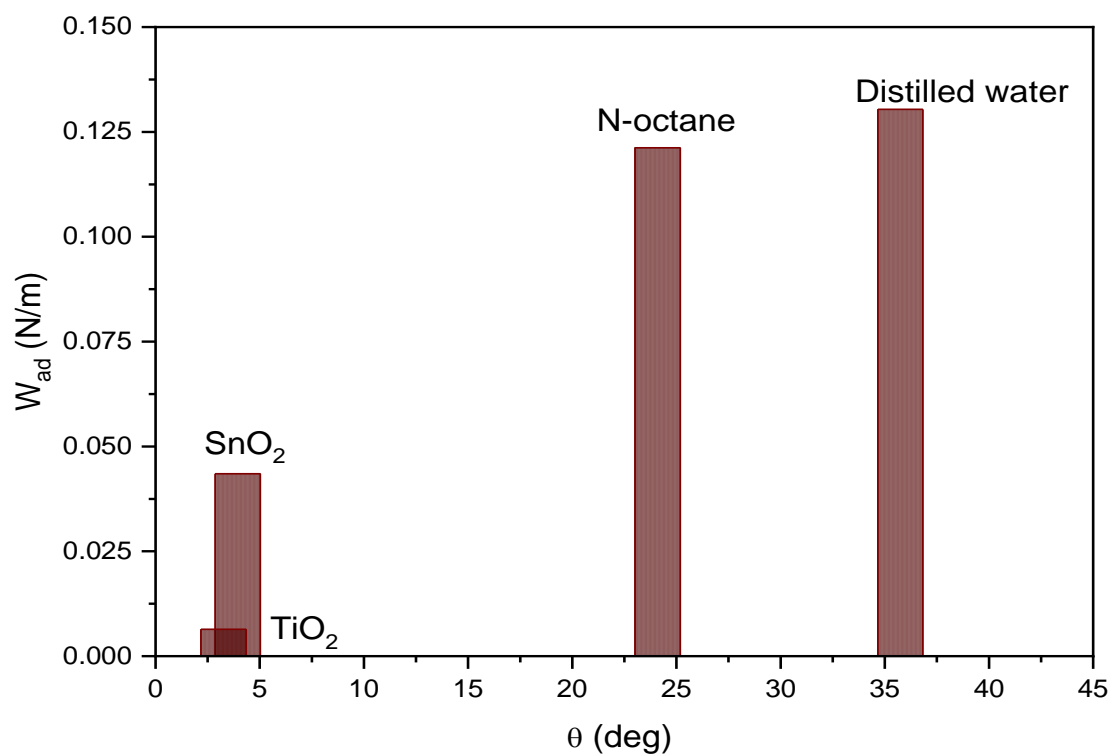


Figure.3.43. Variation of adhesion strength vs. Contact angle of SL.

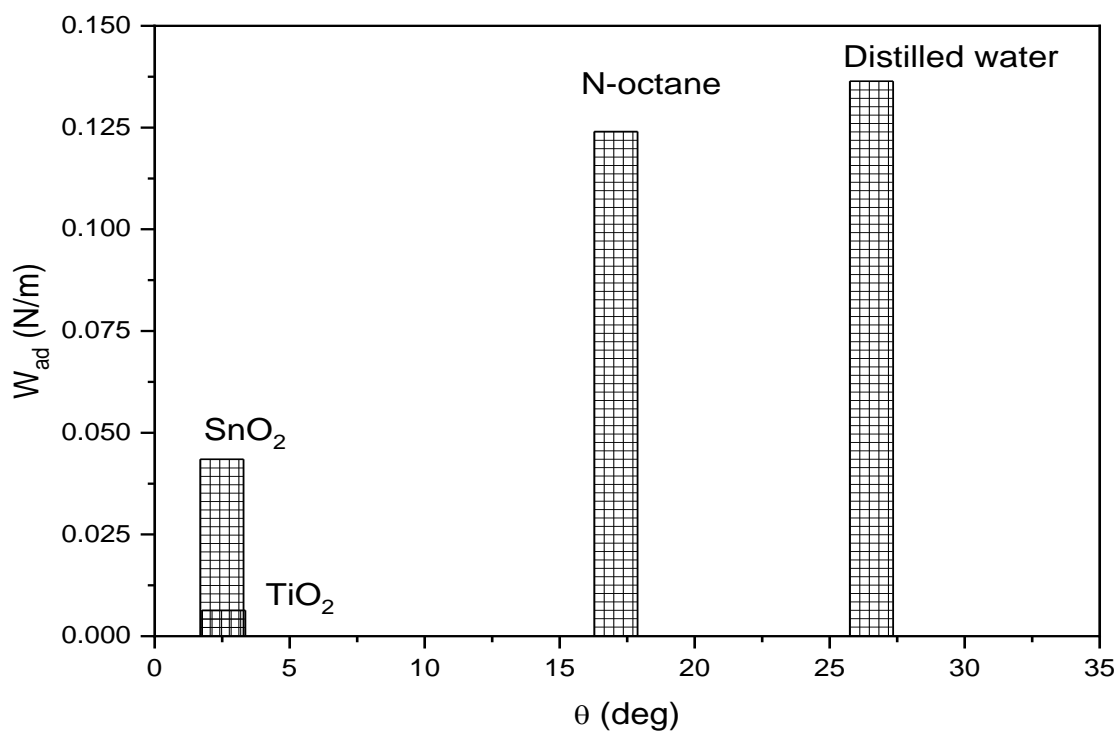


Figure 3.44. Variation of adhesion strength vs. Contact angle of B270.

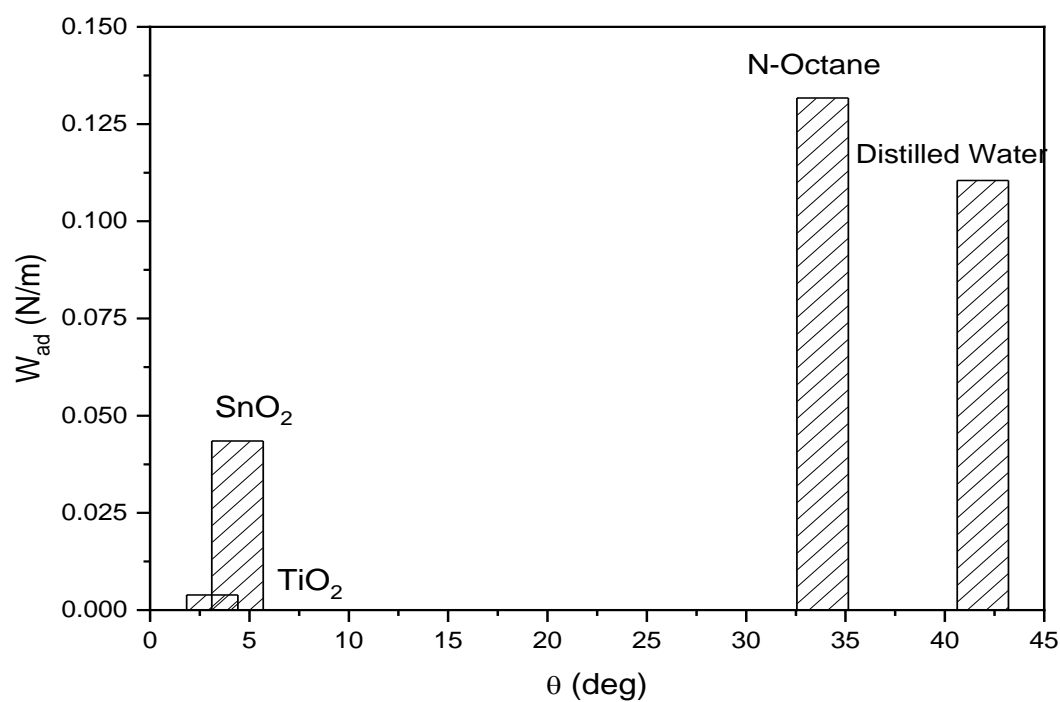


Figure 3.45. Variation of adhesion strength vs. Contact angle of PC.

The Figures 3.46- 3.48 below represent the results of adhesion and spreading coefficient effect of glass (SL, B270, and PC).

CHAPTER.3PRACTICAL STUDY

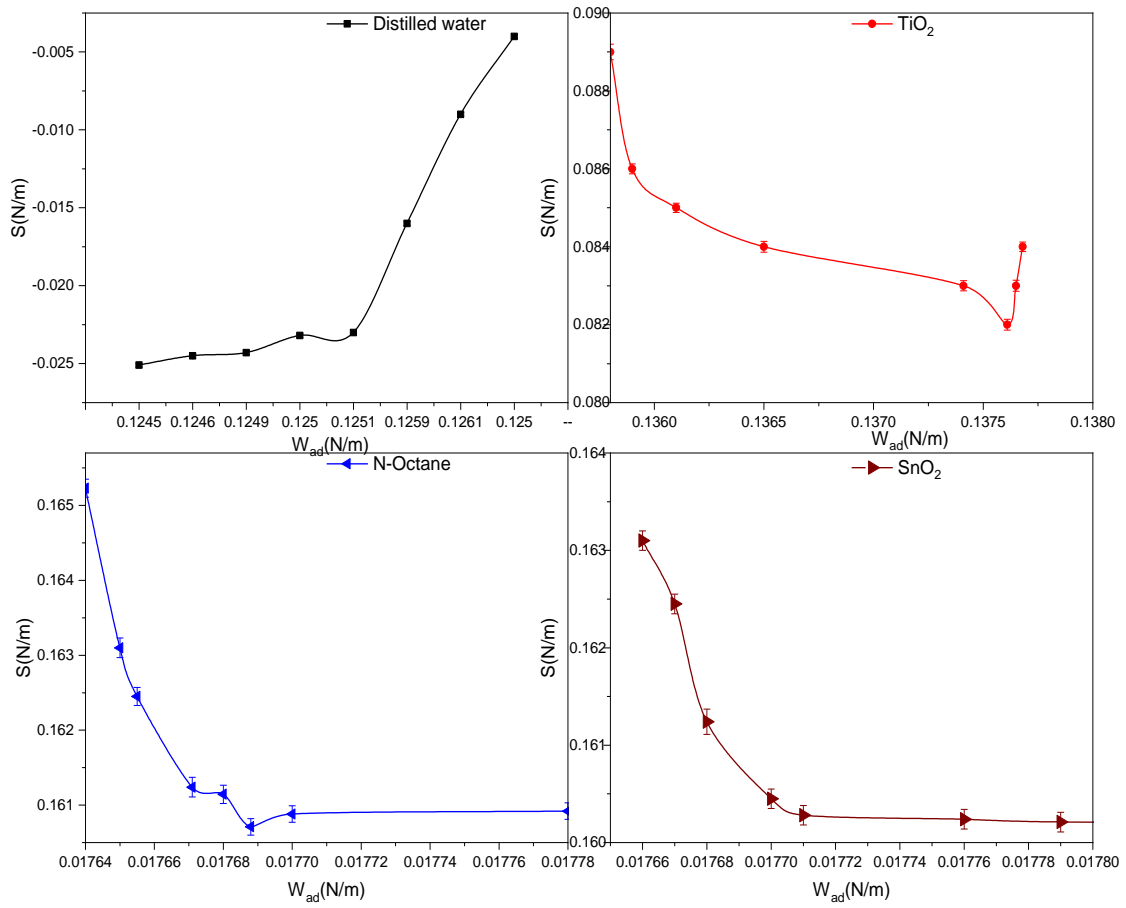


Figure 3.46. Variation of adhesion strength vs. Spreading coefficient effect on SL.

CHAPTER.3PRACTICAL STUDY

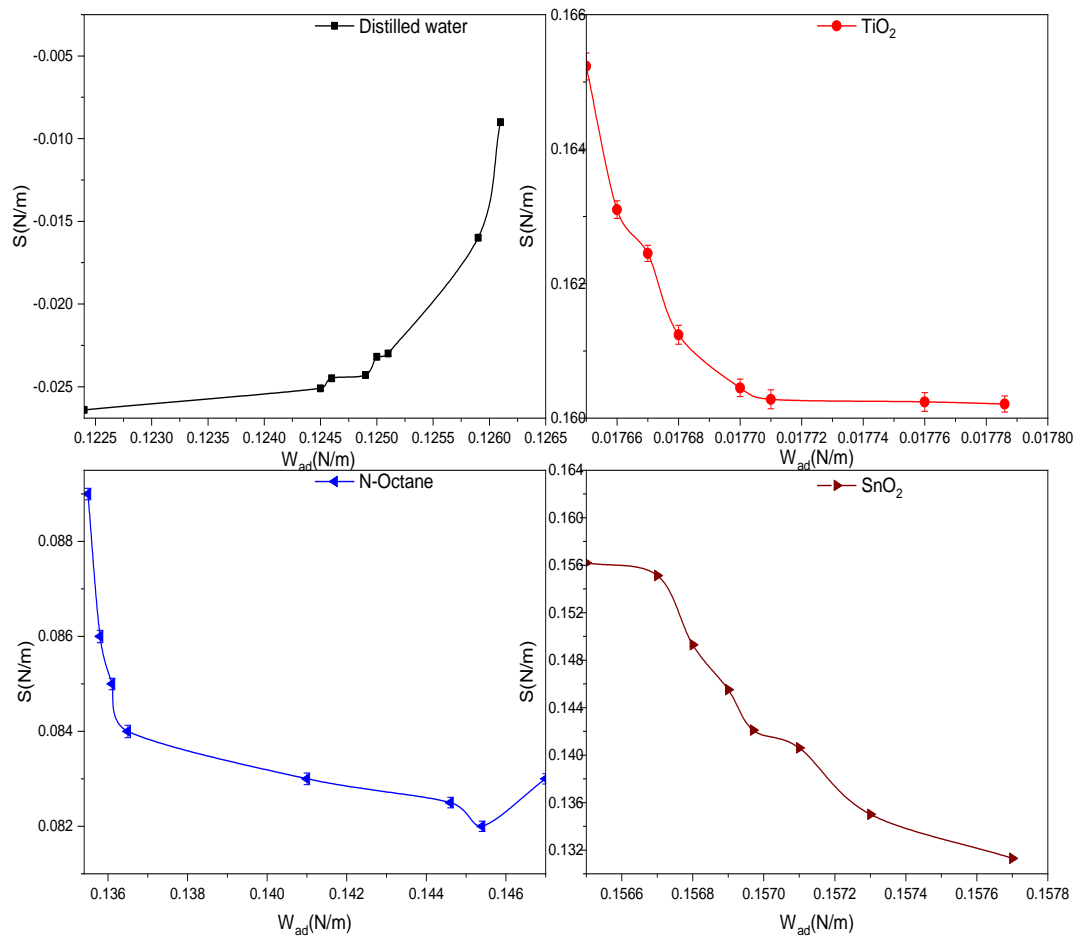


Figure 3.47. Variation of adhesion strength vs. Spreading coefficient effect on B270.

CHAPTER.3 PRACTICAL STUDY

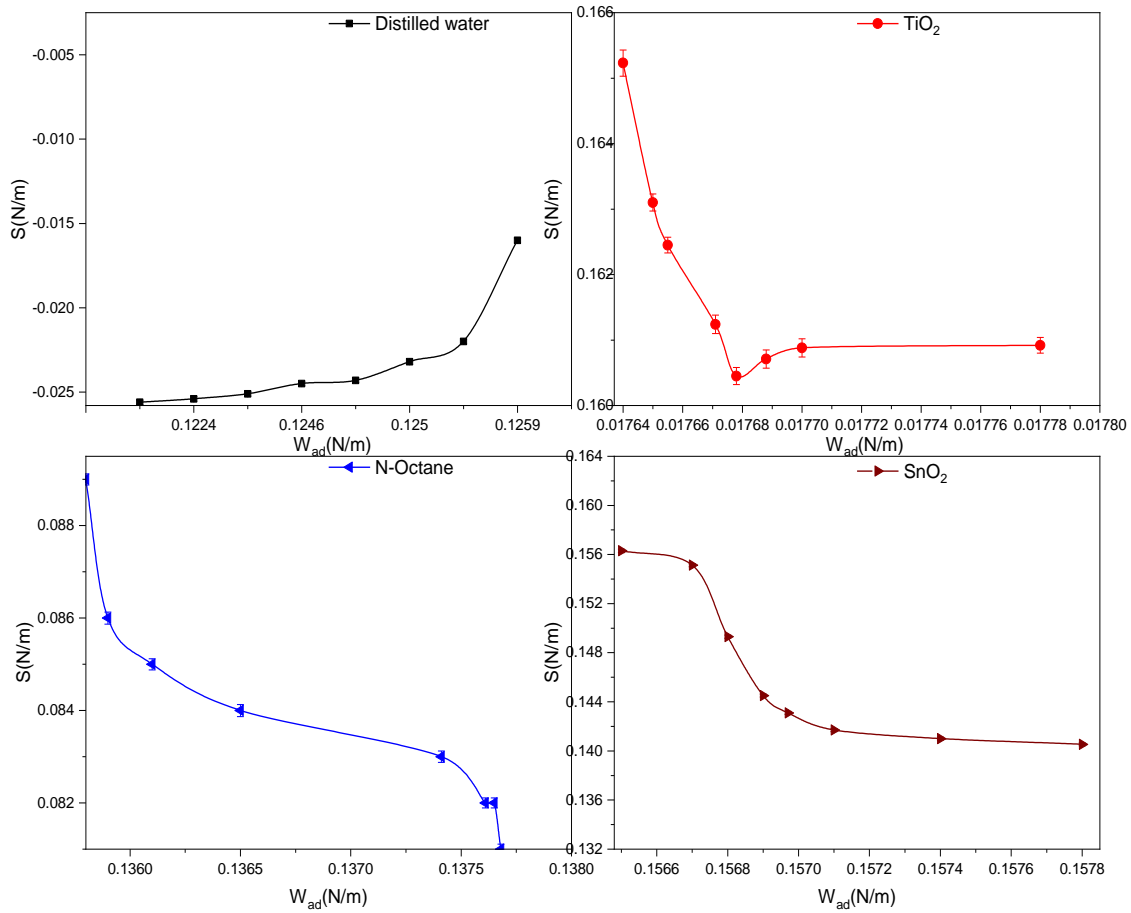


Figure 3.48. Variation of adhesion strength vs. Spreading coefficient effect on PC.

The preview results showed that the hydrophilic of the Titanium dioxide (TiO_2) liquid is better, this can induce the high cohesion of this liquid when deposited on polycarbonate surfaces.

Actually, the decreasing roughness of polycarbonate approves the high adhesion interaction of the substrate; in the fact the spreading coefficient (S) might enable its influence on the adhesion parameters and interfacial phenomena.

It is to be noticed that temperature, chemical nature, concentration of the thin film's solutions has a big influence on the studied factors as proved in previous works [203].

The adhesion behavior for the different types of samples indicates the influence of the type of material on this phenomenon which is obvious if knowing that the optical materials have different chemical compositions as well different properties.

GENERAL CONCLUSION

The adhesion of thin films is a very useful reliability and quality factor in the optical field. In this study, the adhesion behavior of stored and polished optical materials was investigated.

Several tests have been invested such as index measurement, Abbe number, transmission, Raman and FTIR synthesis, surface roughness measurement as well as: optical profilometry, AFM and TIS techniques; in addition, the measurement of the contact angle using the Digi-Drop technique to determine the adhesion and cohesion of the glasses (SL,B270,and PC) showed the hydrophilic properties of the liquids deposited on each substrate used, this means that the effect of the spreading coefficient on the polycarbonate surfaces is better.

The results obtained have led to several conclusions; the long-term storage of optical materials has changed their surface quality and slightly their optical properties. In addition, the quality of the thin film is closely related to the chemical compositions of the solutions.

Observation of this set of results leads us to explain the behavior of a very common phenomenon in the preparation of optical components film deposition which is adhesive force.

The variation in the contact angle for the different optical samples shows the influence of the type of material on this phenomenon, which is obvious if we know that optical materials have different compositions and chemical properties.

The surface condition, which can change from one substrate to another and depending on the conditions under which the samples are prepared, also affects the adhesive and spreading coefficient properties. Especially the different concentration of layers deposited

The surface quality control allowed the verification of the optical properties of the optical samples stored for 3 years in two solutions (CK and PEG) to study their storage effect on the adhesion of thin films.

The storage effect, surface roughness, and adhesion test have been identified to be applicable to optical materials and thin films spreading factor. Especially the different concentrations (SG20,and ZnS20) of layers deposited; which could be changed as function polishing time, duration, medium of storage(PEG and CK), chemical composition of optical glasses and polymers substrates.

The concentration of silica and Zinc Sulfide solutions has a considerable effect on the quality of the thin film. The thin film adhesion can be improved by using specific concentrations (SG20, ZnS20) with the lowest roughness of the chosen substrate.

A very frequent parameter, surface quality is a major factor in the adhesive behavior and wettability when depositing thin films. The high surface quality allows the performance of high quality films and improves wettability during the deposition of zinc Sulfide and Silica solutions.

It has been shown that for different surface states we have obtained different contact angle this can be explained by the fact that the surface roughness, reduced to the maximum without being completely removed, may interfere with the spreading of the liquid TiO_2 (Titanium dioxide) on the surface, causing a change in the adhesion phenomenon. A number of experimental factors influence the spreading factor such as:

- Chemical nature: the heavier and larger the molecules of the CK and PEG, the more difficult their movement relative to each other becomes.
- Temperature: Viscosity decreases when temperature increases due to release of interactions.
- Concentration: the higher the SG20 and ZnS20 concentrations, the greater the viscosity.

The influence of the concentrations of Silica and Zinc Sulfide thin films on the hydrophilic of selected liquids of the following sols were used: 20, 30, and 40%. In consequence, on the value of surface free energy components determined by Sol-gel and CBD methods were studied.

The adhesion between the depositing liquid and the substrate is not so clear in most cases, thus making deposition defects very common.

The photoluminescence of ZnS thin films is very complicated, as it depends on the preparation conditions, defects states, particle size and shape. The most intense photoluminescence was possessed by ZnS (20%) made on PMMA polished for 14 min.

The spreading effect on the physical properties of ZnS films has been studied. The experimental results indicated that the hydrophilic affects the surface morphology and optical properties of ZnS films significantly.

The behavior of optical constants such as refractive index and extinction coefficient was analyzed. The variation of the transmission coefficient (BK7, PMMA), and refractive index with an Abbe number was explained on the basis of the contribution from the packing density of SG20 and ZnS20 thin films.

The use of the invested technique will allow the specialist in the field of surface treatment to predict with speed and precision the quality of their deposits before producing it by the measurement of the adhesion behavior and the spreading factor.

REFERENCE

- [1] Chen P. Holbrook C. Boolchand P et al . Intermediate phase, network demixing, boson and floppy modes, and compositional trends in glass transition temperatures of binary AsxS1-x system.2008, Physical Review B.2008. 78. 224208.
- [2] Shydka D. Karpov V G.Nanodipole Photovoltaics. Applied Physics letter.2008.92(5):053507.
- [3] KiteyR.Geubelle H P,.,SottosNR.Mixed-mode interfacial adhesive strength of a thin film on an anisotropic substrate. Journal of the Mechanics and Physics of Solids .2009;57(1): 51-66 .
- [4] Yu J.Zhao X. Du J et al.Preparation, Microstructure and Photocatalytic Activity of the Porous TiO_2 Anatase Coating by Sol-Gel Processing. Science and Technology. 2000; 17:163-171.
- [5]Mehra R. Proc. Application of refractive index mixing rules in binary systems of hexadecane and heptadecane with n-alkanols at different temperatures .Proc,Indian Acad. Chemical Science.2003;115(2): 147-154.
- [6] Zhang L D.LiuL.Xu W H. Synthesis and characterization of superhydrophobic and super paramagnetic film based on maghemite-polystyrene composite nanoparticles. Journal of Applied Surface Science. 2012.259:719-725.
- [7] Cengiz U.Cansoy C E. Applicability of Cassie-Baxter equation for superhydrophobic fluoropolymer-silica composite films. Journal of Applied Surface Science.2015. 335:99-106.
- [8] Weber M J.Handbook of optical material.3Ed. CRC Press LLC. Boca Raton,U.S.2003.
- [9]Okatov M A. Optical Engineer's Handbook . Ed. St. Petersburg.2004.
- [10] Parsons W F. Optical materials research.Journal of Applied Optics.1972. 11:43–49 .
- [11] Doyle B K. Kahan A M. Design strength of optical glass. Proceedings of the SPIE. 2003.5176: 14-25.
- [12] Baumann SM, Martner CC, Martin D W et al. A study of electron beam evaporated SiO_2 , TiO_2 , and Al_2O_3 films using RBS, HFS, and SIMS.Beam.Intr.with Mater and Atom .1990;45: 664-668.
- [13] Yoshida M. Prasad PN. Fabrication of channel waveguides from sol-gel-processed polyvinylpyrrolidone/ SiO_2 composite materials. Journal of Applied Optics.1996. 35(9): 1500-1506 .
- [14] Kurkjian C R . Prindle W R.Perspectives on the history of glass composition.Journal of the American Ceramic Society .1998.81: 795–813.
- [15] Harper C A. Handbook of ceramics, glasses, and diamonds.1 Ed. McGraw-Hill, Lutherville, Maryland. 2001.

- [16] Rouxel T et al. Indentation deformation mechanism in glass: Densification versus shear flow. *Journal of applied physics*.2010.107: 1-5.
- [17] Launey E M. Ritchie O. R. On the Fracture Toughness of Advanced Materials. *Advanced Materials*. 2009.21:2103–2110
- [18] Wang J et al. Evaluating subsurface damage in optical glasses. *Journal of the European Optical Society - Rapid Publications*. 2011. 6: 1-16.
- [19] Rouxel T et al. Indentation deformation mechanism in glass: Densification versus shear flow. *Journal of applied physics*.2010.107:1-5.
- [20] Anees A . *Handbook of Optomechanical Engineering*.2 Eds. CRC Press. London SW1P 1WG. UK.2021.
- [21] (<https://www.schott.com/en-gb/products/optical-glass>)
- [22] Abiona A D. sinkolu A G. Gamma-irradiation induced property modification of polypropylene. *International Journal of Physical Science*. 2010.5(7):960-967
- [23] Breitbart A .Ablaza, V J. 2007 *Implant materials*. 2Eds. Lippincott Williams & Wilkins, Philadelphia.PA. US.2007.
- [24] Henri L. *Thermohydroelastic Properties of Polymethylmethacrylate*.Ed .Taylor and Francis. Netherlands.2007.
- [25] Demir M M. Memesa, M. Castignolles P. Wegner G. PMMA/zinc oxide Nanocomposites prepared by in-situ bulk polymerization. *Macromolecular Rapid Communications*. 2006. 27 (10): 763–770.
- [26] Charles A H. Edward M P. *Plastics Materials and Processes*, in *Concise Encyclopedia*. Ed. Wiley: NJ. 2003.
- [27] Van Krevelen D W. Nijenhuis K T. *Properties of Polymers*.3Ed. Elsevier: Amsterdam. 2000
- [28] Rouxel D. Thevenot C. Vincent B. *Brillouin spectroscopy of polymer nanocomposites*. *Spectroscopy of polymer nanocomposites*. 2Ed. William Andrew Publishing 2016.
- [29] (<https://www.gsoptics.com/>)
- [30] Whitehouse D J. Surface metrology. *Measurement Science & Technology* 1997.8 (9):955–972.
- [31] Lee S S. Chen J C. On-line surface roughness recognition system using artificial neural networks system in turning operations. *International Journal of Advanced Manufacturing Technology*.2003. 22: 498–509.
- [32] Lee B Y. Yu S F. Juan H. The model of surface roughness inspection by vision system in turning. *Mechatronics*. 2004. 14 (1):129–141.
- [33] Kumar R. Kulashekar P. Dhansekar B. Ramamoorthy B. Application of digital image magnification for surface roughness evaluation using machine vision. *Machine Tools & Manufacture*.2005.45:228–234.

- [34] Barányi I. Czifra A. Kalácska G. Height-independent topographic parameters of worn surfaces. *Sustainable Construction and Design*.2011. 2(1): 35–40.
- [35] Blunt L A. Jiang X . Advanced techniques for assessment surface topography. Kogan Page Science, London.2003.
- [36] Jiang X. Scott P J. Whitehouse D J. Blunt L . Paradigm shifts in surface metrology. *Proceedings of the Royal Society A*.2007.463:2049–2099.
- [37]Leach R K.Fundamental principles of engineering nanometrology. Elsevier. Amsterdam.2009
- [38] Löberg J. Mattisson I. Hansson S.Ahlberg E. Characterization of titanium dental implants I: critical assessment of surface roughness parameters. *Open Biomater*.2010. 2:18–35.
- [39] McGarigal K. TagilS.Cushman A. Surface metrics: an alternative to patch metrics for the quantification of landscape structure. *Landscape Ecology* .2009.24(3):433–450.
- [40] Muralikrishnan B, Raja J. Computational surface and roundness metrology.Springer .London.2009.
- [41] Gliech S. Steinert J. Duparré A .Light-scattering measurements of optical thin-film components at 157 and 193 nm .*Applied Optics*. 2002.41(16): 3224–3235
- [42] Lequime M. Zerrad M. DeumiéC .Amra C. A goniometric light scattering instrument with high-resolution imaging. *Optics Communications*.2009. 282: 1265–1273.
- [43] Shin M J. Cho H J. Lim K A. Moon Y K . Lee J C .Measurement of losses in mirror using cavity ring down method. *Korean Journal of Optic and Photon*.2000. 11:123-129.
- [44] Verbiest T. Clays K. Rodriguez V. In *Second-Order Nonlinear Optical Characterization Techniques: An Introduction*. Taylor & Francis Group.2Eds. Boca Raton. 2009.
- [45] Bosshard C. Gubler U. Kaatz P. Mazerant W. Meier U. Non-Phase-Matched Optical Third-Harmonic Generation in Noncentrosymmetric Media: Cascaded Second-Order Contributions for the Calibration of Third-Order Nonlinearities. *Physical Review B - Condensed Matter and Materials Physics*. 2000.61:10688-10701.
- [46] Dussauze M. Rodriguez V. Lipovskii A. Petrov M. Smith C. Richardson K. Cardinal T. Fargin E. Kamitsos I. How does Thermal Poling Affect the Structure of Soda-Lime Glass. *Journal of Physical Chemistry*. 2010. 114:12754-12759.
- [47] Koudelka L. Horák J. Pisárcik M. Sakál L. Structural Interpretation of Raman Spectra of (As₂S₃)_{1-X}(AsBr₃)_X System Glasses. *Journal Non Crystalline Solids*. 1979. 31:339-345.
- [48] Wilson T. Massournian F. Juskaitis R. Generation and Focusing of Radially Polarized Electric Fields. *Optical Engineering*. 2003.42:3088-3089.
- [49] De Cumis M S. D'Amato F. Viciani S. Patrizi B. Foggi P. Galea C L. First quantitative measurements by IR spectroscopy of dioxins and furans by means of broadly tunable quantum cascade lasers. *Laser Physics*. 2013.23.

- [50] Patrizi B. de Cumis M S. Viciani S. D'Amato F. Foggi P. Characteristic vibrational frequencies of toxic polychlorinated dibenzo-dioxins and -furans. *J. Hazard. Mater.* 2014. 274: 98–105
- [51] Smith B. *Fundamentals of Fourier Transform Infrared Spectroscopy*. 2 Eds. CRC Press: Boca Raton, USA 2011.
- [52] Bruning D J. Digital wave front measuring interferometer for testing optical surfaces and lenses. *Applied Optics*. 1974.13(11):2693–2703.
- [53] Makosch G . Drollinger B .Surface profile measurement with a scanning differential ac interferometer. *Applied Optics*.1984. 23(24):4544-4553.
- [54] Finot E. Passian A. Thundat T. Measurement of mechanical properties of cantilever shaped materials. *Sensors*. 2008. 8: 3497-3541.
- [55] Jalili N. Laxminarayana K A. review of atomic force microscopy imaging systems: application to molecular metrology and biological sciences. *Mechatronics*. 2004.14: 907-945.
- [56] Hersam M C. Monitoring and analyzing nonlinear dynamics in atomic force microscopy. *Small* .2006.2:1122-1124.
- [57] Wei Z.Zhao Y P. Growth of liquid bridge in AFM. *Journal of Physics D Applied Physics*. 2008. 40: 4368-4375.
- [58] Yacoot A. Koenders L. Aspects of scanning force microscope probes and their effects on dimensional measurement. *Journal of Physics D Applied Physics* .2008. 41(10): 103001.
- [59] Lee S I. Howell S W. Raman A. Reifenberger R. Nonlinear dynamics of microcantilevers in tapping mode atomic force microscopy: a comparison between theory and experiment. *Physical Review B* .2002.66(11): 115409.
- [60] Zhao X. Dankowicz H. Characterization of intermittent contact in tapping-mode atomic force microscopy. *ASME Journal of Computational and Nonlinear Dynamics* . 2006. 1:109-115.
- [61] Kruchinin D Y. Yakovlev O B. Andronov M P. Gluing of optical parts having purity class-0 polished surfaces. *Optical of technology*.2011.78 (4).73 – 75.
- [62] Potelov V V. Particulars for working optical glass during the manufacture of prism modules. *Glass Ceram.* 2009.66(8):284 – 287.
- [63] K. Hirao K. Todoroki S.D.H. Cho D H. Soga N. Room-temperature persistent hole burning of Sm²⁺ in oxide glasses. *Optics Letter*. 1993.18(19): 1586-1587.
- [64] Rakuljic G A . Victor L. Yariv A. Optical data storage by using orthogonal wavelength-multiplexed volume holograms . *Optics Letter*. 1992 .17(20) . *Optics Letter* 1471-1474.
- [65] Bertzig E. Trauman J K. Wolfe R. Gyorgy E M. Flinn P L. Near-field magneto-optics and high density data storage .*Applied. Physics. Letter*.1992. 61(2). 142-144.

- [66] Verney-Carron A. Gin S. Libourel G A. fractured roman glass block altered for 1800 years in seawater: analogy with nuclear waste glass in a deep geological repository. *GeochimCosmochim Acta* .2008.72:5372–5385.
- [67] Kunicki-Goldfinger J J. Unstable historic glass: symptoms, causes, mechanisms and conservation. *Rev Conserv*. 2008.9: 47–60.
- [68] Stricker J H. Webb W W. Three-dimensional optical data storage in refractive media by two-photon point excitation. *Optics Letter*. 1991.16(22).1780-1782.
- [69] Kruchinin D Y. Farafontova E P. Ambient Environment Effect on a Polished Optical-Glass Surface. *Glass and Ceramics*. 2016. 72(10): 320–322
- [70] Martin P. Introduction to surface engineering and functionally engineered materials. 1Ed. John Wiley and Sons. 2011.
- [71] Akinlabi E T .MahamoodRM. Akinlabi S A. Advanced Manufacturing Techniques Using Laser Material Processing. *Advances in Civil and Industrial Engineering* n IGI Global, 2016.1–23.
- [72] Kashani H, Amadeh A, Ghasemi H .Room and high temperature wear behaviors of nickel and cobalt base weld overlay coatings on hot forging dies. *Wear* .2007.262: 800–806.
- [73] Mellali M. Fauchais P. Grimaud A. Influence of substrate roughness and temperature on the adhesion/cohesion of alumina coatings, surface and Coating Technology. 1996.81(2):275-286
- [74] Orava J. Kohoutek T. Wagner T. Deposition techniques for chalcogenide thin Films. Woodhead. Oxford. 2014.
- [75] Seshan K. Thin-Film Deposition Processes And Techniques Principles, Methods, Equipment and Applications. 2Ed. Noyes Publications. 2002.
- [76] Kasap S. Capper P. Handbook of electronic and photonic materials. 2Ed. Springer. Switzerland .2017.
- [77] RahemiArdekani S. SabourRouhAghdamA. Nazari M et al. A comprehensive review on ultrasonic spray pyrolysis technique: mechanism. main parameters and applications in condensed matter, *Journal of Analytical and Applied Pyrolysis*. 2019.141-631.
- [78] Shan R . Yi J. Zhong J. Yang S. Effect of sulphur pressure on properties of ZnS thin film prepared by chemical bath deposition technique. *Journal of Materials Science: Materials in Electronics*. 2019.30 : 13230–13237.
- [79] Velanganni S. Manikandan A .Prince J. Mohan C N. Thiruneelakandan R. Nanostructured ZnO coated Bi₂S₃ thin films: enhanced photocatalytic degradation of methylene blue dye. *Phys B: Condensed. Matter*. 2018. 545 :383–389.
- [80] Das M R, Mitra P. SILAR-synthesized CdO thin films for improved supercapacitive photocatalytic and LPG-sensing performance. *Chemical Paper*. 2019.73:1605–1619.

- [81] Fairose S . Ernest S. Nanostructured ZnO sensor fabricated by successive ionic layer adsorption and reaction method for ammonia sensing application, *Phys B:Condensed Matter* .2019.557 : 63–73.
- [82] Ziti A. Hartiti B. Labrim H . Fadil S et al. Characteristics of kesterite CZTS thin films deposited by dip-coating technique for solar cells applications. *Journal of Materials Science Mater Electron*.2019.30: 13134–13143.
- [83] Zhang M. LE R. Zhang R. Liu Z. The effect of SiO₂ on TiO₂-SiO₂ composite film for self-cleaning application, *Surface and Interface*. 2019.16: 194–198.
- [84] Ravichandiran C . Sakthivelu A . Davidprabu R . Valanarasu S, In-depth study on structural, optical photoluminescence and electrical properties of electrodeposited Cu₂O thin films for optoelectronics: an effect of solution Ph. *Microelectronic Engineering*.2019. 210:27–34.
- [85] Martins A S. Cordeiro-Junior J M. Bessegato G G et al. Electrodeposition of WO₃ on Ti substrate and the influence of interfacial oxide layer generated in situ: a photoelectrocatalytic degradation of propyl paraben, *Appl. Surf. Sci.* 2019.464 :664–672.
- [86] Fay S . Steinhäuser J . Oliveira N. Vallat-Sauvain E. Ballif C. Opto-electronic properties of rough LP-CVD ZnO:B for use as TCO in thin-film silicon solar cells. *Thin Solid Films*.2007.515:8558–8561
- [87] Bigiani L. Barreca D. Gasparotto A. Sada C. Controllable vapor phase fabrication of F:Mn₃O₄ thin films functionalized with Ag and TiO₂. *Cryst Eng Comm*.2018.20 :3016–3024
- [88] Martinet C. Paillard V. Gagnaire A. Joseph J. Deposition of SiO₂ and TiO₂ thin films by plasma enhanced chemical vapor deposition for antireflection coating. *Journal of Non-Crystalline Solids*.1997.216 :77–82.
- [89] Yang W. Wolden C A. Plasma-enhanced chemical vapor deposition of TiO₂ thin films for dielectric applications, *Thin Solid Films*.2006.515: 1708–1713.
- [90] Maeda M. Watanabe T. Evaluation of photocatalytic properties of titanium oxide films prepared by plasma-enhanced chemical vapor deposition, *Thin Solid Films* 2005.489: 320–324.
- [91] Liu B. Zhao X . Zhang N. Zhao Q. Photocatalytic Mechanism of TiO₂ – CeO₂ Films Prepared by Magnetron Sputtering under UV and Visible Light. *Surface science*.2005 .595(1): 203–211
- [92] Arulraj A. Subramanian B. Ramesh M. Senguttuvan G. Effect of active sites in pulsed laser deposited bimetallic NiMoS₂ thin films for solar energy conversion. *Mater Letters*. 2019.241:132–135.

- [93] Olvera-Rodríguez I. Hernández R. Medel A. Guzmán C et al. TiO₂/Au/TiO₂ multilayer thin-film photoanode synthesized by pulsed laser deposition for photoelectrochemical degradation of organic pollutants, *Separation and Purification Technology*. 2019. 224: 189–198.
- [94] Pessoa R. Fraga M. Santos L. et al. Nanostructured thin films based on TiO₂ and/or SiC for use in photoelectrochemical cells: A review of the material characteristics, synthesis and recent applications. *material science in semiconductor processing*. 2015. 29: 56–68.
- [95] Kommu S. Wilson G M. Khomami B . A Theoretical/Experimental Study of Silicon Epitaxy in Horizontal Single-Wafer Chemical Vapor Deposition Reactors. *Electrochemical Society* .2000. 147: 1538–1550.
- [96] Pedersen H. Simon D E . Studying chemical vapor deposition processes with theoretical chemistry. *Theoretical Chemistry accounts*, 2014. 5(133): 1476-1490..
- [97] Fuller C B . Mahoney M W . Bingel W H . Friction stir weld tool and method. U.S. Patent .2006. 6:994,242.
- [98] Toku H, Pessoa R S. Maciel H S et al. Influence of Process Parameters on the Growth of Pure-Phase Anatase and Rutile TiO₂ Thin Films Deposited by Low Temperature Reactive Magnetron Sputtering. *Brazilian Journal of Physics*. 2010. 40: 340–343.
- [99] Sousa P. Silvestre A. Popovici N et al. Morphological and structural characterization of CrO₂/Cr₂O₃ films grown by Laser-CVD. *Applied Surface Science* .2005. 247: 423–428.
- [100] Shwetharani R . Chandan H R. Sakar M et al. Photocatalytic semiconductor thin films for hydrogen production and environmental applications. *International Journal of Hydrogen Energy*. 2019. 45(36):5-17.
- [101] Wei Q. Wang Y. Textile Surface Functionalization by Physical Vapor Deposition (PVD) . 2009:58-90.
- [102] Mattox D M . Handbook of physical vapor deposition (PVD) processing, 2 Eds. William Andrew. London. 2010.
- [103] Park S . Ikegami T. Ebihara K et al. Structure and properties of transparent conductive doped ZnO films by pulsed laser deposition. *Applied Surface Science*. 2006. 253: 1522–1527.
- [104] Helmersson U. Lättemann M. Bohlmark J et al. Review Ionized physical vapor deposition (IPVD): A review of technology and applications. *Thin Solid Films*. 2006. 513: 1–24.
- [105] Yang T. Shiu C. Wong M. Structure and Hydrophilicity of Titanium Oxide Films Prepared by Electron Beam Evaporation. *Surface Science*. 2004. 548(1): 75–82,
- [106] Shan R. Yi J. Zhong J. Yang S. Effect of sulphur pressure on properties of ZnS

thin film prepared by chemical bath deposition technique. *Journal of Materials Science Mater Electron*. 2019.30: 13230–13237

[107] Kim J K. Thomas S. Saha P. *Multicomponent Polymeric Materials*. 1st Ed. Springer. Dordrecht. 2016.

[108] Lokhande A C. Chalapathy RBV. He M. Jo E et al. Development of Cu₂SnS₃ (CTS) thin film solar cells by physical techniques: A status review. *Sol. Ener. Mater. Sol. Cells*. 2016.153:84–107.

[109] Barranco A. Borras A. Elisei ARG. Palmero A. Perspectives on oblique angle deposition of thin films: From fundamentals to devices. *Progress in Materials Science*. 2016.76:59–153.

[110] Merkel J J. Sontheimer T. Rech B. Becker C. Directional growth and crystallization of silicon thin films prepared by electron-beam evaporation on oblique and textured surfaces. *Journal of Crystal Growth*. 2013. 367:126–130.

[111] Mukherjee S. Gall D. Structure zone model for extreme shadowing conditions. *Thin Solid Films*. 2013.527:158–163.

[112] Schulz U. Terry S G. Levi CG. Microstructure and texture of EB-PVD TBCs grown under different rotation modes. *Materials Science and Engineering: A*. 2003.360(1–2):319–329.

[113] Yang B. Duan H. Zhou C. Gao Y. Yang J. Ordered nanocolumn- array organic semiconductor thin films with controllable molecular orientation. *Applied Surface Science*. 2013.286:104–108.

[114] Lorenz M. Rao M S. 25 years of pulsed laser deposition. *Journal of Physics D: Applied Physics*. 2014.47:30301–30303

[115] Y. Huang, H. Liu, C. Ma, P. Yu, Y. Chu, Pulsed laser deposition of complex oxide heteroepitaxy, 60 (2019) 481–501.

[116] Mishra M. Chun D M. α -Fe₂O₃ as a photocatalytic material: a review *Applied Catalysis A: General*. 2015. 498:126–141

[117] Ashfold M N. Claeys F. Fuge G M. Henley S J. Pulsed laser ablation and deposition of thin films. *Chemical Society Reviews*. 2004.33(1):23–31.

[118] Grigore E. Ruset C. X. Li X. Dong H. Zirconium carbonitride films deposited by combined magnetron sputtering and ion implantation (CMSII). *Surface and Coatings Technology*. 2010. 204: 1889–1892.

[119] Abadías G. Pailloux F. Dub S N. Epitaxial growth and mechanical properties of (001) ZrN/W nanolaminates. *Surface and Coatings Technology*. 2008.202(15):3683–3687.

[120] Qiu Z Y. Chen C. Wang X M. Lee I S. Advances in the surface modification techniques of bone-related implants for last 10 years. *Regenerative Biomaterials*. 2014.1(1):67-79.

- [121] Chen C, Lee I-S, Zhang S-M, et al. Biomimetic fibronectin/mineral and osteogenic growth peptide/mineral composites synthesized on calcium phosphate thin films. *Chemical Communications*. 2011.47(39):11056-11080.
- [122] Dumitru V, Morosanu C, Sandu V, Stoica A. Optical and structural differences between RF and DC Al_xNy magnetron sputtered films. *Thin Solid Films*. 2000.359:17–20.
- [123] Barranco A, Borrás A, Elípe A, Palmero A. Perspectives on oblique angle deposition of thin films: From fundamentals to devices. *Progress in Materials Science*. 2016.76:59–153.
- [124] Angus Macleod H. Recent developments in deposition techniques for optical thin films and coatings.. *Optical Thin Films and Coatings from Materials to Applications*. 2013: 3-25.
- [125] Dubey P, Arya V, Srivastava S, Singh D, Chandra R, Effect of nitrogen flow rate on structural and mechanical properties of Zirconium Tungsten Nitride (Zr–W–N) coatings deposited by magnetron sputtering, *Surface and Coatings Technology*. 2013.236:182–187.
- [126] Silva E, Figueiredo M R, Franz R, Galindo R E et al Structure–property relations in ZrCN coatings for tribological applications, *Surface and Coatings Technology*. 2010.205(7):2134–2141.
- [127] Braic M, Balaceanu M, Vladescu A. Study of (Zr,Ti)CN, (Zr,Hf)CN and (Zr,Nb)CN films prepared by reactive magnetron sputtering. *Thin Solid Films*. 2011.519(12): 4092–4096.
- [128] Abadías G, Koutsokeras L E, Guerin P, Patsalas P. Stress evolution in magnetron sputtered Ti–Zr–N and Ti–Ta–N films studied by in situ wafer curvature: role of energetic particles, *Thin Solid Films*. 2009. 518(5):1532–1537.
- [129] Tetsuhide S, Yoshikazu T, Morikawa K, Hidetoshi K et al. Impact of pulse duration in high power impulse magnetron sputtering on the low-temperature growth of wurtzite phase (Ti,Al)N films with high hardness. *Thin Solid Films*. 2015. 581:39–47.
- [130] Ishihara M L, Yumoto H et al. Control of preferential orientation of AlN films prepared by the reactive sputtering method. *Thin Solid Films*. 1998. 316: 152–157.
- [131] M. Naguib M, Mashtalir O, Carle J et al. *Two-dimensional transition metal carbides*. *ACS Nano*. 2012.6(2):1322-1331 .
- [132] Nable J C, Gulbinska, Kmetz M A et al. Aluminum Oxide and Chromium Oxide Coatings on Ceramic Fibers via MOCVD. *Chemistry of Materials*. 2003.15(25): 4823– 4829.
- [133] Livage J, Sanchez C, Henry M, Doeuff S. The chemistry of sol-gel process. *Solid State Ionics*. 1989;32(2):633–638.
- [134] Attia S M, Wang J, Wu G, Shen J, Ma J. Review on sol- Gel derived coatings: process, techniques and optical applications, *J. Mater. Sci. Mater. Technol*. 2002.18(3):211-217.
- [135] Znaidi L. Sol – gel-deposited ZnO thin films Review: *Materials Science and Engineering B* .2010.174: 18–30.

- [136] Livage J. Ganguli D. Sol-gel electrochromic coatings and devices: A review. *Solar Energy Materials and Solar Cells*. 2001.68:365–381
- [137] Pierre A C. Introduction to sol-gel processing. Springer.1998.
- [138] Zhang H.Yang D. Ji Y.Ma X. Xu J. Que D. Low temperature synthesis of flowerlike ZnO nanostructures by cetyltrimethylammonium bromide-assisted hydrothermal process. *Journal of Physical Chemistry B*. 2004.108:3955-3958.
- [139]. Nagarale R K. Shina W. Singh PK. Progress in ionic organic-inorganic composite membranes for fuel cell applications. *Polymer Chemistry*.2010.1:388–408.
- [140] Hench LL. Sol-Gel silica: properties, processing and technology transfer. Elsevier.1998.
- [141] Corriu R J, Leclercq D. Recent developments of molecular chemistry for sol-gel processes. *Angewandte Chemie International Edition* .1996.35(13):1420-1436.
- [142] Corriu R J, Guerin C, Henner B J.Wang Q. Role of pentacoordinate intermediates in the hydrolysis reaction of organic silicates. *Organometallics* .1999.18(9):3200-3205.
- [143] Klein L C. Sol–Gel Optics: Processing and Applications.1Ed. Kluwer Academic . Dordrecht. Netherlands .1994.
- [144] Norrman K.Ghanbari A.Larsen N B .Studies of Spin-coated Polymer Films, *Annual Reports on the Progress of Chemistry, Section C*. 2005.101:174–201
- [145] Mohd Yusoff M F. Abdul Kadir M R. Iqbal N. Hassan M A. Hussain R. Dipcoating of poly(ϵ -caprolactone)/hydroxyapatite composite coating on Ti6Al4V for enhanced corrosion protection, *Surface and Coatings Technology*. 2014.245:102-107
- [146] Yamaguchi T. Suzuki T. Shimizu S. Fujishiro Y. Awano M. Examination of wet coating and co-sintering technologies for micro-SOFCs fabrication. *Journal of Membrane Science*.2007.300 (2) : 45-50.
- [147] Mahmud L S. Muchtar A. Somalu M R. Challenges in fabricating planar solid oxide fuel cells: a review. *Renewable and Sustainable Energy Reviews*.2017. 72 : 105-116.
- [148] Klein LC. Sol-Gel Technology for Thin Films, Fiber, Preform, Electronics and Specialty Shapes. Park Ridge .2 Eds. Noyes. USA.1987.
- [149] Setz L F. Santacruz I. Colomer M T. Mello-Castanho S R .Tape casting of strontium and cobalt doped lanthanum chromite suspensions. *Journal of the European Ceramic Society*.2010.30(14): 2897-2903.
- [150] Wang D. Bierwagen G P. Progress in Organic Coatings Sol – gel coatings on metals for corrosion protection.2009. 64: 327–338.
- [151] Tikkanen H. C. Suci C. Wærnhus I. Hoffmann A C. Dip-coating of YSZ nanopowder

for SOFC applications. *Ceramics International*. 2011.37 (7) : 2869-2877.

[152] Torabi A. Etsell T H. Sarkar P. Dip coating fabrication process for micro-tubular SOFCs, *Solid State Ionics* .2011.192 (1) : 372-375.

[153] Kim S D et al. Effects of anode and electrolyte microstructures on performance of solid oxide fuel cells. *Journal of Power Sources* .2007.169 (2) :265-270.

[154] Somalu M R. Yufit V. Shapiro I P. Xiao P. Brandon N P. The impact of ink rheology on the properties of screen-printed solid oxide fuel cell anodes, *International Journal of Hydrogen Energy*.2013. 38 (16): 6789-6801.

[155] Yamaguchi T. Suzuki T. Shimizu S. Fujishiro Y. Awano M. Examination of wet coating and co-sintering technologies for micro-SOFCs fabrication, *Journal of Membrane Science*.2007.300 (2) : 45-50.

[156] Mohd Yusoff M F. Abdul Kadir M R et al. Dipcoating of poly(ϵ -caprolactone)/hydroxyapatite composite coating on Ti6Al4V for enhanced corrosion protection, *Surface and Coatings Technology*. 2014.245 : 102-107.

[157] Wang W. Winkler M T. Gunawan O.. Gokmen T. Todorov T K. Zhu . Mitzi D B. Device Characteristics of CZTSSe Thin-Film Solar Cells with 12.6% Efficiency. *Advanced Energy Materials*. 2014. 4(7): 1301465

[158] Ramasamy K. Malik A M. O'Brien P. Routes to copper zinc tin sulfide $\text{Cu}_2\text{ZnSnS}_4$ a potential material for solar cells. *Chemical Communications*.2012.48. 5703-5714 .

[159] Mukherjee A. Mitra P. Characterization of Sn doped ZnS thin films synthesized by CBD. *Materials Research*.2017.20(2): 430–435.

[160] Padmavathy V. Sankar S. Ponnuswamy V. Influence of thiourea on the synthesis and characterization of chemically deposited nano structured zinc sulphide thin films. *Journal of Materials Science: Materials in Electronics*. 2018.29(9): 7739–7749.

[161] Mane R S. Lokhande C D. Chemical deposition method for metal chalcogenide thin films. *Materials Chemistry and Physics*.. 2000.1:1–31.

[162] Delhaes P .Chemical vapor deposition and infiltration processes of carbon materials.2002.40: 641–657.

[163] Zhang T. Fu L. Controllable chemical vapor deposition growth of two-dimensional heterostructures. *Chem*. 4(4).2018 :671–689.

[164] Ludowise M J. Metalorganic chemical vapor deposition of III-V semiconductors. *Journal of Applied Physics*.1985. 58(8): 31–55.

- [165] Kommu S .Wilson G M.Khomami B . A Theoretical/Experimental Study of Silicon Epitaxy in Horizontal Single-Wafer Chemical Vapor Deposition Reactors. *Journal of the Electrochemical Society* 2000.147: 1538–1550.
- [166] Pedersen H .Elliott SD .Studying chemical vapor deposition processes with theoretical chemistry. *Theoretical Chemistry Accounts*.2014(5).133: 1476.
- [167] Martin P M. Deposition technologies: an overview, *Handbook of deposition technologies for films and coatings*, 3 Eds. William Andrew.2010
- [168] Mattox D M .Handbook of physical vapor deposition (PVD) processing.2Eds. William Andrew.2010.
- [169] Carlsson J.artin PM. Chemical Vapor Deposition, In: Martin PM, *Handbook of Deposition Technologies for Films and Coatings: science, applications and technology*, 3 Eds. Boston: William Andrew .2010.
- [170] Fuller C B.Mahoney M W.Bingel WH .Friction stir weld tool and method.2Ed.Patent. US. 2006.
- [171] Wang D N.White J M. Law KS et al. Thermal CVD/PECVD reactor and use for thermal chemical vapor deposition of silicon dioxide and in-situ multi-step planarized process. Patent .US .1991.
- [172] Hirose Y. Terasawa Y. Synthesis of diamond thin films by thermal CVD using organic compounds. *Japanese Journal of Applied Physics*.1986.25: L519.
- [173] Cao G .Nanostructures and nanomaterials: synthesis, properties and applications, 2 Eds. World Scientific Publishing Company.2004.
- [174] Chen M. Chen C M. Chen C F. Preparation of high yield multi-walled carbon nanotubes by microwave plasma chemical vapor deposition at low temperature . *Journal of materials science*. 2002.37(17). 3561-3567.
- [175] Hitchman M L.Jensen K F . Chemical vapor deposition: principles and applications, 1 Ed.Elsevier.1993 .
- [176] Jose YM. Miki Y M. Rendon L .Santiesteban J G. Catalytic growth of carbon microtubules with fullerene structure . *Applied physics letters*.1993. 62(2): 202-204.
- [177] OhringM.The material science of thin films.1 Ed. Academic Press.Boston.1992.
- [178] Wilcock J D. Campbell D S. The internal stress in evaporated silver and gold films. *Thin Solid Films*. 1969.3(3): 13-34
- [179] Palmieri VG. Caldarella G. Cisternino S et al. The way of thick films toward a flat q-curve In sputtered cavities. 18th International Conference on RF Superconductivity.2017 :378-381

- [180] Malzbender J. Comment on hardness definitions. *Journal of the European Ceramics Society*. 2003. 23(9):1355-1359
- [181] Blau P J. A Comparison of Four Microindentation Hardness Test Methods Using Copper, 52100 Steel and an Amorphous Pd-Cu-Si Alloy. *Metallography*. 1983. 16: 1-18.
- [182] Oliver W C. McHargue C J, Characterizing the Hardness and Modulus of Thin Films Using a Mechanical Properties Probe. *Thin Solid Films*. 1988. 161 : 117-125.
- [183] Peter J B. Lawn B R. *Microindentation Techniques in Materials Science*. 2 Eds. ASTM Special Publication. 1986.
- [184] Choy K L. Chemical vapour deposition of coatings. *Science Direct*. 2003. 48(2): 57–170.
- [185] Gorokhovskiy V. Bowman C. Gannon P. Van Vorous D. A. A. Voevodin A. Rutkowski A. Tribological performance of hybrid filtered arc-magnetron coatings. Part II: Tribological properties characterization. *Surface and Coatings Technology*. 2007. 201: 6228-6238.
- [186] Musil J. Hardness nanocomposite coatings: Thermal stability, oxidation, resistance and toughness *Surface and Coatings Technology*. 2012. 207: 50-56
- [187] Müller L D. *Density Determination in: Physical Methods in Determinative Mineralogy*. Academic Press. 1977.
- [188] Pratten N A. The Precise Measurement of the Density of Small Samples. *Journal of Materials Science*. 1981. 16:1737-1747.
- [189] Jing X. Maiti S. Subhash G. A new analytical model for estimation of scratch induced damage in brittle solids, *Journal of the American Ceramic Society*. 2007. 90 : 885–892.
- [190] Junyuan Feng J. Zhenping W et al. Crack behaviors of optical glass BK7 during scratch tests under different tool apex angles. *Wear*. 2019. 430–431 : 299–308.
- [191] Castaneda L. Garcia-Valenzuela A. Zironi E P. Canetas-Ortega J et al. Formation of indium-doped zinc oxide thin films using chemical spray techniques: The importance of acetic acid content in the aerosol solution and the substrate temperature for enhancing electrical transport. *Thin Solid Films*. 2006. 503(2): 212-218.
- [192] Tec-Yam S et al. High quality antireflective ZnS thin films prepared by chemical bath deposition. *Materials Chemistry and Physics*. 2021. 252: 124366 (2-3) 386-393.
- [193] Lide D L. *CRC handbook of chemistry and physics - a ready-reference book of chemical and physical data*. 89 Eds. CRC Press. 2009
- [194] Borah J P. Barman J. Sarma K. Structural and optical properties of ZnS Nanoparticles. *Chalcogenide Letters*. 2008. 5 (9):201-208.
- [195] Akhtar M S. Saira R. Rana Farhat M et al. Surfactant and template free synthesis of porous ZnS nanoparticles *Materials Chemistry and Physics*. 2017. 189 : 28-34

- [196] Law K. H. Zhao H. Surface Wetting Characterization, Contact Angle, and Fundamentals. Springer. 2016.
- [197] Allahkarami M. Hanan J C. Three-dimensional x-ray diffraction detection and visualization Measurement. Science and Technology. 2014. 25 : 957-233
- [198] Rao A V. Latthe S . Nadargi D Y et al. Preparation of MTMS based transparent superhydrophobic silica films by sol-gel method. Journal of Colloid and Interface. 2009. 332(2):484–490.
- [199] Min H. Jianjun W. Huiling L. Yanlin S. Super-hydrophobic surfaces to condensed micro-droplets at temperatures below the freezing point retard ice/frost formation. Royal Society of Chemistry .2011. 7: 3993–4000
- [200] Mittal K L. Adhesion measurements of films and coatings. 2 Eds. VSP Utrecht. The Netherlands. 1995.
- [201] Mittal K L Adhesion Measurement of Thin Films. Electrocomponent Science and Technology. 1976. 3: 21-42.
- [202] Prater T. Moss R W. Effect of the coating structure on the adherence of sputter-deposited oxide coatings. Thin Solid Films. 1983. 107- 455.
- [203] Mellali M. Fauchais P. Grimaud A. Influence of substrate roughness and temperature on the adhesion/cohesion of alumina coatings. Surface and Coatings Technology. 1996. 81 (2–3) : 275-285
- [204] Evans A G. Dory M D . Hu M S. The cracking and decohesion of thin films on ductile substrates. Journal of Materials Research. 1988. 3 (5): 1043-1053.
- [205] Grosskreutz J C. McNeil M B. The fracture of surface coatings on a strained substrate. Journal of Applied Physics. 1969. 40 : 355-359.
- [206] Wojciechowski P H. Mendolia M S, Fracture and cracking phenomena in thin films adhering to high elongation substrates. Physics of Thin Film, Academic Press. 1992. 19: 271-280.
- [207] Zito R R, Failure of reflective metal coatings by cracking, Thin Solid Films. 87(1) .1982: 87-95
- [208] Mattox D M, Thin film adhesion and adhesive failure – a perspective .Thick Films and Bulk Coatings. 1978. 54-62
- [209] Tuteja A . Choi W. M. Ma M. Mabry J M. Designing superoleophobic surfaces, Science. 318 .2007. 318:1618–1622,
- [210] Kendall K . Interfacial cracking of a composite. Journal of materials Science. 1976. 11: 638-644.
- [211] Dowson D. History of tribology. Professional Engineering Publication. London. 1998.
- [212] Bhushan B. Introduction to Tribology, 2 Eds. Willey . 2013.

- [213] Stalder A F. Melchior T. Muller M et al. Low-bond axisymmetric drop shape analysis for surface tension and contact angle measurements of sessile drops. *Colloids Surfaces A: Physicochemical and Engineering Aspects*.2010.364(3):72-81.
- [214] Karagüzel C. Can M F. Sönmez E. Çelik MS.2005. Effects of electrolyte on Surface Free Energy Components of Feldspar Minerals Using Thin- Layer-Wicking Method, *J. of Colloid and Interface Science*.2005. 285:190- 200.
- [215] Li D .Drop size dependence of contact angles and line tensions of solid-liquid Systems. *Colloids Surfaces A: Physicochemical and Engineering Aspects*. 1996. 116(2):1-23.
- [216] Rjiba N. NardinM . Drean J Y. Frydrych R. *Journal of Colloid and Interface Science*. 2007:314, 373.
- [217] Reitz M. Gerhardt H. Schmitt C et al. Analysis of chemical profiles of insect adhesion secretions by gas chromatography-mass spectrometry. *Analytica Chimica Acta*.2015. 854: 47–60
- [218]Bikerman J J.A Method of Measuring Contact Angles. *Industrial Engineering Chemistry and Analytical Edition*.1941. 13(6):443–444.
- [219] Chau T T .A review of techniques for measurement of contact angles and theirapplicability on mineral surfaces. *Minerals Engineering*. 22(3): 213–219.
- [220] Fuller K N G. Tabor D. The effect of surface roughness on the adhesion of elastic solids. *Proceedings of the Royal Society A* .1975.34: 327–342
- [221]Chen H. Jesus L M. Amirfazli A. Contact angle measurement with a smartphone. *REVIEW OF SCIENTIFIC INSTRUMENTS*.2018. 89: 035117
- [222] WilhelmyL.Ueber die Abhangigkeit der Capillaritats-Constanten des Alkohols von Substanz und Gestalt des benetztenfestenKorpers. *Annals of Physics*.1863. 195(6): 177–217.
- [223] Mack G L. Lee D A. The Determination of Contact Angles from Measurements of the Dimensions of Small Bubbles and Drops. I. The spheroidal segment method for acute angles. *Physical Chemistry A*.1935.40(2): 169–176.
- [224]Bracco G. Holst B. *Surface science techniques*. Springer. 2013.
- [225] Roma´nszki L. MohosM.TelegdiJ.Keresztes Z. Nyikos L. A comparison of contact angle measurement results obtained on bare, treated, and coated alloy samples by both dynamic sessile drop and Wilhelmy method. *PeriodicaPolytechnica Chemical Engineering*. 58.2014:53:59.
- [226] LunkenheimerK. Wantke K D.Determination of the surface tension of surfactant solutions applying the method of Lecomte du Nouy (ring tensiometer).*Colloid Polymer Science* .1981. 259(3): 354–366.
- [227] Du Nouy P L. A New apparatus for measuring surface tension. *Journal of General Physiology*. 1919: 521–524.

- [228] Harkins W. Jordan H.A. Method for the Determination of Surface and Interfacial Tension from the Maximum Pull on a Ring. *Journal of the American Chemical Society*.1930. 52(5): 1751–1772.
- [229] Fox H. Chrisman C. The Ring Method of Measuring Surface Tension for Liquids of High Density and Low Surface Tension. *J. Phys. Chem.* 1952.56(2):284–287.
- [230] Taggart A F. Taylor T C. Ince C R. Experiments with flotation reagents. *Transactions of the American Institute of Mining and Metallurgical Engineers*. Incorporated. 1929.
- [231] Wark I. Cook A. An experimental study of the effect of xanthates on contact angles at mineral surfaces. *Transactions of the American Institute of Mining, Metallurgical Engineers*.1934.112:189-244.
- [232] Hu X .Miller R. Guo L .Experimental study on interfacial characteristics during bubble dissolution. *Colloids Surfaces A: Physicochemical and Engineering Aspects*.2016.505:179-185.
- [233] Zhang X. Shi F. Niu J et al. Superhydrophobic surfaces: from structural control to functional application. *Journal of Materials Chemistry* .2008. 18: 621–633.
- [234] Hoorfar M. Neumann A W. Axisymmetric drop shape analysis (adsa) for the determination of surface tension and contact angle. *Journal of Adhesion*. 2004.80 (8). 727–743.
- [235] Zhang W. Wahlgren M .Sivik B. Membrane characterization by the contact angle technique: II. Characterization of UF-membranes and comparison between the captive bubble and sessile drop as methods to obtain water contact angles. *Desalination* .1989.72(3):263-273
- [236] Lipowsky R. Lenz P. Swain S. *Colloids surfaces A: Physicochemical and engineering Aspects*.2000.3 (161):99-120.
- [237] Snowden W E. Aksay I A. Measurement of thick film adhesion by impact separation technique, LLNL, *Journal of Materials Science*.2008.14 (81): 651-660.
- [238] Turunen M P. Laurila L .Kilvilahti J K. Evaluation of the surface free energy of spin-coated photo definable epoxy. *Journal of Polymer Science*. 2002. 40(18): 2137-2149.
- [239] Persson B N J. Biological adhesion for locomotion on rough surfaces: basic principles and a theorist's view. *MRS Bulletin*. 2007.32: 486–490.
- [240] King T B. The surface tension and structure of silicate slags. *Society of Glass Technology*.1995.35: 241-259.
- [241] Harkins D. Brown E. Determination of surface tension and the weight of falling drops the surface tension of water and benzene by the capillary height method. *Journal of the American Chemical Society*.1999.41:499-524.

- [242] Jasper J J. Surface tension of pure compounds. Journal of Physical and Chemical. ReferenceData.1972.12 (4).1972:841-1009.
- [243] Jo H .Hwang K .Kim D et al. Loss of superhydrophobicity of hydrophobic micro/nano structures during condensation .Scientific Reports.2015.5: 9901.
- [244] Kinloch A J .Adhesion and Adhesives:Science and Technology. 1Ed. Chapman and Hall. New York.1987
- [245] Rubio J. MazoA.Martín-Ilana A et al .FT-IR study of the hydrolysis and condensation of 3-(2-amino-ethylamino) propyl-trimethoxy silane. Journal of the Spanish Ceramic and Glass Society.2018: 57:160-168.
- [246] Soriano D. Mazo A. Rubio J et al. Spectral pH dependence of erythrosin B in sol-gel silica coatings and buffered solutions. Journal of the Spanish Ceramic and Glass Society . 2006.45: 39-47.
- [247] Abchi A. Belkhir N. Rubio J. Effect of storage and surface roughness on the SiO₂ thin films adhesion behavior. Journal of Adhesion Science and Technology. 2021. <https://doi.org/10.1080/01694243.2021.1916259>.
- [248] Sugden S. XC VII. The determination of surface tension from the maximum pressure in bubbles. Journal of the Chemical Society. 1922; 121:858.
- [249] Zhang Z Z. Shen D Z. Zhang J Y. Shan C C et al. The growth of single cubic phase ZnS thin films on silica glass by plasma-assisted metalorganic chemical vapor deposition. Thin Solid Films. 2006.513 :114-117.
- [250] Jiang Y. Meng X M. Liu J et al. ZnS nano wires with wurtzite type modulated structure. Advanced Materials . 2003.15 :1195-1198
- [251] Wageh S, Zhao S L and Xu X R . Growth and optical properties of colloidal ZnS nanoparticles. Journal of Crystal Growth .2003.255(4):332-337
- [252] Kumbhojkar N. Nikesh V V .Kshirsagar A . Photophysical properties of ZnS nanoclusters. Journal of Applied Physics. 2000.88(11): 6260-6264.

RÉSUMÉ

Les propriétés de surface peuvent affecter l'efficacité et le comportement du matériau optique, ainsi leur amélioration est plus que souhaitable. L'une des solutions préconisées est le dépôt de couches minces. Les couches minces sont importantes pour des applications dans les différents domaines, tels que les dispositifs optiques, les applications environnementales, les dispositifs de télécommunications, les dispositifs de stockage d'énergie ...etc. Cependant, le dépôt des couches minces doit être réussi afin de réaliser les objectifs souhaités. En effet, une meilleure adhérence et qualité de dépôt sont le facteur essentiel pour le jugement d'une couche mince.

Dans cette optique, cette thèse a pour objectif d'étudier l'effet des conditions de stockage et la qualité de surface de certains matériaux optiques sur l'adhésion des couches minces. Pour cela, des essais ont été menés dans la synthèse et le dépôt des couches minces par sol -gel et La technique de déposition par bain chimique (CBD), ainsi que l'étude du comportement adhésif du sulfure de zinc et de silice des couches minces déposées avec des concentrations différentes: 20, 30 et 40% sur des substrats optiques. Les essais ont été réalisés sur des substrats en matériaux optiques (verre minéral et polymère) stockés pendant une longue durée dans différentes solutions (CK et PEG). Les surfaces optiques ont été caractérisées avec plusieurs techniques (interférométrie optique, TIS, AFM...) leurs rugosités de surfaces ont été mesurées et comparées, les solutions préparées ont été analysées par FTIR, Raman et spectroscopie de photoluminescence. Les résultats obtenus sont de grandes variances et par conséquent les conclusions claires ne sont pas facilement tirées. L'effet de stockage des matériaux optiques et leur rugosité de surfaces sur le phénomène d'adhésion et le facteur d'étalement des couches minces déposées sont établis.

Mots clés: Verre optique, PMMA, coefficient d'étalement, films minces, adhérence, angle de contact, sol-gel, CBD, Silice, Sulfure de Zinc, FTIR, spectroscopie Raman.

ملخص

يمكن أن تؤثر خصائص السطح على كفاءة وسلوك المادة البصرية، وبالتالي فإن تحسينها أكثر من غوبفيه. ومنه فإن

أحد الحلول الموصى بها هو ترسيب الطبقات الرقيقة. تعتبر

الطبقات الرقيقة مهمة للتطبيقات الفيزيائية المختلفة، مثل الأجهزة الضوئية، والتطبيقات البيئية، وأجهزة الاتصالات السلكية واللاسلكية، وأجهزة تخزين الطاقة، وما إلى ذلك. ومع ذلك، يجب أن يكون ترسيب الطبقات الرقيقة ناجحاً من أجل تحقيق الأهداف المرجوة. في الواقع، يعد الالتصاق وجودة الترسيب أفضل عاملاً أساسياً لتأثير على الطبقة الرقيقة.

معوضعي عينا لا اعتبار التقنيات الحديثة

المتاحة، تهدف هذه الأطروحة إلى دراسة تأثير ظروف التخزين وجودة سطح بعض المواد البصرية على الالتصاق بالطبقات الرقيقة. ولهذا الغرض، أجرينا اختبار بارافيت حصر وترسيب الطبقات الرقيقة بواسطة محلول لهاميو ترسيب

الحمام الكيميائي، وكذلك دراسة السلوك اللاصق لكريتيد الزنكوسيليكات الطبقات الرقيقة المترسبة بتركيز مختلفة: 20 و 30 و 40

في المائة على ركائز البصرية. تم إجراء الاختبار على ركائز مصنوعة من مواد بصرية (الزجاج المعدني والبوليمر)

للتخزين طويلاً لأجل فهم حاليل مختلفة. تتميز الأسطح الضوئية بعدة تقنيات

(قياس الاندخال البصري، وتكمال الكوة البصرية، ومجهر القوة الذرية، وما إلى ذلك) وقياس خشونة سطحها ومقارنتها، ثم

تحليل المحلول المحضر بواسطة التحليل الطيفي للأشعة تحت الحمراء، التحليل الطيفي لأمانو التحليل الطيفي الضوئي. إن النتائج التي تم التوصل إليها هي فروق كبيرة، وليس من السهل استخلاص استنتاجات واضحة.

يتم تحديد تأثير التخزين للمواد البصرية وخشونة سطحها على ظاهرة الالتصاق معاملاً لانتشار للطبقات الرقيقة المترسبة

الكلمات المفتاحية : الزجاج البصري، معاملاً لانتشار، الأغشية الرقيقة، الالتصاق، زاوية الالتصاق، محلول لهامي، ترسيب

الحمام الكيميائي، بوليمر، كبريتيد الزنك، سيليكات، التحليل الطيفي للأشعة تحت الحمراء، التحليل الطيفي لأمانو.